



UNH-08-02
JLAB-THY-08-830
NT@UW-08-11

HADRONIC INTERACTIONS FROM LATTICE QCD *

Silas R. Beane

*Department of Physics,
University of New Hampshire,
Durham, NH 03824-3568, USA.*

Kostas Orginos

*Department of Physics,
College of William and Mary,
Williamsburg, VA 23187-8795, USA
and Jefferson Laboratory,
12000 Jefferson Avenue,
Newport News, VA 23606, USA.*

Martin J. Savage

*Department of Physics,
University of Washington,
Seattle, WA 98195-1560, USA.*

Abstract

We present an overview of recent efforts to calculate the interactions among hadrons using lattice QCD. After outlining the techniques that are used to extract scattering parameters, we detail the latest calculations of meson-meson scattering, baryon-baryon scattering and multi-meson systems obtained with domain-wall valence quarks on the staggered MILC lattices by the NPLQCD collaboration. Estimates of the computational resources required to achieve precision results in the baryon sector are presented.

* Review prepared for the *International Journal of Modern Physics C*.

Contents

I. Introduction	4
A. Aspects of QCD and Nuclear Physics	5
B. Aspects of Lattice QCD	5
C. Diversion into Sociology	6
II. Formal Aspects of Lattice Calculations for Nuclear Physics	7
A. Physics From Euclidean Space Correlation Functions	8
B. Hadronic Interactions, the Maiani-Testa Theorem and Lüscher's Method	9
1. Is it a Bound-State or a Scattering-State ?	12
C. Finite-Lattice Spacing Artifacts and Mixed-Action Effective Field Theories	13
D. Potentials From Lattice Calculations	15
E. Statistical Errors Associated with Calculations of Observables in the Nucleon and Systems of Nucleons	16
III. Our Current Techniques and Resources	17
A. Domain Wall and Staggered Fermions	20
B. The Lattice Actions	21
C. Mixed Action Tuning	24
D. Method of Contractions	24
E. Data Analysis	25
F. Resources	27
IV. Two-Body Physics	27
A. $\pi\pi$ Scattering	27
1. Introduction	27
2. Data Analysis and Chiral and Continuum Extrapolation	28
3. Systematic Uncertainties	31
4. Discussion	32
B. $K\pi$ Scattering	33
1. Introduction	33
2. Analysis and Chiral Extrapolation	34
C. KK Scattering	39
1. Introduction	39
2. Mixed-Action χ -PT at One Loop	39
3. Extrapolation to the Physical Point	41
D. Thoughts on Meson-Meson Scattering	42
E. NN Scattering	42
F. YN Scattering	45
1. Introduction	45
2. Results	46
3. Discussion	47
G. Exploratory Quenched Calculations	48
1. BB Potentials	48
2. J/ψ -Hadron Scattering	50
V. n-body Interactions	50

VI. Resource Requirements for Further Progress	52
VII. Concluding Remarks	54
References	55

I. INTRODUCTION

Lattice Quantum Chromodynamics (QCD) is emerging from —what should be considered to be— a thirty year research and development (R and D) phase, into the production phase, where it will produce precise and accurate calculations of non-perturbative strong interaction quantities. The last five years has seen the field evolve from an era of quenched calculations in small spatial volumes at large lattice spacings, to the present day, where fully-dynamical calculations with chiral symmetry at finite lattice-spacing are standard, the lattice volumes have a spatial extent of $L \sim 2.5 - 3.5$ fm and lattice spacings are $b \lesssim 0.13$ fm. Unfortunately, it is still the case that the light-quark masses, m_q , are larger than those of nature, with typical pion masses $m_\pi \sim 300$ MeV. However, the next five years will see calculations at the physical light-quark masses, $m_\pi \sim 140$ MeV, in large volumes, $L \gtrsim 6$ fm, and at small lattice spacings, $b \lesssim 0.06$ fm become standard. This impressive evolution will continue with the increasing computer power dedicated to Lattice QCD calculations, and development of new and faster algorithms with which to generate lattice configurations, and to compute quark propagators and hadronic observables.

The impact on nuclear physics of being able to reliably compute strong interaction quantities directly from QCD, the underlying theory of the strong interactions, cannot be overstated. While it is important to recover what is known experimentally to high precision, that is obviously not the main objective, and certainly not a good reason to pursue such an effort. The reason for investing (both money and careers) in this area is to be able to calculate quantities of importance that cannot be accessed experimentally, or which can be measured with only limited precision. Nuclear physics is an incredibly rich field, whose phenomenology has been explored for decades. However, there is still little understanding of the connection to QCD and the basic building blocks of nature, quarks and gluons. Such a connection will be firmly established with lattice QCD, and as a consequence, the calculation of quantities that are not experimentally accessible will finally become possible. On a more academic level, Lattice QCD will allow for an exploration of how nuclei and nuclear interactions depend upon the fundamental parameters of nature, and an understanding of the fine-tunings that permeate nuclear physics will finally be translated into (the possible) fine-tunings of the light-quark masses.

Two important examples of how Lattice QCD calculations can impact nuclear physics are in the evolution of a supernova and in the structure of nuclei. In the evolution of supernova, one of the key ingredients that determines whether a supernova evolves into a black-hole or a neutron star is the nuclear equation of state (NEOS). The NEOS is determined by the dynamical degrees of freedom and their interactions. The degrees of freedom at a given density are determined by the mass of the hadrons in the medium, which depends upon their interactions. For instance, the mass of the Σ^- is expected to be significantly less than in free-space due to its interactions with neutrons, however, the precise mass-shift is uncertain due to the model dependence of existing calculations [1]. As the Σ^- carries the same charge as the electron, it can become energetically favorable to have the nuclear material composed of neutrons, protons and Σ^- 's, as opposed to just neutrons and protons, due to the location of the fermi-levels. Experimentally, little is known about the Σ^- -neutron interaction, and a precise Lattice QCD calculation of this interaction, and others, will greatly reduce the theoretical uncertainty in this particular potential contribution to the NEOS in hadronic systems with densities of a few times that of nuclear matter. As regards the structure of nuclei, we now have refined many-body techniques, such as Greens function Monte-Carlo

(GFMC) [2] with which to calculate the ground states and excited states of light nuclei, with atomic number $A \lesssim 14$. Using only the modern nucleon-nucleon (NN) potentials that reproduce all scattering data below inelastic thresholds with $\chi^2/dof \sim 1$, such as AV_{18} [3], one fails quite dramatically to recover the structure of light nuclei. The inclusion of a three-nucleon interaction greatly improves the predicted structure of nuclei [2]. Lattice QCD will be able to calculate the interactions of multiple nucleons, bound or unbound in the same way it can be used to determine the two-body scattering parameters. For instance, a calculation of the three-neutron interaction will be possible.

A. Aspects of QCD and Nuclear Physics

The structure and interactions of all nuclei are determined completely by QCD and by the electroweak interactions, primarily electromagnetism. The Lagrange density of QCD is written in terms of the quark and gluon fields, and is manifestly invariant under local $SU(3)_c$ transformations. At short-distances the coupling between the quarks and gluons, and between the gluons and themselves, $\alpha_s(Q)$, is small and allows for processes to be computed as an asymptotic series in $\alpha_s(Q)$ —*asymptotic freedom*. However, as the typical length scale of the process grows, $\alpha_s(Q)$ becomes large, and perturbative calculations fail for $Q^2 \lesssim 1 \text{ GeV}^2$. At long-distances, and hence low energies, the appropriate degrees of freedom are not the quarks and gluons that the QCD Lagrange density is written in terms of, but the hadrons, such as pions and nucleons. It is the properties of collections of nucleons, hyperons and mesons that defines the field of nuclear physics, a field that, simply put, is the exploration of the non-perturbative regime of QCD. In this low-energy regime, the approximate chiral symmetry of the QCD Lagrange density is spontaneously broken by the vacuum, giving rise to pseudo-Goldstone bosons and the approximate isospin symmetry. With such rich dynamics present in what naively looks like a simple theory it is not surprising that relatively little progress has been made in determining the properties and interactions of nuclei, even the simplest nuclei, directly from QCD. Understanding and calculating the properties and interactions of nuclei is further complicated by the fact that nuclear physics, and hence QCD, exhibits one or more fine-tunings. The values of the light quark masses, the scale of chiral symmetry breaking, Λ_χ , and the electromagnetic coupling constant take values such that the scattering lengths in the two-nucleon systems are both unnaturally large compared with the range of the nuclear interaction. Further, the location of energy-levels in carbon and oxygen are such that the triple- α process can proceed to produce enough carbon for us to be writing this review. Of course, one looks toward an anthropic explanation (for a lengthy discussion of the anthropic principle see Ref. [4]) of these fine-tunings, but at present we have no understanding of how the fine-tunings exhibited in nuclear systems translate into fine-tunings in the fundamental parameters of nature (if in fact they are fine-tuned).

B. Aspects of Lattice QCD

The only known way to solve QCD in the low-energy regime is numerically using Lattice QCD. Lattice QCD is a technique in which Euclidean space correlation functions are calculated by a Monte-Carlo evaluation of the Euclidean space path integral. The calculations are performed in Euclidean space so that contributions to any given correlation function that have a large action are exponentially suppressed. This is in contrast with Minkowski

space in which large action contributions result in a complex phase which will average to an exponentially small contribution with nearby paths. Space-time is discretized with the quarks residing on the lattice sites, and the gluon fields residing on the links between lattice sites. The lattice spacing, b , (the distance between adjacent lattice sites) is required to be much smaller than the scale of chiral symmetry breaking (or any physical length scale in the system) for its effects to be small. The effects of a finite lattice spacing can be systematically removed by combining lattice calculations of the same correlation functions at several lattice spacing with the low-energy effective field theory (EFT) constructed to explicitly include the lattice spacing. The EFTs describing such calculations are somewhat more complicated than their continuum partners as they must reproduce that matrix elements of the Symanzik action constructed with higher dimension operators induced by the lattice spacing[5]. While the action lacks Lorentz invariance and rotational symmetry, it does possess hypercubic symmetry. As computers have finite memory and performance, the lattice volumes are finite in all four space-time directions. Generally, periodic boundary conditions (BC's) are imposed on the fields in the space-directions (a three torus), while anti-periodic BC's are imposed on the fields in the time-direction, which in many cases is much larger than the space-directions¹. For the calculations we will be discussing in this review, the lattice volumes are large compared with the Compton wavelength of the pion, and deviations in single particle properties from their infinite volume values are exponentially small, generically $\sim e^{-m_\pi L}$. Finally, the cost of performing lattice calculations increases dramatically with decreasing quark mass, and presently, calculations at the physical quark masses, $m_\pi \sim 140$ MeV are not possible. Currently, lattice calculations are performed at unphysical values of the quark masses, and the light quark mass dependence of the observable of interest, which can be determined perturbatively in the low-energy EFTs, is used to extrapolate to the physical light quark masses. Therefore, the practical situation with current Lattice QCD calculations is that they are performed at finite lattice spacing, within finite volumes and at unphysical quark masses. The appropriate EFT (e.g. χ -PT, heavy-baryon- χ -PT) is then used to extrapolate to the infinite volume, continuum limit of QCD where the parameters of nature reside.

C. Diversion into Sociology

Many of the members of the NPLQCD collaboration (of which the authors are a part of and with the logo displayed in Fig. 1) spent years developing EFTs for nuclear physics, and more generally performing calculations of strong interaction processes in the low-energy regime. Around 2005, it started to become apparent to us that in order to make progress in low-energy QCD, the approximate chiral symmetries of QCD were, in many cases, no longer sufficient to make predictions for quantities at the precision required to impact experiments, or to shed light on fundamental questions in strong interaction physics. Basically, the number of counterterms that were commonly appearing in calculations beyond leading order (LO) or next-to-leading order (NLO) were large, and in many instances exceeded the number of experimental measurements that were available or would become available in the near future. We decided that the only path forward in this area was to use Lattice QCD to calculate these

¹ A linear combination of propagators generated with periodic and anti-periodic boundary conditions can be used to effectively double the length of the time-direction

counterterms. The focus of the NPLQCD collaboration is to calculate nuclear reactions from Lattice QCD, and our initial efforts have focused on calculating the elastic scattering of the lightest hadrons. It is these calculations that are the focus of this review.



FIG. 1: The NPLQCD logo.

We wish to stress that we would not have been able to perform the calculations in the time frame that we have if it were not for the Lattice QCD infrastructure that existed in 2005 and continues to exist and grow in the United States, namely USQCD and the efforts of the lattice group at Jefferson Laboratory. The USQCD collaborative effort ² has allowed for the large scale production, and more importantly for us, sharing of lattice resources. The MILC collaboration has produced, and continues to produce, multiple staggered (Kogut-Susskind) lattice ensembles at different quark masses, lattice spacing and lattice volumes. Further, NPLQCD has shared resources with the LHP collaboration ³. Another significant contribution to our program is the software package *Chroma* [6, 7], developed by Robert Edwards and his team at Jefferson Laboratory, which we have used extensively to perform our calculations.

II. FORMAL ASPECTS OF LATTICE CALCULATIONS FOR NUCLEAR PHYSICS

In this section we highlight the formal aspects of Lattice QCD that have direct bearing on the extraction of scattering and reaction processes in multi-hadron systems. Intricate details of Lattice QCD calculations are beyond the scope of this review. In later sections, however, we discuss specific aspects of Lattice QCD calculations that are relevant to the discussions at hand. For even finer details, we refer the reader to a number of excellent texts on the subject [8, 9, 10]. Throughout, we will be discussing lattices with cubic symmetry in the spatial directions, each of length L in lattice units. The time direction is assumed to be much larger than the spatial directions so that all calculations are assumed to be at zero temperature, $T = 0$. Further, while the lattice spacing is conventionally denoted by “a”, we will use “b” in order to avoid conflict with the notation for scattering lengths which are universally denoted by “a”.

² <http://www.usqcd.org/>

³ <http://www.jlab.org/~dgr/lhpc/>

A. Physics From Euclidean Space Correlation Functions

In the continuum limit, the Euclidean space correlations functions (suitably Fourier transformed) are the sums of exponential functions, whose arguments are the product of Euclidean time with the eigenvalues of the Hamiltonian in the finite-volume associated with eigenstates that couple to the hadronic sources and sinks. At large times, the correlation function becomes a single exponential dictated by the ground state energy and the overlap of the source and sink with the ground state. As an example, consider the pion two-point function, $C_{\pi^+}(t)$ generated by a source (and sink) of the form $\pi^+(\mathbf{x}, t) = \bar{u}(\mathbf{x}, t)\gamma_5 d(\mathbf{x}, t)$,

$$C_{\pi^+}(t) = \sum_{\mathbf{x}} \langle 0 | \pi^-(\mathbf{x}, t) \pi^+(\mathbf{0}, 0) | 0 \rangle = \sum_{\mathbf{x}} \langle \pi^-(\mathbf{x}, t) \pi^+(\mathbf{0}, 0) \rangle \quad . \quad (1)$$

The sum over all lattice sites at each time-slice, t , projects onto the spatial momentum $\mathbf{p} = \mathbf{0}$ states. The source $\pi^+(\mathbf{x}, t)$ not only produces single pion states, but also all possible states with the same quantum numbers as a single pion. More generally, the source and sink are smeared over lattice sites in the vicinity of (\mathbf{x}, t) to increase the overlap onto the ground state and lowest-lying excited states. Translating the sink operator in time via $\pi^+(\mathbf{x}, t) = e^{\hat{H}t} \pi^+(\mathbf{x}, 0) e^{-\hat{H}t}$ gives ⁴

$$C_{\pi^+}(t) = \sum_n \frac{e^{-E_n t}}{2E_n} \sum_{\mathbf{x}} \langle 0 | \pi^-(\mathbf{x}, 0) | n \rangle \langle n | \pi^+(\mathbf{0}, 0) | 0 \rangle \rightarrow A_0 \frac{e^{-m_\pi t}}{2m_\pi} \quad . \quad (2)$$

At finite lattice spacing, the correlation functions for Wilson fermions remain the sum over exponential functions, but for particular choices of parameters used in domain-wall fermions, the correlation functions exhibit additional sinusoidally modulated exponential behavior at short-times (with a period set by the lattice spacing).

It is straightforward to show that the lowest energy extracted from the correlation function in Eqs. (1) and (2) correspond to the mass of the π^+ (and more generally the mass of the lightest hadronic state that couples to the source and sink) in the finite volume. Finite volume effects are exponentially suppressed [11], therefore, while every lattice calculation is performed in a finite volume, as long as the volume is large compared to the pion mass, the mass of stable single particle states can be extracted with high accuracy.

Once any correlation function, e.g. $C_{\pi^+}(t)$, is calculated, the most common objective is to extract the argument of the exponential function that persists at large times. One way to do this is to simply fit the function over a finite number of time-slices to a single exponential function. A second method that is perhaps a bit more “pleasing to the eye”, is to form the effective mass function, e.g.

$$M_{\text{eff.}}(t) = \log \left(\frac{C_{\pi^+}(t)}{C_{\pi^+}(t+1)} \right) \rightarrow m_\pi \quad , \quad (3)$$

where both t and $M_{\text{eff.}}(t)$ are in lattice units. At large times, $M_{\text{eff.}}(t)$ becomes a constant equal to the mass of the lightest state contributing to the correlation function ⁵.

⁴ We assume the absence of external electroweak fields that exert forces on hadrons in the lattice volume.

⁵ This is obviously the most simplistic approach one can take to this problem. To extract the ground state

B. Hadronic Interactions, the Maiani-Testa Theorem and Lüscher's Method

Extracting hadronic interactions from Lattice QCD calculations is far more complicated than the determination of the spectrum of stable particles. This is encapsulated in the Maiani-Testa theorem [13], which states that S-matrix elements cannot be extracted from infinite-volume Euclidean-space Green functions except at kinematic thresholds⁶. This is clearly problematic from the nuclear physics perspective, as a main motivation for pursuing Lattice QCD is to be able to compute nuclear reactions involving multiple nucleons. Of course, it is clear from the statement of this theorem how it can be evaded, one computes Euclidean-space correlation functions at finite volume to extract S-matrix elements, the formulation of which was known for decades in the context of non-relativistic quantum mechanics [14] and extended to quantum field theory by Lüscher [15, 16]. Lüscher showed that the energy of two particles in a finite volume depends in a calculable way upon their elastic scattering amplitude and their masses for energies below the inelastic threshold. As a concrete example consider $\pi^+\pi^+$ scattering. A $\pi^+\pi^+$ correlation function in the A_1 representation of the cubic group [17] (that projects onto the s-wave state in the continuum limit) is

$$C_{\pi^+\pi^+}(p, t) = \sum_{|\mathbf{p}|=p} \sum_{\mathbf{x}, \mathbf{y}} e^{i\mathbf{p}\cdot(\mathbf{x}-\mathbf{y})} \langle \pi^-(t, \mathbf{x}) \pi^-(t, \mathbf{y}) \pi^+(0, \mathbf{0}) \pi^+(0, \mathbf{0}) \rangle . \quad (4)$$

In relatively large lattice volumes the energy difference between the interacting and non-interacting two-meson states is a small fraction of the total energy, which is dominated by the masses of the mesons. In order to extract this energy difference the ratio of correlation functions, $G_{\pi^+\pi^+}(p, t)$, can be formed, where

$$G_{\pi^+\pi^+}(p, t) \equiv \frac{C_{\pi^+\pi^+}(p, t)}{C_{\pi^+}(t)C_{\pi^+}(t)} \rightarrow \sum_{n=0}^{\infty} \mathcal{A}_n e^{-\Delta E_n t} , \quad (5)$$

and the arrow denotes the large-time behavior of $G_{\pi^+\pi^+}$. The energy eigenvalue, E_n , and its deviation from the sum of the rest masses of the particle, ΔE_n , are related to the center-of-mass momentum p_n by

$$\Delta E_n \equiv E_n - 2m_\pi = 2\sqrt{p_n^2 + m_\pi^2} - 2m_\pi . \quad (6)$$

To obtain $p \cot \delta(p)$, where $\delta(p)$ is the phase shift, the square of the center-of-mass momentum, p , is extracted from this energy shift and inserted into [14, 15, 16, 18]

$$p \cot \delta(p) = \frac{1}{\pi L} \mathbf{S} \left(\left(\frac{pL}{2\pi} \right)^2 \right) , \quad (7)$$

which is valid below the inelastic threshold. The regulated three-dimensional sum is [19]

$$\mathbf{S}(x) \equiv \sum_{\mathbf{j}}^{|j|<\Lambda} \frac{1}{|\mathbf{j}|^2 - x} - 4\pi\Lambda , \quad (8)$$

and excited states one can implement the method of Lüscher and Wolff [12] in which the correlation functions resulting from different sources and sinks are calculated. The resulting matrix of correlation functions is diagonalized, and the effective mass function for each resulting eigenvalue can be used to extract the spectrum.

⁶ An infinite number of infinitely precise calculations would allow one to circumvent this theorem.

where the summation is over all triplets of integers \mathbf{j} such that $|\mathbf{j}| < \Lambda$ and the limit $\Lambda \rightarrow \infty$ is implicit. Therefore, by measuring the energy-shift, ΔE_n , of the two particles in the

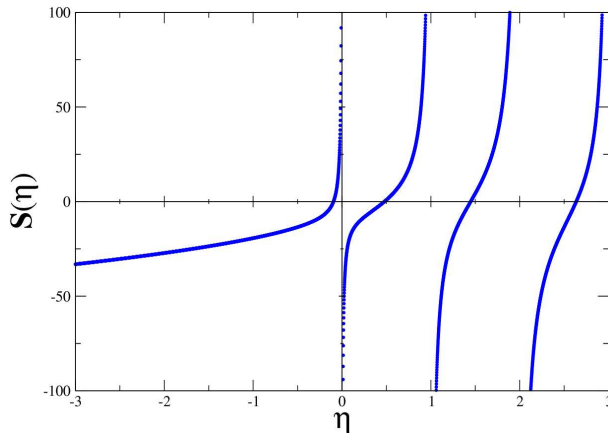


FIG. 2: The function $\mathbf{S}(\eta)$ vs. η , defined in Eq. (8), has poles only for $\eta \geq 0$.

finite lattice volume, the scattering phase-shift is determined at ΔE_n . In the absence of interactions between the particles, $|p \cot \delta| = \infty$, and the energy eigenstates in the finite volume occur at momenta $\mathbf{p} = 2\pi\mathbf{j}/L$. It is important to re-emphasize that this relation in Eq. (7) is valid relativistically [15, 16]. Perhaps most important for nuclear physics is that this expression is valid for large and even infinite scattering lengths [19]. The only restriction is that the lattice volume be much larger than the range of the interaction between the hadrons, which for two nucleons, is set by the mass of the pion.

For the scattering of two nucleons, the scattering length is known to be unnaturally large at the physical pion mass, and therefore, the relation in Eq. (7) will need to be used to extract the scattering parameters. For systems that are not finely-tuned, such as the $\pi^+\pi^+$ system, an expansion in the volume can be used. In the large volume limit ($L \gg |a|$) the energy of the two lowest-lying continuum states in the A_1 representation of the cubic group [17] are [15, 16]

$$\begin{aligned} \Delta E_0 &= +\frac{4\pi a}{ML^3} \left[1 - c_1 \frac{a}{L} + c_2 \left(\frac{a}{L} \right)^2 + \dots \right] + \mathcal{O}(L^{-6}) \\ \Delta E_1 &= \frac{4\pi^2}{ML^2} - \frac{12 \tan \delta_0}{ML^2} \left[1 + c'_1 \tan \delta_0 + c'_2 \tan^2 \delta_0 + \dots \right] + \mathcal{O}(L^{-6}) \quad , \end{aligned} \quad (9)$$

where δ_0 is the s-wave phase-shift evaluated at $p = 2\pi/L$. The coefficients, which result from sums over the allowed momenta [15, 16] in the finite cubic volume, are $c_1 = -2.837297$, $c_2 = +6.375183$, $c'_1 = -0.061367$, and $c'_2 = -0.354156$. (Note that we use the nuclear physics sign convention for the scattering length.) In addition, for $a > 0$ with an attractive

interaction ⁷ a bound state exists with energy [19] (in the large volume limit)

$$\Delta E_{-1} = -\frac{\gamma^2}{M} \left[1 + \frac{12}{\gamma L} \frac{1}{1 - 2\gamma(p \cot \delta)'} e^{-\gamma L} + \dots \right] , \quad (11)$$

where $(p \cot \delta)' = \frac{d}{dp^2} p \cot \delta$ evaluated at $p^2 = -\gamma^2$. The quantity γ is the solution of

$$\gamma + p \cot \delta|_{p^2=-\gamma^2} = 0 , \quad (12)$$

which yields the bound-state binding energy in the infinite-volume limit. As expected, the finite volume corrections are exponentially suppressed by the binding momentum. This is consistent with the corrections to a single particle state where the lightest hadronic excitation is the zero-momentum two-particle continuum state, as opposed to a state containing an additional pion for, say, the finite volume corrections to the single nucleon mass ⁸.

In the limit where $L \ll |(p \cot \delta)^{-1}|$, which is a useful limit to consider when systems have unnaturally-large scattering lengths, the solution of Eq. (7) gives the energy of the lowest-lying state to be

$$\begin{aligned} \Delta \tilde{E}_0 &= \frac{4\pi^2}{ML^2} [d_1 + d_2 L p \cot \delta_0 + \dots] \\ \Delta \tilde{E}_1 &= \frac{4\pi^2}{ML^2} [d'_1 + d'_2 L p \cot \delta_0 + \dots] , \end{aligned} \quad (13)$$

where the coefficients are $d_1 = -0.095901$, $d_2 = +0.0253716$, $d'_1 = +0.472895$, $d'_2 = +0.0790234$ and where $p \cot \delta_0$ in $\Delta \tilde{E}_0$ is evaluated at an energy $\Delta E = \frac{4\pi^2}{ML^2} d_1$, while $p \cot \delta_0$ in $\Delta \tilde{E}_1$ is evaluated at an energy $\Delta E = \frac{4\pi^2}{ML^2} d'_1$. The values of the $d_i^{(n)}$ are determined by zeros of the three-dimensional zeta-functions, and the expressions for ΔE_i and $\Delta \tilde{E}_i$, excluding ΔE_{-1} , are valid for both positive and negative scattering lengths.

Recently, we have performed Lattice QCD calculations of the energy of multiple π^+ 's, from which both the two-body scattering parameters and three-body interaction were determined [22, 23]. In order to make use of the lattice calculations, the ground-state energy of n identical bosons in a finite volume was required. The calculation of the energy-shift of n identical bosons at $\mathcal{O}(L^{-7})$ is straightforward but tedious. The energy-shift of the ground

⁷ The extension of the Chowla-Selberg formula to higher dimensions [20] gives

$$\mathbf{S}(-x^2) \rightarrow -2\pi^2 x + 6\pi e^{-2\pi x} + \dots , \quad (10)$$

for large x , where the ellipses denote terms exponentially suppressed by factors of $e^{-2\sqrt{2}\pi x}$, or more.

⁸ The finite volume dependence of bound states has been explored numerically in Ref. [21].

state is [24, 25, 26]

$$\begin{aligned}
\Delta E_0(n, L) = & \frac{4\pi a}{M L^3} \binom{n}{2} \left\{ 1 - \left(\frac{a}{\pi L} \right) \mathcal{I} + \left(\frac{a}{\pi L} \right)^2 [\mathcal{I}^2 + (2n - 5)\mathcal{J}] \right. \\
& - \left(\frac{a}{\pi L} \right)^3 [\mathcal{I}^3 + (2n - 7)\mathcal{I}\mathcal{J} + (5n^2 - 41n + 63)\mathcal{K}] \\
& + \left(\frac{a}{\pi L} \right)^4 [\mathcal{I}^4 - 6\mathcal{I}^2\mathcal{J} + (4 + n - n^2)\mathcal{J}^2 + 4(27 - 15n + n^2)\mathcal{I}\mathcal{K} \\
& \left. + (14n^3 - 227n^2 + 919n - 1043)\mathcal{L}] \right\} \\
& + \binom{n}{2} \frac{8\pi^2 a^3 r}{M L^6} \left[1 + \left(\frac{a}{\pi L} \right) 3(n - 3)\mathcal{I} \right] + \binom{n}{3} \frac{\bar{\eta}_3^L}{L^6} \left[1 - 6 \left(\frac{a}{\pi L} \right) \mathcal{I} \right] \\
& + \binom{n}{3} \left[\frac{192 a^5}{M \pi^3 L^7} (\mathcal{T}_0 + \mathcal{T}_1 n) + \frac{6\pi a^3}{M^3 L^7} (n + 3) \mathcal{I} \right] + \mathcal{O}(L^{-8}) . \quad (14)
\end{aligned}$$

where the geometric constants that enter are

$$\begin{aligned}
\mathcal{I} &= -8.9136329 & \mathcal{J} &= 16.532316 & \mathcal{K} &= 8.4019240 \\
\mathcal{L} &= 6.9458079 & \mathcal{T}_0 &= -4116.2338 & \mathcal{T}_1 &= 450.6392 \\
\mathcal{S}_{\text{MS}} &= -185.12506 & & & &
\end{aligned} \quad (15)$$

and $\binom{n}{k} = n!/(n-k)!/k!$. The last term in the last bracket of Eq. (14) is the leading relativistic contribution to the energy-shift. Deviations from the energy-shift of n -bosons computed with non-relativistic quantum mechanics arise only for three or more particles as the two-particle energy-shift has the same form when computed in non-relativistic quantum mechanics and in quantum field theory [15, 16]. The renormalization-scale independent, but volume dependent, three-body quantity

$$\bar{\eta}_3^L = \eta_3(\mu) + \frac{64\pi a^4}{m} (3\sqrt{3} - 4\pi) \log(\mu L) - \frac{96a^4}{\pi^2 m} \mathcal{S} \quad (16)$$

was determined in recent Lattice QCD calculations [22, 23], where $\eta_3(\mu)$ is the coefficient of the three-body interaction in the Hamiltonian. In Eq. (15), \mathcal{S}_{MS} is the value of the scheme-dependent quantity \mathcal{S} in the Minimal Subtraction (MS) scheme used to renormalize the theory. The naive dimensional analysis (NDA) estimate of $\bar{\eta}_3^L$ is $\bar{\eta}_3^L \sim 1/(m_\pi f_\pi^4)$. The leading terms in Eq. (14) evaluated at $n = 2$ reproduce those terms shown in Eq. (9).

1. Is it a Bound-State or a Scattering-State ?

Obviously it is important to understand what infinite-volume physics can be extracted from finite-volume calculations. One important question that arises is: if a negative energy shifted state is calculated on the lattice at finite-volume, does it correspond to a bound state or to a scattering state? Clearly, calculations of the same correlation function in multiple volumes will allow for the exponential volume dependence of a bound state⁹ to be distinguished from

⁹ Corrections to the bound-state pole-condition in terms of $i \cot \delta$ that depend exponentially upon the volume [21] are equivalent to the corrections to the bound state mass [19] that have the same form.

the power-law volume dependence of a scattering state. However, one can make an educated guess about the nature of the state by the magnitude of the energy shift. Consider a simple system whose scattering amplitude is dominated at low-energies by the scattering length and effective range, as is the case for the scattering of two nucleons. The location of the states in the lattice volume are determined by the solution of Eq. (7). In Fig. 3 we show the graphical

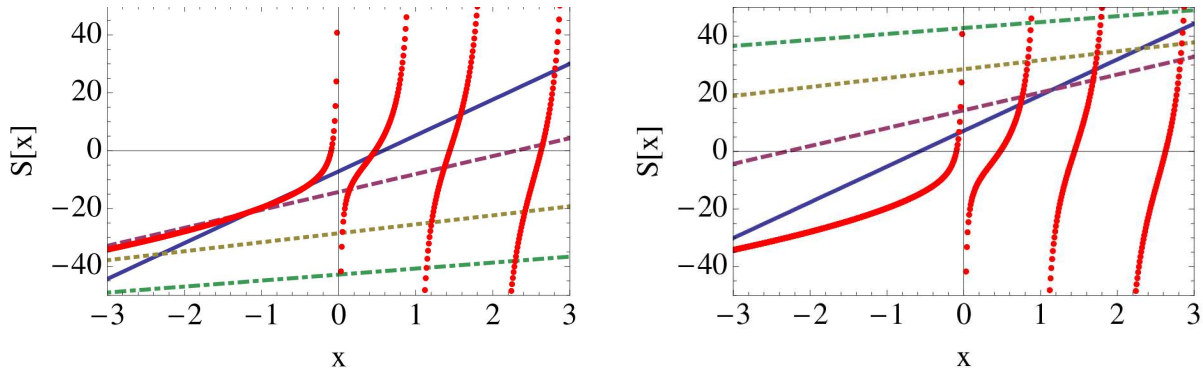


FIG. 3: The functions $\mathbf{S}(x)$ and $p \cot \delta$ vs. x , where $p \cot \delta$ is evaluated at $p^2 = \frac{4\pi^2}{L^2}x$. The left panel is evaluated for scattering parameters $a = +1.1$ fm and $r = 0.5$ fm and all other scattering parameters vanish. The volume parameters are those of coarse MILC lattices with $L = 20$ (solid, blue), $L = 40$ (dashed, purple), $L = 80$ (dashed, tan), and $L = 120$ (dot-dashed, green) and $b = 0.125$ fm. The right panel is evaluated at the same parameters as the left except $a = -1.1$ fm. The intercepts of the two curves corresponds to the location of the energy-eigenstates in the finite volume.

solution to Eq. (7) for two systems, one with $a = +1.1$ fm and $r = 0.5$ fm (left panel) and the other with $a = -1.1$ fm and $r = 0.5$ fm (right panel). One finds that for energies giving a value of $x = \left(\frac{pL}{2\pi}\right)^2$ less than $x_0 = -0.0959006$ ($p \cot \delta < 0$) the state will likely become a bound state in the infinite-volume limit. In contrast, states with energies giving a value of $x \gtrsim x_0$ ($p \cot \delta > 0$) will likely become a continuum state in the infinite-volume limit. These statements are at best rules of thumb, and one can construct obvious exceptions. Further, one can imagine scattering parameters in $p \cot \delta$ that modify these rules.

Numerical explorations of the spectrum of compact scalar QED containing a loose bound state have been performed in multiple volumes [21]. The results of that work confirm the large-volume behavior of the spectrum expected from Eq. (7) [19] and shown in Fig. 3.

C. Finite-Lattice Spacing Artifacts and Mixed-Action Effective Field Theories

As space-time has been discretized in the process of performing the Lattice QCD calculation of any given observable, there is a systematic deviation between the calculation and the actual physical value of the quantity. One anticipates that in the limit that the lattice spacing is much smaller than any physical length scale associated with the strong interactions, the finite-lattice spacing effects can be neglected for practical purposes. For a fixed lattice volume, this requires a lattice with a large number of lattice sites, and at present time typical lattice spacing are $b \sim 0.125$ fm on the coarse MILC lattices, $b \sim 0.09$ fm on the fine

MILC lattices, and $b \sim 0.06$ fm on the super-fine MILC lattices. It is clear that the lattice spacing of the coarse MILC lattices is not that much smaller than the scale of chiral symmetry breaking, $\Lambda_\chi \sim 1$ GeV ~ 0.2 fm. Naively, such lattice spacing would clearly be problematic if the leading lattice-spacing artifacts entered at order $\mathcal{O}(b)$ which is the case for naive Wilson fermions, but most calculations today are performed with improved-fermions, such as Clover, Domain-Wall, Staggered or Overlap fermions which all have lattice spacing artifacts entering at $\mathcal{O}(b^2)$ ¹⁰. The work we will review is performed with a mixed-action. With the exception of the potentials between B-mesons, the staggered lattice discretization of the quark action is used to describe the sea-quarks, while the Domain-Wall lattice discretization is used for the valence quarks. The two discretizations have their advantages and disadvantages, and the mixed-action scheme has proved to be an effective way to perform the calculations that we are interested in.

Once the lattice calculation has been performed and the quantities of interest, such as scattering lengths, have been extracted using the finite-volume techniques described above, the finite-lattice spacing effects must be removed. Ideally, one would calculate the same quantity at multiple lattice spacings, and then extrapolate to the continuum using the appropriate finite-lattice spacing expression [27, 28, 29] computed in the low-energy EFT, such as mixed-action chiral perturbation theory (MA χ -PT)¹¹. At present, we do not have sufficient computer resources to perform calculations at multiple lattice spacings. We have just completed our work on the available coarse MILC lattices and we are currently calculating with the fine MILC lattices. However, one of the very exciting results to emerge from MA χ -PT is that when certain mesonic observables are written as an expansion in m_π/f_π (for two-flavors), and more generally M_M/f_M for three-flavors, as measured in the lattice calculation¹², lattice spacing artifacts can be eliminated at low-orders in the expansion by a field redefinition, due to the good chiral symmetry properties of the domain-wall (more generally Ginsparg-Wilson) fermions used in the valence sector. The mixed-action corrections for the $\pi^+\pi^+$ scattering length have been determined in Ref. [30]. It was demonstrated that when the extrapolation formulae for this system are expressed in terms of the lattice-physical parameters there are no lattice-spacing-dependent counterterms at $\mathcal{O}(b^2)$, $\mathcal{O}(b^4)$ or $\mathcal{O}(m_\pi^2 b^2) \sim \mathcal{O}(b^4)$. This was explained to be a general feature of the two-meson systems at this order, including the non-zero momentum states [31]. There are additional lattice-spacing corrections due to the hairpin interactions present in mixed-action theories, but for domain-wall valence propagators calculated on the asqtad improved MILC gauge configurations, these contributions are completely calculable without additional counterterms at NLO. They depend only upon the valence meson and staggered taste-identity meson mass splitting [30, 31] which has been computed [32]. This allows for a precise determination

¹⁰ There are chiral symmetry breaking corrections entering at $\mathcal{O}(b)$, but they are exponentially suppressed, a measure of which is the value of the residual mass.

¹¹ MA χ -PT is the low energy effective field theory describing the dynamics of the pseudo-Goldstone bosons in the situation where the sea-quarks are governed by one lattice action, while the valence quarks are governed by a different one, in our case domain-wall valence quarks and staggered sea quarks. This is a partially-quenched theory that allows for the lattice spacing to be systematically included as a small expansion parameter, starting at $\mathcal{O}(b^2)$.

¹² We denote quantities that are computed directly from the correlation functions, such as m_π , as lattice-physical quantities. These are not extrapolated to the continuum, to infinite-volume or to the physical point.

of the mixed-action corrections to the scattering lengths at the various pion masses. In two-flavor MA χ -PT (i.e. including finite lattice-spacing corrections) the chiral expansion of the scattering length at NLO is [31]

$$m_\pi a_{\pi\pi}^{I=2} = -\frac{m_\pi^2}{8\pi f_\pi^2} \left\{ 1 + \frac{m_\pi^2}{16\pi^2 f_\pi^2} \left[3 \log \left(\frac{m_\pi^2}{\mu^2} \right) - 1 - l_{\pi\pi}^{I=2}(\mu) - \frac{\tilde{\Delta}_{ju}^4}{6m_\pi^4} \right] \right\}, \quad (17)$$

where it is understood that m_π and f_π are the lattice-physical parameters [31] and

$$\tilde{\Delta}_{ju}^2 \equiv \tilde{m}_{jj}^2 - m_{uu}^2 = 2B_0(m_j - m_u) + b^2\Delta_I + \dots, \quad (18)$$

contains the leading lattice-spacing artifacts. u denotes a valence quark and j denotes a sea-quark, and isospin-symmetry is assumed in both the sea and valence sectors. \tilde{m}_{jj} (m_{uu}) is the mass of a meson composed of two sea (valence) quarks of mass m_j (m_u) and the dots denote higher-order corrections to the meson masses. Clearly Eq. (17), which contains all $\mathcal{O}(m_\pi^2 b^2)$ and $\mathcal{O}(b^4)$ lattice artifacts, reduces to the continuum expression for the scattering length [33] in the QCD limit where $\tilde{\Delta}_{ju}^2 \rightarrow 0$ ¹³. The three-flavor MA χ -PT expression for K^+K^+ and $K^+\pi^+$ scattering are somewhat more complicated, for obvious reasons and we refer the reader to Ref. [34].

The fact that baryons do not have the same special status with respect to chiral symmetry as the pseudo-Goldstone bosons means that the field redefinitions that parametrically suppress finite-lattice spacing contributions to $\pi^+\pi^+$ scattering, do not exist for baryons. Therefore one expects to see finite lattice spacing contributions to the scattering lengths for nucleon-nucleon, and hyperon-nucleon scattering at $\mathcal{O}(b^2)$ (and residual mass-type contributions). In order to achieve high precision calculations of baryon-baryon scattering, calculations on lattices with a small lattice spacing will be required.

D. Potentials From Lattice Calculations

One remarkable feature of nuclear physics is that one can understand and compute to reasonable accuracy the properties and interactions of nuclei working with an energy-independent two-nucleon potential alone. Phenomenologically, one finds that the three-nucleon interaction is required to improve agreement with experiment, as is the inclusion of meson exchange currents into electroweak matrix elements. But the fact remains that the two-nucleon potential is the dominant interaction in nuclei.

There is a burning desire to construct a nucleon-nucleon potential¹⁴ directly from QCD, and hence from Lattice QCD. One can extract an energy-dependent and source/sink-dependent potential, defined at one energy (the energy of the two nucleons determined in the finite volume), however, this contains no more information than the phase-shift at the energy determined with Lüscher's method. One such potential was calculated in quenched QCD in Ref [35] but, for the reasons mentioned above, it cannot be used as an input in nuclear calculations and it cannot be meaningfully compared to traditional nucleon-nucleon potentials.

¹³ The counterterm $l_{\pi\pi}^{I=2}(\mu)$ is the same counterterm that appears in continuum χ -PT.

¹⁴ In this context, the word *potential* means an energy-independent potential.

A nucleon-nucleon potential may be defined from Lattice QCD calculations in the same way that potentials are determined from experimental measurements of the elastic scattering cross-section. A large number of calculations are performed, producing values for the phase-shift, along with an uncertainty, over a wide range of low-energies, and a potential is defined that minimizes the χ^2/dof in a global fit to the lattice calculations. At present, there is no practical program underway to perform such an analysis due to limited computational power.

E. Statistical Errors Associated with Calculations of Observables in the Nucleon and Systems of Nucleons

Lattice QCD calculations of quantities are performed by a Monte-Carlo evaluation of the path integral. As such, an important aspect of any such calculation is its statistical error and it is useful to consider a discussion presented by Lepage [36]. Consider an observable that is extracted from the correlation function $\langle\theta(t)\rangle$, such as a correlation function resulting from a pion source at time $t = 0$ and a pion sink at time t . In any calculation there are a finite number of configurations on which to perform measurements and a finite number of lattice sites on each lattice. For N statistically independent measurements of $\theta(t)$, the noise to signal ratio of this correlator behaves as $1/\sqrt{N}$ in the limit of large N . However, the time-dependence of this ratio depends upon the specific correlation function that is being calculated.

Consider the case where $\langle\theta(t)\rangle$ is the correlation function associated with n pions, each with a source of the form $\pi^+(\mathbf{x}, t) = \bar{u}(\mathbf{x}, t)\gamma_5 d(\mathbf{x}, t)$, or one that is smeared over neighboring lattice sites,

$$\langle\theta(t)\rangle = \left\langle \left(\sum_x \pi^-(\mathbf{x}, t) \right)^n \left(\pi^+(\mathbf{0}, 0) \right)^n \right\rangle \rightarrow A_0 e^{-nm_\pi t} , \quad (19)$$

where the interactions between the pions have been neglected in the large time behavior. The variance of this correlator is estimated to be

$$\begin{aligned} N\sigma^2 &\sim \langle\theta(t)^\dagger\theta(t)\rangle - \langle\theta(t)\rangle^2 \\ &= \left\langle \left(\sum_x \pi^-(\mathbf{x}, t) \right)^n \left(\sum_y \pi^+(\mathbf{y}, t) \right)^n \left(\pi^+(\mathbf{0}, 0) \right)^n \left(\pi^-(\mathbf{0}, 0) \right)^n \right\rangle - \langle\theta(t)\rangle^2 \\ &\rightarrow (A_2 - A_0^2) e^{-2nm_\pi t} , \end{aligned} \quad (20)$$

where the large time behavior of the variance is dictated by the lightest intermediate state that can be formed from the propagators emerging from the sources associated with $\theta(t)^\dagger\theta(t)$ and coupling to the sinks (annihilation diagrams are not included). It then follows that the ratio of noise to signal behaves as

$$\frac{\sigma}{\bar{x}} = \frac{\sigma(t)}{\langle\theta(t)\rangle} \sim \frac{\sqrt{(A_2 - A_0^2)} e^{-nm_\pi t}}{\sqrt{N} A_0 e^{-nm_\pi t}} \sim \frac{1}{\sqrt{N}} , \quad (21)$$

which is independent of time. (Here σ/\bar{x} denotes the ratio of standard deviation to mean.) That is to say that for the single pion correlator and correlators involving arbitrary numbers

of pions the errors are time-independent, and importantly do not exponentially grow with time.

The situation is, unfortunately, not so pleasant for systems involving any number of baryons. For the case of a single proton, the correlation function has the form

$$\langle \theta^{ii}(t) \rangle = \sum_{\mathbf{x}} \langle p^i(\mathbf{x}, t) \bar{p}^i(\mathbf{0}, 0) \rangle \rightarrow A_{p0}^{ii} e^{-m_p t} , \quad (22)$$

where an interpolating field that has non-vanishing overlap with the proton is $p^i \sim u^{a,T} C \gamma_5 d^b u^{i,c} \epsilon_{abc}$, where a, b, c are color indices and i is a spin-index. The variance of this correlation function is

$$\begin{aligned} N\sigma^2 &\sim \langle \theta^{ii\dagger}(t) \theta^{ii}(t) \rangle - \langle \theta^{ii}(t) \rangle^2 = \sum_x \langle p^i(\mathbf{x}, t) \bar{p}^i(\mathbf{x}, t) p^i(\mathbf{0}, 0) \bar{p}^i(\mathbf{0}, 0) \rangle - \langle \theta^{ii}(t) \rangle^2 \\ &\rightarrow A_{p2} e^{-3m_\pi t} - A_{p0}^2 e^{-2m_p t} \rightarrow A_{p2} e^{-3m_\pi t} , \end{aligned} \quad (23)$$

and therefore the noise to signal ratio behaves as

$$\frac{\sigma}{\bar{x}} = \frac{\sigma(t)}{\langle \theta(t) \rangle} \sim \frac{1}{\sqrt{N}} e^{(m_p - \frac{3}{2}m_\pi)t} . \quad (24)$$

More generally, for a system of A nucleons, the noise to signal ratio behaves as

$$\frac{\sigma}{\bar{x}} \sim \frac{1}{\sqrt{N}} e^{A(m_p - \frac{3}{2}m_\pi)t} . \quad (25)$$

Therefore, in addition to the signal itself falling as $G \sim e^{-Am_p t}$, the noise associated with the correlator grows exponentially as in Eq. (25).

III. OUR CURRENT TECHNIQUES AND RESOURCES

The Lattice formulation of QCD is the perfect tool for evaluating the correlation functions required to extract physical observables, such as hadron masses and phase shifts. It both provides an ultraviolet regulator of the continuum field theory and converts functional integrals into regular integrals of very high dimension. In the continuum, the QCD path integral is

$$\mathcal{Z} = \int \mathcal{D}A_\mu \mathcal{D}\bar{\psi} \mathcal{D}\psi e^{\int d^4x \left(-\frac{1}{4} F_{\mu\nu}^a F^{a\mu\nu} - \bar{\psi} [D_\mu \gamma_\mu + m] \psi + \mathcal{L}_{G.F.} \right)} \quad (26)$$

where A_μ is the gauge field representing the gluons, $F_{\mu\nu}^a$ is the gauge field strength and $\bar{\psi}, \psi$ are the fermion fields representing the quarks. D_μ is the covariant derivative which ensures gauge invariance and γ_μ are matrices satisfying the Clifford algebra. The physical quantities in this theory can be calculated from correlation functions of operators \mathcal{O} that are functions of the quantum fields (quarks and gluons).

$$\langle \mathcal{O} \rangle = \frac{1}{\mathcal{Z}} \int \mathcal{D}A_\mu \mathcal{D}\bar{\psi} \mathcal{D}\psi \mathcal{O} e^{\int d^4x \left(-\frac{1}{4} F_{\mu\nu}^a F^{a\mu\nu} - \bar{\psi} [D_\mu \gamma_\mu + m] \psi + \mathcal{L}_{G.F.} \right)} \quad (27)$$

We can now discretize the continuum path integral introducing a discrete space time. In order to preserve gauge invariance the gauge fields are discretized as special unitary matrices,

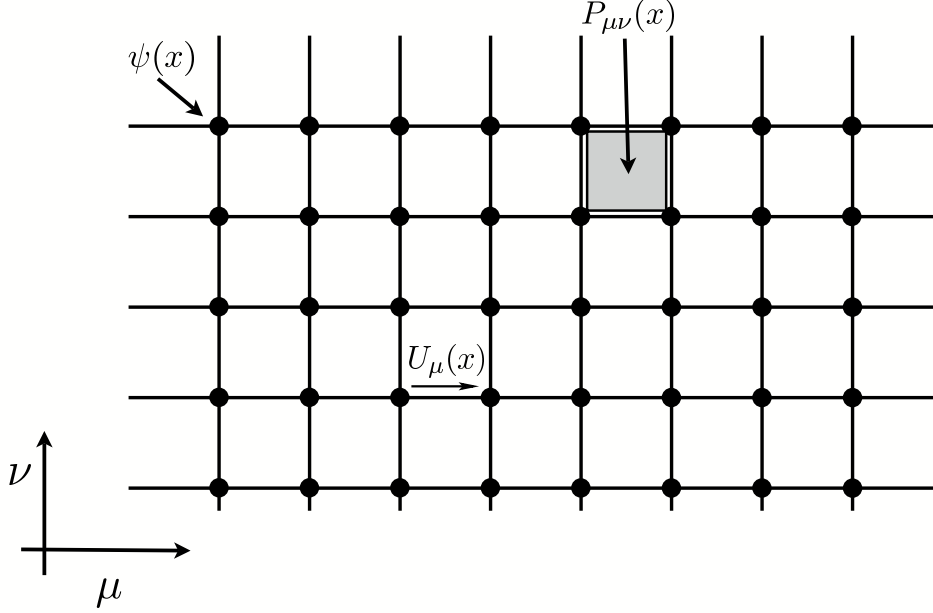


FIG. 4: A two dimensional slice of the four dimensional lattice.

$SU(3)$, living on the links of the lattice (see Figure 4). The discrete gauge action is given by the sum over all plaquettes $P_{\mu\nu}(x)$ which are the product of the links U going around the elementary plaquettes of the lattice.

$$S_g(U) = \beta \sum_{x\mu\nu} \left(1 - \frac{1}{3} \text{ReTr} P_{\mu\nu}(x) \right) \quad (28)$$

with

$$P_{\mu\nu} = U_\mu(x) U_\nu(x + \hat{\mu}) U_\mu^\dagger(x + \hat{\nu}) U_\nu^\dagger(x), \quad (29)$$

and β is the lattice gauge coupling. Taking the lattice spacing to zero, the above action becomes the continuum gauge action $-\int d^4x \frac{1}{4} (F_{\mu\nu}^a(x))^2$. This is the well known Wilson gauge [37] action. This discretization is not unique but it is the simplest. One can modify this discrete action by adding larger loops with coefficients appropriately chosen in order to achieve better convergence to the continuum limit, which is the ultimate goal of the calculation.

The fermions, which live on the vertices of the lattice, present a more challenging problem. Naive discretization results in the so called fermion doubling problem, i.e. lattice fermions

come naturally in sixteen copies, too many for describing real QCD which has three light quarks (up, down and strange) and three heavy quarks (top, bottom and charm). The doublers can be avoided by several ingenious formulations of lattice fermions. Wilson fermions, which were introduced first [37], eliminate the doublers by adding irrelevant dimension five operators in the action that lift the masses of the doublers, leaving only the light fermion in the spectrum. The price to pay is breaking of chiral symmetry and the introduction of lattice artifacts that scale as $O(b)$. Kogut-Susskind fermions [38] provide another way to remove some of the doublers and re-interpret the remaining four as four degenerate flavors. In this approach a $U(1)$ chiral symmetry still remains unbroken and lattice artifacts scale as $O(b^2)$. Kogut-Susskind fermions become problematic when the required number of flavors is not a multiple of four (as is the case for QCD). In addition, the broken flavor and chiral symmetries introduce large lattice artifacts, although they scale as $O(b^2)$. Finally, the so called domain wall fermions [39, 40, 41] and overlap fermions [42, 43] are fermionic actions that both preserve chiral symmetry at finite lattice spacing and are doubler free. Unfortunately, such formulations are computationally significantly more expensive. In all cases the lattice fermion action is of the form

$$S_f = \bar{\psi} D(U) \psi \quad (30)$$

where ψ is the fermion "vector" and $D(U)$ is a sparse matrix¹⁵ acting on this vector, that depends on the gauge field U .

The partition function in the case of two quark flavors is

$$\begin{aligned} \mathcal{Z} &= \int \prod_{\mu, x} dU_{\mu}(x) \prod_x d\bar{\psi} d\psi e^{-S_g(U) - S_f(\bar{\psi}, \psi, U)} \\ &= \int \prod_{\mu, x} dU_{\mu}(x) \det(D(U)^{\dagger} D(U)) e^{-S_g(U)}. \end{aligned} \quad (31)$$

The integration over the quark fields, which are represented by Grassman numbers, can be done exactly. In addition, the quark matrix $D(U)$ represents one flavor, however since $\det D(U)^{\dagger} = \det D(U)$, the determinant $\det(D(U)^{\dagger} D(U))$ represents two flavors. In the case of correlation functions, integrating out the quarks gives the following expression

$$\langle \mathcal{O} \rangle = \frac{1}{\mathcal{Z}} \int \prod_{\mu, x} dU_{\mu}(x) \mathcal{O}\left(\frac{1}{D(U)}, U\right) \det(D(U)^{\dagger} D(U)) e^{-S_g(U)}, \quad (32)$$

resulting in operators \mathcal{O} that depend on the inverse of the quark matrix. The above manipulation is only valid in the case of two flavors of quarks (the up and the down) which both have the same mass, which is a good approximation to the low energy physics of QCD. A strange quark can be easily added by including $\det(D(U)^{\dagger} D(U))^{1/2}$ in the partition function.

The computation of Eq. (32) is the main numerical task faced in Lattice QCD calculations. The integral in Eq. (32) over the gauge fields is of extremely large dimensionality. Considering that we have discretized QCD, which has a fundamental scale of ~ 1 fm (10^{-13} cm), we need to work with a lattice that has a physical size much larger than 1 fm in order to control

¹⁵ In certain cases such as the overlap fermions the matrix is not sparse but has sparse like properties i.e. the matrix vector multiplication is a "cheap" operation.

finite volume effects, and a lattice spacing much smaller than 1 fm in order to control the continuum limit. With moderate choices for the volume and the lattice spacing, a typical lattice size of 32^4 is arrived at. Counting the color, flavor and spin degrees of freedom, the calculation involves $\approx 10^8$ degrees of freedom. The only way this computation can be done is by using Monte Carlo integration. Fortunately, the combination of the quark determinant and the gauge action,

$$\mathcal{P}(U) = \frac{1}{\mathcal{Z}} \det(D(U)^\dagger D(U)) e^{-S_g(U)}, \quad (33)$$

is a positive definite quantity which can be interpreted as a probability and hence importance sampling can be employed. The basic algorithm is to produce N gauge field configurations $\{U\}$ with probability distribution $\mathcal{P}(U)$ and then evaluate

$$\langle \mathcal{O} \rangle = \lim_{N \rightarrow \infty} \frac{1}{N} \sum_{i=1}^N \mathcal{O}(U_i, \frac{1}{D(U_i)}). \quad (34)$$

At finite N , the estimate of \mathcal{O} is approximate, with an error that converges to zero as $\mathcal{O}(1/\sqrt{N})$. Both for the gauge field configuration generation and the evaluation of Eq. (34), the linear system of equations

$$D^\dagger(U)[m]D(U)[m]\chi = \phi, \quad (35)$$

needs to be solved where the dependence of the quark matrix on the quark mass m is made explicit. Since the quark matrix is sparse, iterative solvers such as conjugate gradient can be used. The condition number of the quark matrix is inversely proportional to the quark mass. Since the physical quark masses for the up and down quarks are quite small, the quark matrix has a large condition number. With current computer resources this linear system cannot be solved exactly at the physical quark mass. For that reason the calculation is performed at heavier quark masses and then extrapolated to the physical point. The vast majority of the computer time used in these calculations is devoted to the solution of this linear system both in the context of gauge field generation and in the later stage of the calculation of physical observables through Eq. (34).

Realistic lattice calculations require quark masses that result in pion masses below 400 MeV, allowing chiral effective field theories to be used with some reliability. In addition, a dynamical strange quark is required in order to guarantee that the low energy constants of the EFT match those of the physical theory. Although this task seems formidable, in the last several years there have been developments that make phenomenologically interesting calculations now possible.

A. Domain Wall and Staggered Fermions

The emergence of fermions that respect chiral symmetry [39, 40, 41, 42, 43] on the lattice was one of the major recent developments in Lattice QCD. These formulations of lattice fermions allow us to reduce the lattice spacing errors and approach the continuum limit in a smoother manner. However, the cost of calculating with these fermions is an order of magnitude larger than any other variant of lattice fermions. In addition, the development of improved Kogut-Susskind fermion actions [44, 45] that significantly reduce the $O(b^2)$ errors, allowed for cheap inclusion of quark loop effects in the QCD correlation functions computed

on the lattice. With this formulation, volumes with spatial extent as large as $L \sim 3.5$ fm are possible with light-quark masses as low as 1/10th of the strange quark mass depending on available computing resources. However the fact that Kogut-Susskind fermions represent four flavors of quarks complicates calculations when two or one flavors are needed. From the operational point of view the problem is solved by introducing into the path integral the Kogut-Susskind determinant raised to the $n_f/4$ power (rooted), where n_f is the desired number of flavors. The non-integer power of the quark determinant introduces non-localities in the lattice action. It has been argued, however, that the long distance physics that survives the continuum limit is not affected by such non-localities [46, 47, 48, 49, 50, 51]. In addition, at finite lattice spacing, the pathologies arising in the Kogut-Susskind fermion formulation can be dealt with in staggered χ -PT [47, 48, 52, 53, 54, 55, 56]. Although no rigorous proof exists, empirical evidence indicates that Kogut-Susskind fermions do describe the correct physics as long as the continuum limit is taken before the chiral limit [51]. It should be noted that there are some members of the lattice community who believe that the rooted-staggered action is fundamentally flawed and its continuum limit does not correspond to QCD (for a summary of these arguments, see Ref. [57]). We disagree with these arguments, however we acknowledge that there is no proof that the continuum limit of the rooted-Kogut-Susskind action corresponds to QCD. All of the work that we present in this review based upon mixed-action calculations on the MILC lattice ensembles assumes that the continuum limit is, in fact, QCD.

In our calculations we use Kogut-Susskind fermions to represent the QCD vacuum polarization effects associated with the two light flavors (up/down quarks) and the somewhat heavier strange quark. This is done by using gauge configurations generated with the appropriate Kogut-Susskind fermion determinants incorporated into the probability distribution that enters the path integral. Since this part of the computation is completely disconnected from the calculation of correlation functions, we can use gauge fields generated by other collaborations. In our case we use the gauge configurations generated by the MILC collaboration [58].

For all external quarks we use domain wall fermions. Because of the chiral symmetry that domain wall fermions satisfy, all our correlation functions satisfy chiral Ward identities, ensuring that the leading order chiral behavior is continuum-like. The small corrections appearing due to Kogut-Susskind fermions in the vacuum loops can be taken care of systematically in χ -PT [30, 31, 34]. Compared to calculations with Kogut-Susskind fermions in the valence sector, this formulation results in better control of the chiral behavior and possibly smaller discretization errors. This approach was first introduced by the LHP collaboration for the study of nucleon structure [59, 60, 61, 62, 63].

B. The Lattice Actions

The gauge configurations used in our work were generated by the MILC collaboration using the one loop tadpole improved gauge action [64] where both $\mathcal{O}(b^2)$ and $\mathcal{O}(g^2 b^2)$ errors are removed. This action is defined as

$$S_G[U] = -\frac{\beta}{3} \left(c_0 \sum_{x;\mu<\nu} P[U]_{x,\mu\nu} + c_1 \sum_{x;\mu\neq\nu} R[U]_{x,\mu\nu} + c_2 \sum_{x;\mu<\nu<\sigma} C[U]_{x,\mu\nu\sigma} \right) \quad (36)$$

where $R[U]_{x,\mu\nu}$ and $C[U]_{x,\mu\nu\sigma}$ denote the real part of the trace of the ordered product of SU(3) gauge links along 1×2 rectangles in the μ, ν plane and the $\mu, \nu, \sigma, -\mu, -\nu, -\sigma$ paths,

respectively. The coefficients c_0 , c_1 , and c_2 are determined in one loop tadpole improved perturbation theory [64], and $\beta = 10/g_0^2$ where g_0 is the bare gauge coupling. For the fermions in the vacuum the Asqtad improved Kogut-Susskind action [44, 45, 65, 66, 67, 68] is used. This action is the Naik action [69] ($O(b^2)$ improved Kogut-Susskind action), with smeared links for the one link terms so that couplings to gluons with any of their momentum components equal to π/b are set to zero. The form of the action is the following:

$$\begin{aligned}
S_{Asqtad} = & \frac{1}{2} \left[\sum_{x,y} \sum_{\mu=1,4} \bar{\chi}(x) \eta_\mu(x) (V_\mu(x) \delta_{y,x+\hat{\mu}} - V_\mu^\dagger(x - \hat{\mu}) \delta_{y,x+\hat{\mu}}) \chi(y) - \right. \\
& - \sum_{x,y} \sum_{\mu=1,4} \bar{\chi}(x) \frac{1}{24u_0^2} \eta_\mu(x) (W_\mu(x) \delta_{y,x+\hat{\mu}} - W_\mu^\dagger(x - \hat{\mu}) \delta_{y,x+\hat{\mu}}) \chi(y) \left. \right] + \\
& + \sum_x m \bar{\chi}(x) \chi(x)
\end{aligned} \tag{37}$$

where the V_μ and W_μ links are

$$\begin{aligned}
V_\mu(x) = & \frac{5}{8} U_\mu(x) + \sum_{\nu \neq \mu} \frac{1}{16u_0^2} S_{\mu\nu}(x) + \\
& + \sum_{\nu \neq \mu} \sum_{\rho \neq \mu, \rho \neq \nu} \frac{1}{64u_0^4} S_{\mu\nu\rho}(x) + \\
& + \sum_{\nu \neq \mu} \sum_{\rho \neq \mu, \rho \neq \nu} \sum_{\sigma \neq \mu, \sigma \neq \nu, \sigma \neq \rho} \frac{1}{384u_0^6} S_{\mu\nu\rho\sigma}(x) \\
& - \sum_{\nu \neq \mu} \frac{1}{16u_0^4} L_{\mu\nu}(x)
\end{aligned} \tag{38}$$

$$\begin{aligned}
W_\mu(x) = & U_\mu(x) U_\mu(x + \hat{\mu}) U_\mu(x + 2\hat{\mu}) \\
& \tag{39}
\end{aligned}$$

and

$$S_{\mu\nu}(x) = U_\nu(x) U_\mu(x + \hat{\nu}) U_\nu^\dagger(x + \hat{\mu}) + U_\nu^\dagger(x - \hat{\nu}) U_\mu(x - \hat{\nu}) U_\nu(x - \hat{\nu} + \hat{\mu}) \tag{41}$$

$$\begin{aligned}
L_{\mu\nu}(x) = & U_\nu(x) U_\nu(x + \hat{\nu}) U_\mu(x + 2\hat{\nu}) U_\nu^\dagger(x + \hat{\nu} + \hat{\mu}) U_\nu^\dagger(x + \hat{\mu}) + \\
& + U_\nu^\dagger(x - \hat{\nu}) U_\nu^\dagger(x - 2\hat{\nu}) U_\mu(x - 2\hat{\nu}) U_\nu(x - 2\hat{\nu} + \hat{\mu}) U_\nu(x - \hat{\nu} + \hat{\mu})
\end{aligned} \tag{42}$$

$$\begin{aligned}
S_{\mu\nu\rho}(x) = & U_\nu(x) S_{\mu\rho}(x + \hat{\nu}) U_\nu^\dagger(x + \hat{\mu}) + \\
& + U_\nu^\dagger(x - \hat{\nu}) S_{\mu\rho}(x - \hat{\nu}) U_\nu(x - \hat{\nu} + \hat{\mu})
\end{aligned} \tag{43}$$

$$\begin{aligned}
S_{\mu\nu\rho\sigma}(x) = & U_\nu(x) S_{\mu\rho\sigma}(x + \hat{\nu}) U_\nu^\dagger(x + \hat{\mu}) + \\
& + U_\nu^\dagger(x - \hat{\nu}) S_{\mu\rho\sigma}(x - \hat{\nu}) U_\nu(x - \hat{\nu} + \hat{\mu}) .
\end{aligned} \tag{44}$$

In all of the above u_0 is the tadpole coefficient which was determined self consistently by MILC, $\eta_\mu(x) = (-1)^{\sum_{\rho < \mu} x_\rho}$ and x the four integers describing the lattice coordinates.

For the valence sector we use the five dimensional Shamir domain wall fermion action [40,

41]

$$\begin{aligned}
S_{DW} = & - \sum_{x,x'} \sum_{s=0}^{L_s-1} [\bar{\Psi}(x,s) [D_w(x,x') + 1] \Psi(x',s)] - \\
& - \left[\bar{\Psi}(x,s) \frac{1-\gamma_5}{2} \Psi(x',s+1) + \bar{\Psi}(x,s) \frac{1+\gamma_5}{2} \Psi(x',s-1) \right] + \\
& + m \left[\bar{\Psi}(x,0) \frac{1+\gamma_5}{2} \Psi(x',L_s-1) + \bar{\Psi}(x,L_s-1) \frac{1-\gamma_5}{2} \Psi(x',0) \right], \quad (45)
\end{aligned}$$

with $D_w(x,x')$ the regular four dimensional Wilson fermion action,

$$D_w(x,x') = (4 + M_5) \delta_{x,x'} - \sum_{\mu} \left[\frac{1-\gamma_{\mu}}{2} U_{\mu}(x) \delta_{x+\hat{\mu},x'} + \frac{1+\gamma_{\mu}}{2} U_{\mu}^{\dagger}(x') \delta_{x,x'+\hat{\mu}} \right], \quad (46)$$

and L_s is the extent of the 5th dimension. Hypercubic-smeared (HYP-smeared) [70, 71, 72, 73] gauge links were used in Eq. (45) and (46) to improve chiral symmetry. The physical four dimensional quark fields appear as boundary modes at the surface of the five dimensional space when M_5 lies in the interval $(-2,0)$. The physical quark fields ($\bar{q}(x)$ and $q(x)$) are related to the underlying 5D fermions by

$$\begin{aligned}
q(x) &= \frac{1-\gamma_5}{2} \Psi(x,0) + \frac{1+\gamma_5}{2} \Psi(x,L_s-1) \\
\bar{q}(x) &= \bar{\Psi}(x,L_s-1) \frac{1-\gamma_5}{2} + \bar{\Psi}(x,0) \frac{1+\gamma_5}{2}. \quad (47)
\end{aligned}$$

The parameter m in Eq. (45) is related to the physical quark mass as it introduces in the effective action a $m\bar{q}q$ term. Domain wall fermions in the infinite L_s limit poses an exact chiral symmetry when m vanishes. This symmetry transformation is

$$\Psi(x,s) \rightarrow e^{i\Gamma_5(s)\theta(x)} \Psi(x,s) \quad (48)$$

$$\bar{\Psi}(x,s) \rightarrow \bar{\Psi}(x,s) e^{-i\Gamma_5(s)\theta(x)} \quad (49)$$

where $\Gamma_5(s) = \text{sign}(\frac{L_s-1}{2} - s)$.

However, at finite L_s this chiral symmetry is explicitly broken by the coupling of left handed and right handed modes in the middle of the 5th dimension. As a result one can construct the following partially conserved axial vector current

$$\mathcal{A}_{\mu}(x) = - \sum_{s=0}^{L_s-1} \Gamma_5(s) j_{\mu}(x,s) \quad (50)$$

where j_{μ} is the four dimensional conserved vector current that corresponds to the 4D Wilson fermion action. This current satisfies a Ward-Takahashi identity which in the flavor non-singlet case takes the form [41]:

$$\begin{aligned}
\Delta_{\mu} \langle \mathcal{A}_{\mu}^a(x) O(y) \rangle &= 2m \langle \bar{q}(x) \tau^a \gamma_5 q(x) O(y) \rangle + \\
&+ 2 \langle \bar{q}_{mp}(x) \tau^a \gamma_5 q_{mp}(x) O(y) \rangle + i \langle \delta^a O(y) \rangle \quad (51)
\end{aligned}$$

where

$$\begin{aligned} q_{mp}(x) &= \frac{1 - \gamma_5}{2} \Psi(x, \frac{L_s}{2}) + \frac{1 + \gamma_5}{2} \Psi(x, \frac{L_s}{2} - 1) \\ \bar{q}_{mp}(x) &= \bar{\Psi}(x, \frac{L_s}{2} - 1) \frac{1 - \gamma_5}{2} + \bar{\Psi}(x, \frac{L_s}{2}) \frac{1 + \gamma_5}{2} \end{aligned} \quad (52)$$

are four dimensional fields constructed at the midpoint of the the 5th dimension. The Ward-Takahashi identity of Eq. (51) is the same as the continuum counterpart with just an additional term $2\langle \bar{q}_{mp}(x) \tau^a \gamma_5 q_{mp}(x) O(y) \rangle$. This term is there only at finite L_s ¹⁶ and it is a measure of the explicit chiral symmetry breaking. At long distances this term is proportional to $2\langle \bar{q}(x) \tau^a \gamma_5 q(x) O(y) \rangle$. Using the pseudo-scalar density as a probe operator $O(y)$ the residual mass is defined as

$$m_{res} = \frac{1}{t_{max} - t_0} \sum_{t_0}^{t_{max}} \frac{\langle \bar{q}_{mp}(t) \tau^a \gamma_5 q_{mp}(t) \bar{q}(0) \tau^a \gamma_5 q(0) \rangle}{\langle \bar{q}(t) \tau^a \gamma_5 q(t) \bar{q}(0) \tau^a \gamma_5 q(0) \rangle}, \quad (53)$$

where t_0, t_{max} is the time interval where only the ground state pion contributes to the two correlators in the ratio.

C. Mixed Action Tuning

Because the valence and sea quark actions are different, the calculation is inherently partially quenched. In other words, the calculation violates unitarity. Unlike conventional partially quenched calculations, which become unitary when the valence quark mass is tuned to the sea quark mass, unitarity cannot be restored by tuning the valence quark mass. The next best option is to tune the valence quark mass in such a way that the resulting pions have the same mass as those made of the sea Kogut-Susskind fermions. In this case unitarity should be restored in the continuum limit, where the $n_f = 2$ staggered action has an $SU(8)_L \otimes SU(8)_R \otimes U(1)_V$ chiral symmetry due to the four-fold taste degeneracy of each flavor, and each pion has 15 degenerate additional partners. At finite lattice spacing this symmetry is broken and the taste multiplets are no longer degenerate, but have splittings that are $\mathcal{O}(\alpha^2 b^2)$ [44, 45, 55, 65, 68]. The domain wall fermion mass is tuned to give valence pions that match the Goldstone Kogut-Susskind pion¹⁷. This choice gives pions that are as light as possible, resulting in better convergence of the χ -PT needed to extrapolate the lattice results to the physical quark mass point. This tuning was also done by LHPC collaboration [59, 60, 61, 62, 74, 75].

D. Method of Contractions

Throughout our work, gauge invariant Gaussian smeared quark propagators centered around a single point were used. In order to facilitate the complicated Wick contractions of many

¹⁶ For the flavor singlet current this term survives the infinite L_s limit and gives rise to the anomaly.

¹⁷ This is the only Goldstone boson that becomes massless in the chiral limit at finite lattice spacing.

body interpolating fields, the following strategy was adopted. Noticing that the permutations needed for Wick contractions are in effect "scalar"¹⁸, all the contractions at the annihilation operator point (sink) were performed and all the color and spin indices were left open at the creation operator point (source). The resulting data are Fourier transformed (space indices at the annihilation operator point) and saved on disk. All the two-body (and N-body) correlation functions can then be constructed by appropriate contractions of the source spin and color indices on scalar machines (such as simple work stations).

Code was constructed to automatically perform all permutations, keeping track of the signs associated with fermion exchanges, allowing the construction of complicated diagrams in a relatively simple and efficient manner. This approach works well when quark annihilation diagrams are absent. For this reason such processes (such as the $I=0$ $\pi\pi$ channel), have not been explored in our work to date. Another reason for avoiding such processes is that the mixed action approach has large artifacts in these channels. In the future we plan to address such processes using the so called all-to-all propagator approach [76].

E. Data Analysis

Since Monte-Carlo integration is used to compute the relevant correlation functions, the statistical uncertainty must be carefully determined. The main observables extracted in all calculations presented in this review are energy levels and energy level differences. These results contain information about phase shifts, scattering lengths and the three body interaction as discussed above. The extraction of energy levels is done by fitting the relevant correlation functions to a sum of exponentials (or appropriately hyperbolic cosine functions when anti-periodic boundary conditions in time are imposed). We performed correlated χ^2 minimization fits that take into account the time correlations in the lattice data. In particular, the relevant parameters, such as the masses and the amplitude each state contributes to the correlation function, are determined as those that minimize

$$\chi^2(A) = \sum_{ij} [\bar{G}(t_i) - F(t_i, A)] C_{ij}^{-1} [\bar{G}(t_j) - F(t_j, A)] \quad (54)$$

where $\bar{G}(t)$ are the lattice two point correlation functions, $F(t, A)$ are the fitting functions used, with A denoting the set of fitting parameters over which $\chi^2(A)$ is minimized, and C_{ij} is the covariance matrix. The lattice two point correlation functions are determined as averages over N Monte-Carlo samples $G_k(t)$:

$$\bar{G}(t) = \frac{1}{N} \sum_{k=1}^N G_k(t) \quad (55)$$

and

$$C_{ij} = \frac{1}{N(N-1)} \sum_{k=1}^N [G_k(t_i) - \bar{G}(t_i)] [G_k(t_j) - \bar{G}(t_j)] . \quad (56)$$

The (standard) errors on the fitted parameters are determined by the boundaries of the error ellipsoid, which is defined by the locus of points where $\chi^2 = \chi_{min}^2 + 1$. (For a pedagogical presentation of fitting see the TASI lectures by D. Toussaint [77].)

¹⁸ In parallel computing language "scalar" refers to operations that are not data parallel.

In computing scattering lengths, the procedure for determining the statistical errors is a little more involved due to the highly non-linear relation between the scattering length and the energy levels of the two particle system. First one is interested in the energy differences between the energy levels of the two particle system and the sum of the masses of the two free particles (similarly for the case of more than two particles). These energy differences can be determined in two ways. The simplest is the one described in the previous sections where ratios of correlators are constructed in such way so that these ratios are a sum over exponentials parametrized by the desired energy splittings (see for example Eq. (6)). In this case Jackknife is used to determine the covariance matrix and then a correlated χ^2 -fit is performed as described above. For a single elimination Jackknife, the covariance matrix of a ratio of correlators is

$$C_{ij} = \frac{N-1}{N} \sum_{k=1}^N [R_k(t_i) - \bar{R}(t_i)] [R_k(t_j) - \bar{R}(t_j)] \quad (57)$$

where R_k is the desired ratio computed with the k th sample omitted from the full ensemble and \bar{R} is the ratio computed on the full ensemble.

Fitting correlation functions to extract the ground state energy requires fitting ranges that start at time separations from the source that are large enough so that excited states have negligible contributions. The determination of the minimum time separation that can be included in the fit is sometimes subjective. Hence a systematic error due to the choice of the minimum time separation in the fit is included. This error is determined by observing the variation of the extracted results as a function of the choice of fitting interval. The final errors include both systematic and statistical errors combined in quadrature.

One way to reduce the systematic errors due to coupling to excited states is to use appropriate interpolating fields that reduce these couplings. This can be achieved by using smeared quark sources and sinks. We have used gauge invariant Gaussian smeared sources for the quark propagators which were implemented as

$$\chi(\vec{x}) = \left(1 + \frac{\omega}{4N} \nabla^2\right)^N \delta(\vec{x}_0) \quad (58)$$

where $\delta(\vec{x})$ is a 3D delta function, ∇^2 is the covariant 3D Laplacian, and ω is a parameter controlling the width of the smearing. In the limit of $N \rightarrow \infty$ this becomes an exponential of the Laplace operator. While the value of ω was chosen to optimize the coupling to the nucleon, it also worked very well for the mesons. In addition, we used both point and smeared sinks, both of which produced comparable results.

All of our lattice calculations are performed away from the physical pion mass. For that reason we have to rely on χ -PT to extrapolate to the physical point. Since results from ensembles with different sea quark masses are un-correlated (i.e. the covariance matrix is diagonal), we performed un-correlated χ^2 fits of our data to the χ -PT formulas. In all cases we estimate a systematic error due to these fits and extrapolation. Finally, except for $\pi^+\pi^+$ and K^+K^+ scattering lengths where the leading order lattice spacing effects are calculable, lattice spacing errors are estimated by dimensional analysis.

In order to avoid systematic errors due to scale setting, dimensionless quantities (appropriate products or ratios of dimensional quantities) are used wherever possible. In the few cases we need to quote results in MeV we use the scale determined by the MILC collaboration and confirmed by our own determination using the pion decay constant [78].

An essential parameter for all of our calculations using domain wall fermions in the valence sector is the residual mass m_{res} that measures the degree of explicit chiral breaking. The results of the residual mass calculation are presented in Table I.

TABLE I: The parameters of the MILC gauge configurations and domain-wall propagators used in this work. The subscript l denotes light quark (up and down), and s denotes the strange quark. The superscript dwf denotes the bare-quark mass for the domain-wall fermion propagator calculation.

Ensemble	bm_l	bm_s	bm_l^{dwf}	bm_s^{dwf}	$10^3 \times bm_{res}$
2064f21b676m007m050	0.007	0.050	0.0081	0.081	1.604
2064f21b676m010m050	0.010	0.050	0.0138	0.081	1.552
2064f21b679m020m050	0.020	0.050	0.0313	0.081	1.239
2064f21b681m030m050	0.030	0.050	0.0478	0.081	0.982
2896f2b709m0062m031	0.0062	0.031	0.0080	0.0423	0.380

F. Resources

The computational resources needed for the calculations presented here were obtained from several sources including the USQCD clusters at JLab and FNAL (pentium clusters with infiniband interconnect), Tungsten at NCSA (pentium infiniband cluster) and Mare-Nostrum in Barcelona, Spain (Power PC 970MP IBM with Myrinet interconnect)¹⁹. The total computer power that went into our results reviewed here is about 1.2Tflop-years, an amount of time that is rather small by current standards. This amount of time was sufficient to achieve precision results in the meson sector.

The results presented here are snapshots of an ongoing effort. Not all of them were obtained with the same statistics on a given ensemble. For details on exactly what went into these calculations the reader should refer to the original publications. We typically computed several propagators per configuration by shifting the location of the source, and have cases with as many as 24 propagators per configuration. We carefully monitored the variance reduction as more propagators were added, and concluded that correlation functions were almost statistically independent. The residual correlations were taken care of by averaging correlation functions on a given configuration (blocking) and proceeding with the statistical analysis of data discussed in Section III E. Further blockings over multiple configurations did not change the results.

IV. TWO-BODY PHYSICS

A. $\pi\pi$ Scattering

1. Introduction

Pion-pion scattering at low energies is the simplest and best-understood hadron-hadron scattering process. Its simplicity and tractability follow from the fact that the pions are

¹⁹ We thank Andrew Pochinsky and Balint Joo for essential help in optimizing our code for this machine.

identified as the pseudo-Goldstone bosons associated with the spontaneous breaking of the approximate chiral symmetry of QCD. For this reason, the low-momentum interactions of pions are strongly constrained by the approximate chiral symmetries, more so than other hadrons. The scattering lengths for $\pi\pi$ scattering in the s-wave are uniquely predicted at LO in χ -PT [79]:

$$m_\pi a_{\pi\pi}^{I=0} = 0.1588 \quad ; \quad m_\pi a_{\pi\pi}^{I=2} = -0.04537 \quad , \quad (59)$$

at the charged pion mass. Subleading orders in the chiral expansion of the $\pi\pi$ amplitude give rise to perturbatively-small deviations from the tree level, and contain both calculable non-analytic contributions and analytic terms with new coefficients that are not determined by chiral symmetry alone [33, 80, 81]. In order to have predictive power at subleading orders, these coefficients must be obtained from experiment or computed with Lattice QCD.

Recent experimental efforts have been made to compute the s-wave $\pi\pi$ scattering lengths, $a_{\pi\pi}^{I=0}$ and $a_{\pi\pi}^{I=2}$: E865 [82, 83] (K_{e4} decays), CERN DIRAC [84] (pionium lifetime) and CERN NA48/2 [85] ($K^\pm \rightarrow \pi^\pm \pi^0 \pi^0$). Unfortunately, these experiments do not provide stringent constraints on $a_{\pi\pi}^{I=2}$. However, a theoretical determination of s-wave $\pi\pi$ scattering lengths which makes use of experimental data has reached a remarkable level of precision [86, 87]:

$$m_\pi a_{\pi\pi}^{I=0} = 0.220 \pm 0.005 \quad ; \quad m_\pi a_{\pi\pi}^{I=2} = -0.0444 \pm 0.0010 \quad . \quad (60)$$

These values result from the Roy equations [88, 89, 90], which use dispersion theory to relate scattering data at high energies to the scattering amplitude near threshold. In a striking recent result, this technology has allowed a model-independent determination of the mass and width of the resonance with vacuum quantum numbers (the σ meson) that appears in the $\pi\pi$ scattering amplitude [91]. Several low-energy constants of one-loop χ -PT are critical inputs to the Roy equation analysis. One can take the values of these low-energy constants computed with Lattice QCD by the MILC collaboration [32, 92] as inputs to the Roy equations, and obtain results for the scattering lengths consistent with the analysis of Ref. [86].

The first lattice calculations of $\pi\pi$ scattering were performed in quenched QCD [93, 94, 95, 96, 97, 98, 99, 100, 101, 102, 103, 104, 105, 106, 107, 108, 109, 110, 111, 112, 113], and the first partially-quenched QCD calculation of $\pi\pi$ scattering (the scattering length and phase-shift) was carried through by the CP-PACS collaboration, who exploited the finite-volume strategy to study $I = 2$, s-wave scattering with two flavors ($n_f = 2$) of improved Wilson fermions [114], with pion masses in the range $m_\pi \simeq 0.5 - 1.1$ GeV. The first fully-dynamical calculation of the $I = 2$ $\pi\pi$ scattering length with three flavors ($n_f = 2 + 1$) of light quarks was performed by NPLQCD using domain-wall valence quarks on asqtad-improved staggered sea quarks at four pion masses in the range $m_\pi \simeq 0.3 - 0.5$ GeV at a single lattice spacing, $b \sim 0.125$ fm [78].

2. Data Analysis and Chiral and Continuum Extrapolation

It is convenient to present the results of the lattice calculation in “effective scattering length” plots, simple variants of the effective-mass plots discussed above. The effective energy splitting is formed from the ratio of correlation functions given in Eq. (5),

$$\Delta E_{\pi^+\pi^+}(t) = \log \left(\frac{G_{\pi^+\pi^+}(0, t)}{G_{\pi^+\pi^+}(0, t+1)} \right) \quad , \quad (61)$$

which in the limit of an infinite number of gauge configurations would become a constant at large times that is equal to the lowest energy of the interacting $\pi^+\pi^+$ system in the volume relative to the non-interacting two-pion energy. At each time-slice, $\Delta E_{\pi^+\pi^+}(t)$ is inserted into Eq. (7) (or Eq. (9)), to give a scattering length at each time slice, $a_{\pi^+\pi^+}(t)$. It is customary to consider the dimensionless quantity given by the pion mass times the scattering length, $m_\pi a_{\pi^+\pi^+}$, where $m_\pi(t)$ is the pion effective mass, in order to remove scale-setting uncertainties. For each of the MILC ensembles that were analyzed, the effective scattering lengths are shown in Fig. 5, and the values of the pion masses, decay constants and $\pi\pi$ energy-shifts can be found in Refs. [78, 115]. The mixed-action corrections for the

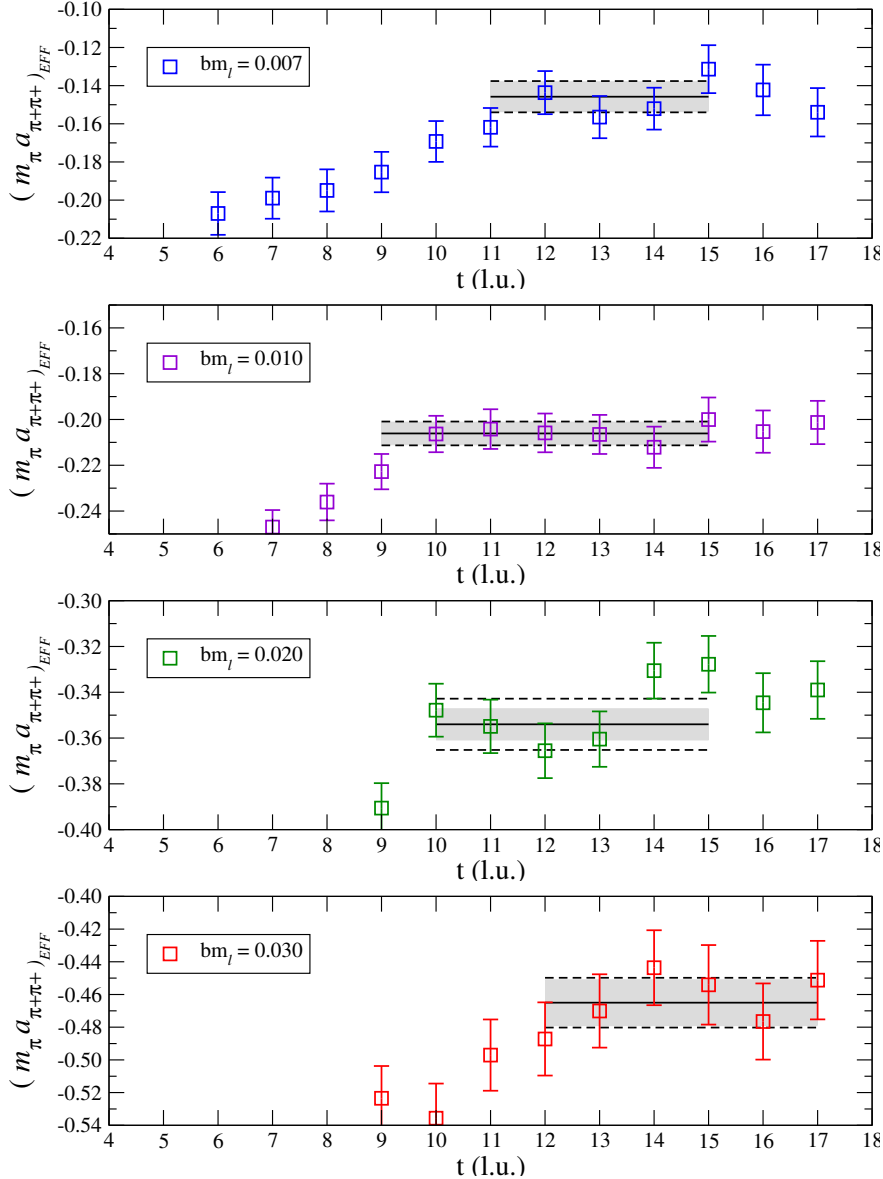


FIG. 5: The effective $\pi^+\pi^+$ scattering length times the effective π mass as a function of time-slice arising from smeared sinks. The solid black lines and shaded regions are fits with 1- σ statistical uncertainties; the dashed lines are estimates of the systematic uncertainty due to fitting.

$I = 2 \pi\pi$ scattering length have been determined in Ref. [30] and have been discussed above.

With domain-wall fermion masses tuned to match the staggered Goldstone pion [74, 75], one finds (in lattice units) $\tilde{\Delta}_{ju}^2 = b^2 \Delta_I = 0.0769(22)$ [32] on the coarse MILC lattices with $b \sim 0.125$ fm. For each ensemble, $m_\pi a_{\pi\pi}^{I=2}$ was determined and the chiral extrapolation formula in Eq. (17) was used to extract a value of the counterterm $l_{\pi\pi}^{I=2}(\mu = f_\pi)$. The results of the two-flavor extrapolation to the continuum are given in Ref. [115].

Fitting to lattice data at the lightest accessible values of the quark masses will optimize the convergence of the chiral expansion. While there are only four different quark masses in the data set, with pion and kaon masses of approximately $(m_\pi, m_K) \sim (290, 580), (350, 595), (490, 640)$ and $(590, 675)$ MeV, fitting all four data sets and then “pruning” the heaviest data set and refitting provides a useful measure of the convergence of the chiral expansion. Hence, in “fit A”, we fit the $l_{\pi\pi}^{I=2}(f_\pi)$ ’s extracted from all four lattice ensembles ($m_\pi \sim 290, 350, 490$, and 590 MeV) to a constant, while in “fit B”, we fit the $l_{\pi\pi}^{I=2}(f_\pi)$ ’s from the lightest three lattice ensembles ($m_\pi \sim 290, 350$, and 490 MeV). In “fit C”, we fit the $l_{\pi\pi}^{I=2}(f_\pi)$ ’s from the lightest two lattice ensembles ($m_\pi \sim 290$ and 350 MeV). Results are given in Table II. Taking the range of parameters spanned by fits A-C one finds:

TABLE II: Results of the fits in two-flavor Mixed-Action χ -PT. The values of $m_\pi a_{\pi\pi}^{I=2}$ correspond to the extrapolated values at the physical point. The first uncertainty is statistical and the second is a comprehensive systematic uncertainty.

FIT	$l_{\pi\pi}^{I=2}(\mu = f_\pi)$	$m_\pi a_{\pi\pi}^{I=2}$ (extrapolated)	χ^2/dof
A	$6.43 \pm 0.23 \pm 0.26$	$-0.043068 \pm 0.000076 \pm 0.000085$	1.17
B	$5.97 \pm 0.29 \pm 0.42$	$-0.043218 \pm 0.00009 \pm 0.00014$	0.965
C	$4.89 \pm 0.64 \pm 0.68$	$-0.04357 \pm 0.00021 \pm 0.00022$	0.054

$$\begin{aligned}
l_{\pi\pi}^{I=2}(\mu = f_\pi) &= 5.4 \pm 1.4 \\
m_\pi a_{\pi\pi}^{I=2} &= -0.04341 \pm 0.00046 .
\end{aligned} \tag{62}$$

In Fig. 6 we show the results of our calculation, along with the lowest mass $n_f = 2$ point from CP-PACS (not included in the fit). The tree-level prediction and the results of the two-flavor fit described in this section are also shown. The experimental point shown in Fig. 6 is not included in the fit and extrapolation. It is interesting that the lattice calculations indicate little deviation from the tree level χ -PT curve. The significant deviation of the extrapolated scattering length from the tree-level result is largely a consequence of fitting to MA χ -PT at one-loop level.

An important check of the systematic uncertainties involved in the chiral extrapolation is to perform the same analysis using three-flavor MA χ -PT [30, 31] as both the real world and our lattice calculation have three active light flavors. In addition to the computations needed for the two-flavor analysis, it is necessary to determine masses and decay constants for the kaon and the η . The Gell-Mann–Okubo mass-relation among the mesons is used to determine the η mass, which is not computed in this lattice calculation due to the enormous computer resources (beyond what is available) required to compute the disconnected contributions. This procedure is consistent to this order in the chiral expansion.

The chiral expansion of the $\pi^+\pi^+$ scattering length in three-flavor mixed-action χ -PT as well as the numerical values for the various ensembles are given in Ref. [115]. For the three-flavor analysis, the pruning analysis gives the results shown in Table III. Taking the

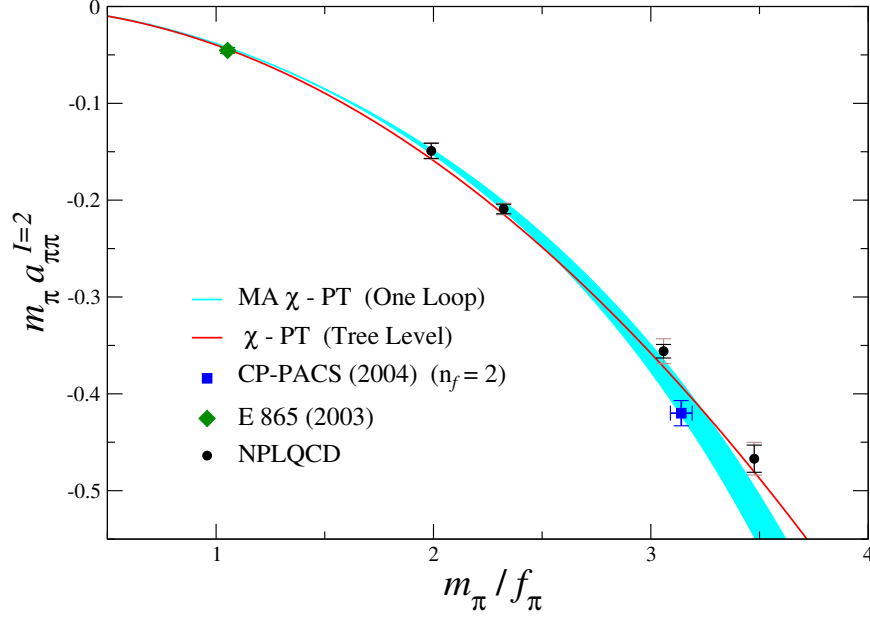


FIG. 6: $m_\pi a_{\pi\pi}^{I=2}$ vs. m_π/f_π (ovals) with statistical (dark bars) and systematic (light bars) uncertainties. Also shown are the experimental value from Ref. [83] (diamond) and the lowest quark mass result of the $n_f = 2$ dynamical calculation of CP-PACS [114] (square). The blue band corresponds to a weighted fit to the lightest three data points (fit B) using the one-loop MA χ -PT formula in Eq. (17) (the shaded region corresponds only to the statistical uncertainty). The red line is the tree-level χ -PT result. The experimental data is not used in the chiral extrapolation fits.

TABLE III: Results of the NLO fits in three-flavor Mixed-Action χ -PT. The values of $m_\pi a_{\pi\pi}^{I=2}$ correspond to the extrapolated values at the physical point. The first uncertainty is statistical and the second is a comprehensive systematic uncertainty.

	FIT $32(4\pi)L_{\pi\pi}^{I=2}(\mu = f_\pi)$	$m_\pi a_{\pi\pi}^{I=2}$ (extrapolated)	χ^2/dof
D	$7.09 \pm 0.23 \pm 0.23$	$-0.042992 \pm 0.000076 \pm 0.000077$	0.969
E	$6.69 \pm 0.29 \pm 0.39$	$-0.04312 \pm 0.00009 \pm 0.00013$	0.803
F	$5.75 \pm 0.63 \pm 0.64$	$-0.04343 \pm 0.00021 \pm 0.00021$	0.073

range of parameters spanned by fits D-F one finds:

$$\begin{aligned}
32(4\pi)L_{\pi\pi}^{I=2}(\mu = f_\pi) &= 6.2 \pm 1.2 \\
m_\pi a_{\pi\pi}^{I=2} &= -0.04330 \pm 0.00042 \quad .
\end{aligned} \tag{63}$$

3. Systematic Uncertainties

There are many sources of systematic uncertainty to be quantified; there are lattice-spacing artifacts that arise at $\mathcal{O}(m_\pi^4 b^2)$; there are exponentially-suppressed finite-volume effects; there are effects due to residual chiral symmetry breaking; there are generic two-loop effects

due to the truncation of the chiral expansion at one loop; and finally, there are range corrections that enter at $\mathcal{O}(L^{-6})$ in Eq. (9). All of these effects have been taken into account [115]. It is noteworthy that the residual mass turns out to be one of the leading systematic errors in our analysis of $\pi^+\pi^+$ scattering.

It is worth emphasizing that the calculations have exact isospin symmetry, as do the extrapolation formulas used to analyze the results. The conventional discussion of the scattering length is in the unphysical theory with $e = 0$ and $m_u = m_d = m$, with $m_\pi = m_{\pi^+} = 139.57018 \pm 0.00035$ MeV and $f_\pi = f_{\pi^+} = 130.7 \pm 0.14 \pm 0.37$ MeV. Hence $m_{\pi^+}/f_{\pi^+} = 1.0679 \pm 0.0032$, where the statistical and systematic uncertainties have been combined in quadrature. The results of the lattice calculations are extrapolated to this value. The leading contribution to isospin breaking in $\pi\pi$ scattering is due to the electromagnetic interaction, and this has been studied extensively²⁰. Such contributions must be removed from the experimentally-determined scattering amplitude in order to make a comparison with the strong-interaction calculations. Isospin breaking due to the difference in mass of the light quarks occurs at next-to-leading order in the chiral expansion, and is expected to be small, as is its contribution to $m_{\pi^+}^2 - m_{\pi^0}^2$.

4. Discussion

The prediction for the physical value of the $I = 2$ $\pi\pi$ scattering length is $m_\pi a_{\pi\pi}^{I=2} = -0.04330 \pm 0.00042$, which agrees within uncertainties with the (non-lattice) determination of CGL [86]. In Table IV and Fig. 7 we offer a comparison between various determinations²¹.

TABLE IV: A compilation of the various calculations and predictions for the $I = 2$ $\pi\pi$ scattering length.

	$m_\pi a_{\pi\pi}^{I=2}$
χ -PT (Tree Level)	-0.04438
NPLQCD (2007)	-0.04330 ± 0.00042
E 865 (2003)	-0.0454 ± 0.0031
NPLQCD (2005)	-0.0426 ± 0.0018
MILC (2006)*	-0.0432 ± 0.0006
MILC (2004)*	-0.0433 ± 0.0009
CGL (2001)	-0.0444 ± 0.0010

²⁰ For discussions of the contributions of virtual photons to $\pi\pi$ scattering see Ref. [116, 117, 118, 119], and for very recent work on the electromagnetic contributions to the extraction of $\pi\pi$ scattering lengths from kaon decays see Ref. [120] and Ref. [121]

²¹ The stars on the MILC results indicate that these are not lattice calculations of the $I = 2$ $\pi\pi$ scattering length but rather a hybrid prediction which uses MILC's determination of various low-energy constants together with the Roy equations), and the Roy equation determination of Ref. [86] (CGL (2001).

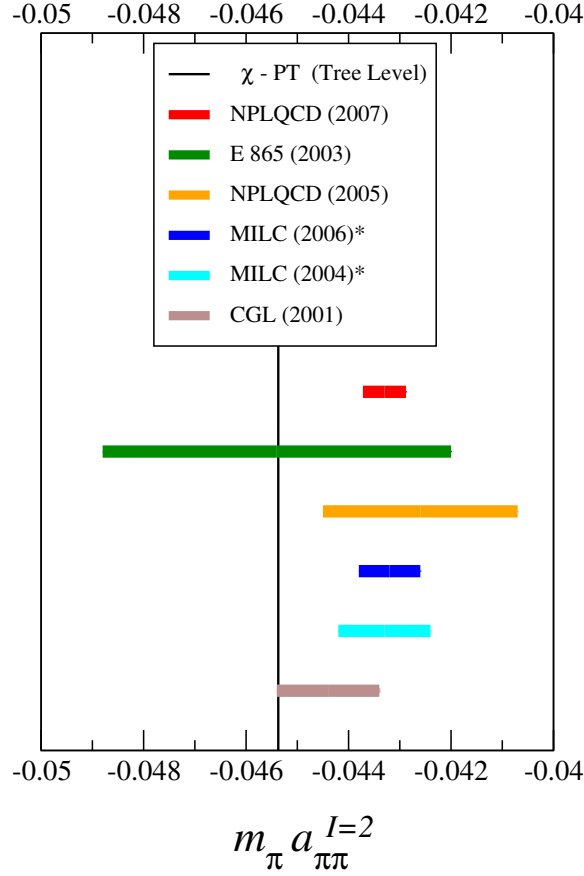


FIG. 7: Bar chart of the various determinations of the $I = 2$ $\pi\pi$ scattering length tabulated in Table IV. See footnote 21.

B. $K\pi$ Scattering

1. Introduction

In hadronic atoms, nature has provided a relatively clean environment in which to explore the low-energy interactions of charged hadrons. The electromagnetic interaction allows for oppositely-charged, long-lived hadrons to form Coulomb bound states. The locations of the energy-levels of these systems are perturbed by the strong interactions, while the lifetimes of the ground states are dictated by the strong interactions that couple the charged hadrons to lighter neutral ones.

Study of the low-energy interactions between kaons and pions with $\pi^- K^+$ bound-states allows for an explicit exploration of the three-flavor structure of low-energy hadronic interactions, an aspect that is not directly probed in $\pi\pi$ scattering. Experiments have been proposed by the DIRAC collaboration [122] to study πK atoms at CERN, J-PARC and GSI, the results of which would provide direct measurements or constraints on combinations of the scattering lengths. In the isospin limit, there are two isospin channels available to the πK system, $I = \frac{1}{2}$ and $I = \frac{3}{2}$. The width of a $\pi^- K^+$ atom depends upon the difference be-

tween scattering lengths in the two channels, $\Gamma \sim (a_{1/2} - a_{3/2})^2$, (where $a_{1/2}$ and $a_{3/2}$ are the $I = \frac{1}{2}$ and $I = \frac{3}{2}$ scattering lengths, respectively) while the shift of the ground-state depends upon a different combination, $\Delta E_0 \sim 2a_{1/2} + a_{3/2}$. Recently, the Roy-Steiner equations (analyticity, unitarity and crossing-symmetry) have been used to extrapolate high-energy πK data down to threshold [123], where it is found that

$$m_\pi (a_{1/2} - a_{3/2}) = 0.269 \pm 0.015 \quad , \quad m_\pi (a_{1/2} + 2a_{3/2}) = 0.134 \pm 0.037 \quad , \quad (64)$$

which can be decomposed to $m_\pi a_{1/2} = 0.224 \pm 0.022$ and $m_\pi a_{3/2} = -0.0448 \pm 0.0077$. (See also Refs. [124, 125] and Ref. [126] for a similar approach.) In addition, three-flavor χ -PT has been used to predict these scattering lengths out to next-to-next-to-leading order (NNLO) in the chiral expansion. At NLO [127, 128, 129],

$$m_\pi (a_{1/2} - a_{3/2}) = 0.238 \pm 0.002 \quad , \quad m_\pi (a_{1/2} + 2a_{3/2}) = 0.097 \pm 0.047 \quad , \quad (65)$$

while at NNLO [130] $m_\pi a_{1/2} = 0.220$ and $m_\pi a_{3/2} = -0.047$ ²². One must be cautious in assessing the uncertainties in these theoretical calculations, as one can only make estimates based on power-counting for the contribution of higher-order terms in the chiral expansion. There has been one determination of the $\pi^+ K^+$ scattering length in quenched QCD [131], however, the chiral extrapolation of the scattering length did not include the non-analytic dependences on the light quark masses that are predicted by χ -PT.

As discussed above, recent work has identified in a model-independent way the lowest-lying resonance in QCD which appears in $\pi\pi$ scattering [91]. Crucial to this development has been the accurate determination of the low-energy $\pi\pi$ scattering amplitude, including the recent Lattice QCD determination of the $I = 2$ scattering length [78]. A similar analysis has very recently been carried out for πK scattering in the $I = \frac{1}{2}$ s-wave in order to determine the lowest-lying strange resonance [132]. Improved accuracy in the low-energy πK scattering amplitude should be welcome to this endeavor.

2. Analysis and Chiral Extrapolation

It is useful to consider the dimensionless quantity of the reduced mass times the scattering length, $\mu_{\pi K} a_{\pi^+ K^+}$, where $\mu_{\pi K}(t)$, the “effective reduced mass” is constructed from the effective mass of the single particle correlators. For each of the MILC ensembles, the effective scattering lengths are shown in Fig. 8, while the results of the lattice calculation of the decay constants, meson masses, $\pi^+ K^+$ energy shifts and scattering lengths are given in Ref. [133]. The scattering lengths as a function of reduced mass are shown in Fig. 9.

In SU(3) χ -PT [33, 134, 135] at NLO, the expansion of the crossing even (a^+) and crossing odd (a^-) scattering length times the reduced mass is known [127, 128, 129] and reproduced in Ref. [133]. The counterterm $L_{\pi K}(\lambda)$ is a renormalization scale, λ , dependent linear combination of the Gasser-Leutwyler counterterms

$$L_{\pi K} \equiv 2L_1 + 2L_2 + L_3 - 2L_4 - \frac{L_5}{2} + 2L_6 + L_8 \quad . \quad (66)$$

²² At tree-level, Weinberg [79] determined that $m_\pi a_{1/2} = 0.137$ and $m_\pi a_{3/2} = -0.0687$.

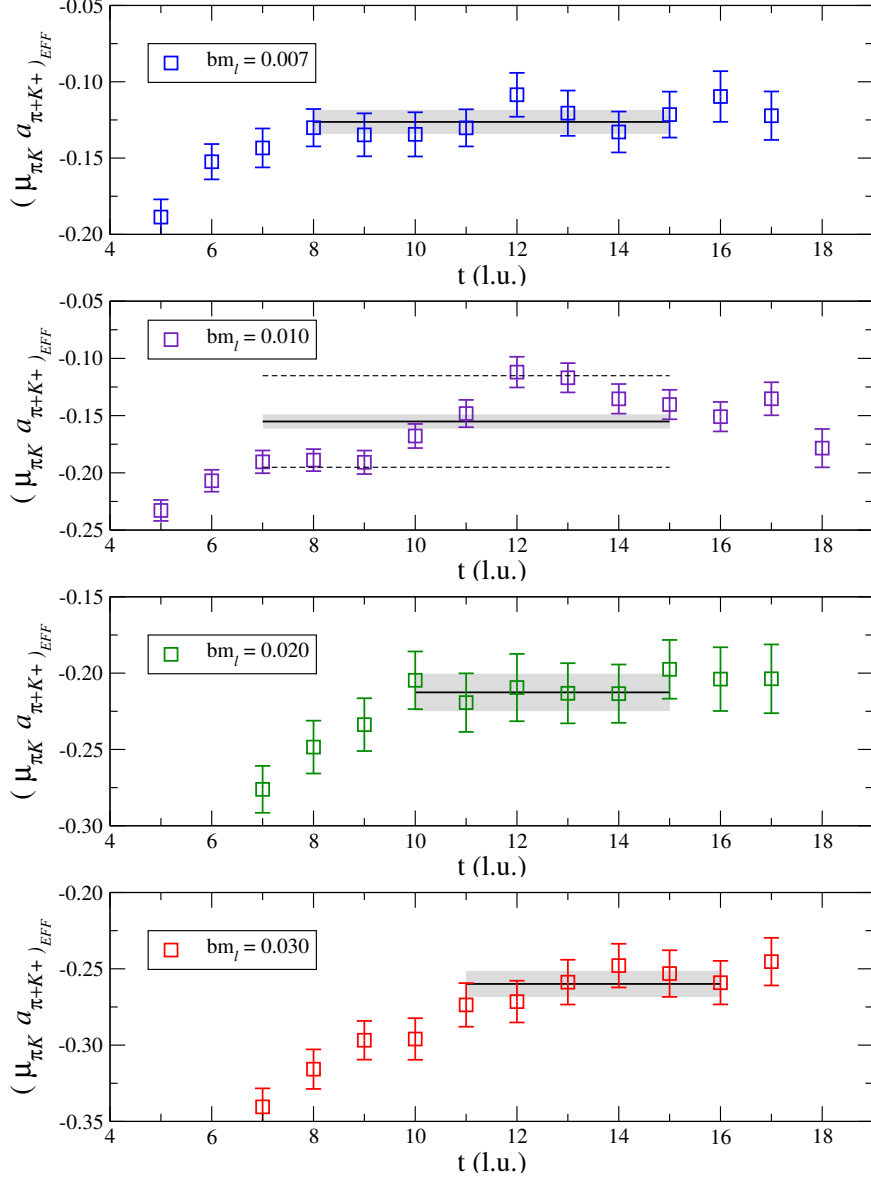


FIG. 8: The effective π^+K^+ scattering length times the reduced mass, $\mu_{\pi K} a_{\pi+K+}(t)$ as a function of time slice arising from smeared sinks. The solid black lines and shaded regions are fits with $1\text{-}\sigma$ errors. The dashed lines on the $m_\pi \sim 350$ MeV ensemble plot are an estimate of the systematic error due to fitting.

The $I = \frac{1}{2}$ and $I = \frac{3}{2}$ scattering lengths are related to crossing even and odd amplitudes by

$$\begin{aligned} a_{1/2} &= a^+ + 2a^- \\ a_{3/2} &= a^+ - a^- = a_{\pi^+K^+} \quad . \end{aligned} \quad (67)$$

It is convenient to define the function Γ via a subtraction of the tree-level and one-loop contributions in order to isolate the counterterms,

$$\Gamma \equiv -\frac{f_\pi^2}{16m_\pi^2} \left(\frac{4\pi f_\pi^2}{\mu_{\pi K}^2} [\mu_{\pi K} a_{\pi+K+}] + 1 + \chi^{(NLO,-)} - 2\frac{m_K m_\pi}{f_\pi^2} \chi^{(NLO,+)} \right) , \quad (68)$$

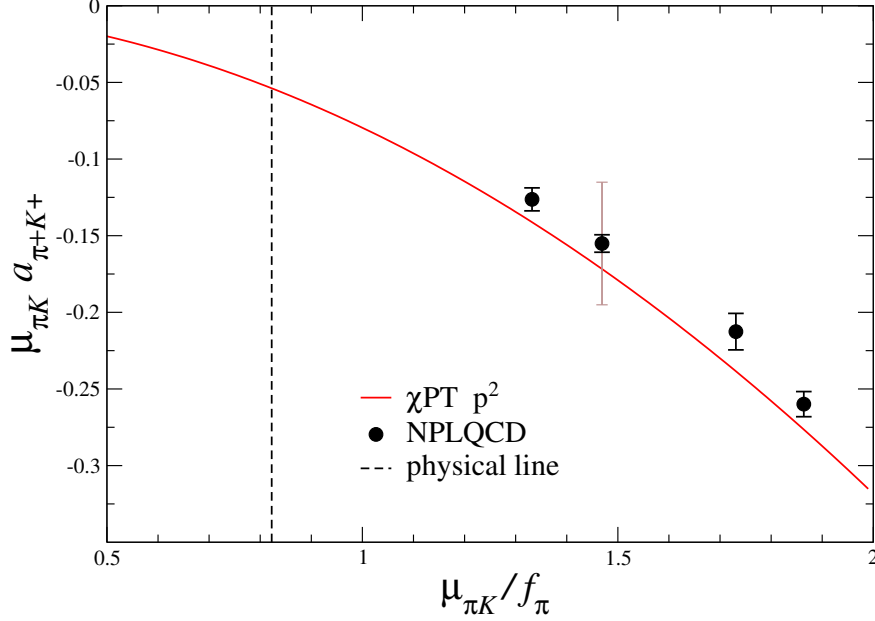


FIG. 9: $\mu_{\pi K} a_{\pi+K+}$ vs. $\mu_{\pi K}/f_\pi$. The data points are the results of this lattice calculation, while the curve is the theoretical prediction at tree level in chiral perturbation theory [79]. The dark error bar is statistical, while the lighter error bar corresponds to the systematic error. The vertical dashed line denotes the physical pion and kaon masses.

and at NLO this becomes

$$\Gamma = L_5(f_\pi^{\text{phys}}) - 2 \frac{m_K}{m_\pi} L_{\pi K}(f_\pi^{\text{phys}}). \quad (69)$$

The dependence of Γ on m_π and m_K determines L_5 and $L_{\pi K}$ and, in turn, allows an extraction of $a_{3/2}$ and $a_{1/2}$. The numerical values of Γ and their errors are plotted in Fig. 10. By fitting a straight line to the values of Γ as a function of m_k/m_π the counterterms L_5 and $L_{\pi K}$ (renormalized at f_π^{phys}) can be determined.

As described in Section IV A 2, the results of the lattice calculations are pruned, to give “fit A” and “fit B”. With this limited data set it is not practical to fit to the NNLO expres-

TABLE V: Results of the NLO fits. The values of $m_\pi a_{3/2}$ and $m_\pi a_{1/2}$ correspond to their extrapolated values at the physical point.

FIT	$L_5 \times 10^3$	$L_{\pi K} \times 10^3$	$m_\pi a_{3/2}$	$m_\pi a_{1/2}$	χ^2/dof
A	3.83 ± 0.49	3.55 ± 0.20	-0.0607 ± 0.0025	0.1631 ± 0.0062	0.17
B	2.94 ± 0.07	3.27 ± 0.02	-0.0620 ± 0.0004	0.1585 ± 0.0011	0.001
C	$5.65 \pm 0.02^{+0.18}_{-0.54}$	4.24 ± 0.17	-0.0567 ± 0.0017	0.1731 ± 0.0017	0.84
D	$5.65 \pm 0.02^{+0.18}_{-0.54}$	4.16 ± 0.18	-0.0574 ± 0.0016	0.1725 ± 0.0017	0.90

sion [130] for the scattering length. However, it is important to estimate the uncertainty in the values of the scattering lengths extrapolated to the physical point that is introduced by the truncation of the chiral expansion at NLO. In our work on f_K/f_π [136] a value of L_5 was extracted as it is the only NLO counterterm that contributes. The numerical value obtained

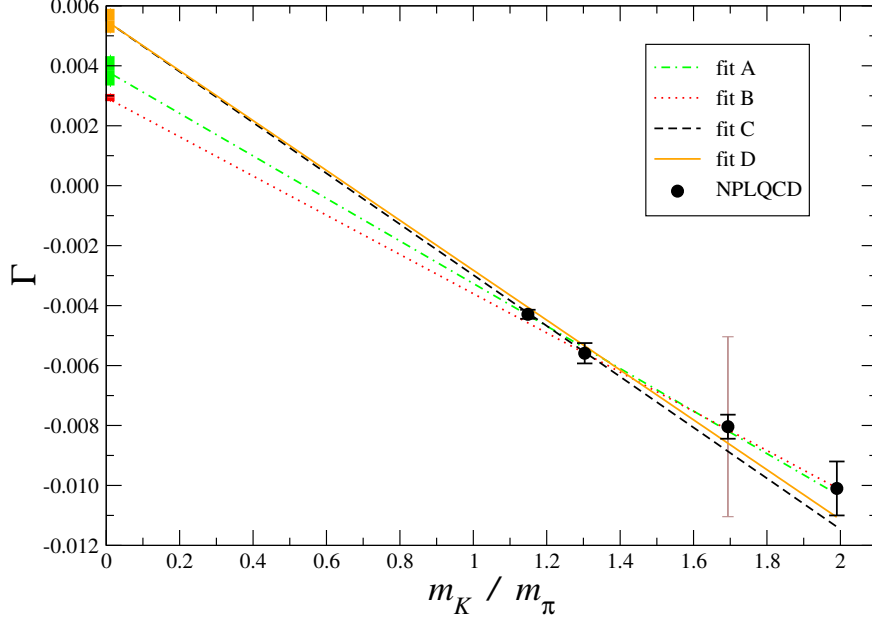


FIG. 10: Γ vs. m_K/m_π . The dark error bar on the data points is statistical, while the lighter error bar corresponds to the systematic error. The lines correspond to the four linear fits (A,B,C,D). The bars on the y axis represent the $1\text{-}\sigma$ errors in the determinations of $L_5 = \Gamma(m_K/m_\pi = 0)$ (see Ref. [133]). (At 95% confidence level, these determinations are in agreement.)

is only perturbatively close to its true value, as it is contaminated by higher-order contributions. Therefore, by fixing the L_5 that appears in Eq. (69) to the value of L_5 extracted from f_K/f_π , an estimate of the uncertainty in both $L_{\pi K}$ and in the extrapolated values of the scattering lengths due to the truncation of the chiral expansion can be made. Specifically, L_5 was sampled from a Gaussian distribution for a range of f_K/f_π values [136] and then $L_{\pi K}$ was fit. This fit is denoted “fit C”, and the same fit but with the $m_\pi \sim 590$ MeV data pruned is denoted “fit D”. The results of the four fits are given in Table V and plotted in Fig. 10. These lead to

$$L_{\pi K} = 4.16 \pm 0.18^{+0.26}_{-0.91} \quad , \quad (70)$$

and a prediction of the scattering lengths extrapolated to the physical point of

$$\begin{aligned} m_\pi a_{3/2} &= -0.0574 \pm 0.0016^{+0.0024}_{-0.0058} \\ m_\pi a_{1/2} &= 0.1725 \pm 0.0017^{+0.0023}_{-0.0156} . \end{aligned} \quad (71)$$

The central values and statistical errors were taken from fit D and the systematic error due to truncation of the chiral expansion was set by taking the range of the various quantities allowed by the four fits, including statistical and systematic errors. Fig. 11 shows the 95% confidence-level error ellipses associated with the four fits in the $m_\pi a_{1/2}$ - $m_\pi a_{3/2}$ plane. For purposes of comparison the current-algebra point [79] is included on the plot as well as $1\text{-}\sigma$ error ellipses from analyses based on fitting experimental data using χ -PT at NLO [127] and using Roy-Steiner equations [123]. As $1\text{-}\sigma$ error ellipses correspond to 39% confidence level, one should be careful in finding discrepancy between the various determinations of the scattering lengths. The crossing-odd scattering length is of special interest as its corrections

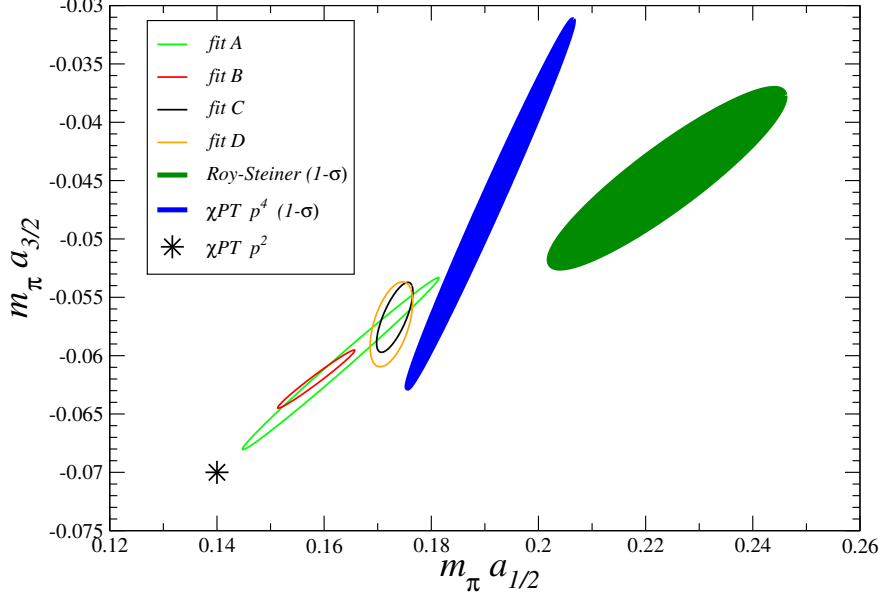


FIG. 11: Error ellipses for the four fits (A,B,C,D) at 95% confidence level. The star corresponds to the current-algebra predictions (χ -PT p^2) from Ref. [79]. The $1\text{-}\sigma$ error ellipses from a χ -PT analysis at NLO [127] (denoted χ -PT p^4) and from a fit using the Roy-Steiner equations [123] are also shown.

are protected by SU(2) chiral symmetry and are therefore of order m_π^4 and expected to be small [137, 138]²³.

Given how well the lattice data fit the NLO continuum χ -PT formulas, it would seem that the $O(b^2)$ discretization errors are comparable or smaller than the systematic error due to omitted $O(m_q^3)$ effects in the chiral expansion. However, one should keep in mind that our determinations of, for instance, the low-energy constants L_5 and $L_{\pi K}$ are subject to $O(b^2)$ shifts. In contrast with the $\pi^+\pi^+$ and K^+K^+ scattering lengths, the mixed-action quantity Δ_{Mix} makes an explicit contribution to the $K^+\pi^+$ scattering length [30, 139]. While this adds an additional unknown contribution to this process, a MA χ -PT analysis of πK scattering, including lattice data from the fine MILC lattices ($b \sim 0.09$ fm), as well as the determination of Δ_{Mix} [140], will be able to address this source of systematic error quantitatively.

We anticipate that with improved statistics, together with calculations on lattices with smaller lattice spacings, the theoretically-predicted regions for $m_\pi a_{3/2}$ and $m_\pi a_{1/2}$ can be further reduced beyond those shown in Fig. 11. These regions can then be compared with the expected measurements from $K^+\pi^-$ atoms, to provide an exciting test of hadronic theory.

We also note that (1) there are calculations underway to calculate the scattering lengths in both isospin channels directly with quenched QCD [141]; (2) an indirect method which uses scalar form factors for exclusive semileptonic decays, calculated with $n_f = 2$ lattice data, gives $m_\pi a_{1/2} = 0.179 \pm 0.017$ [142, 143].

²³ We thank Heiri Leutwyler for emphasizing this point to us.

C. KK Scattering

1. Introduction

Strange hadrons may play a crucial role in the properties and evolution of nuclear material under extreme conditions [1]. The interior of neutron stars provide one such environment in which the densities are high enough that it may be energetically favorable to have strange baryons present in significant quantities, depending upon their interactions with non-strange hadrons. Further, it may be the case that a kaon condensate forms due, in part, to strong interactions between kaons and nucleons [144]. Unfortunately, the theoretical analysis of both scenarios is somewhat plagued by the limited knowledge of the interactions of strange hadrons with themselves and with non-strange hadrons.

Heavy-ion collisions, such as those at the BNL Relativistic Heavy Ion Collider (RHIC), also produce nuclear material in an extreme condition. Recent observations suggesting the formation of a low-viscosity fluid are quite exciting as they provide a first glimpse of matter not seen previously. The late-time evolution of such a collision requires an understanding of the interaction between many species of hadrons, not just those of the initial state, including the interactions between strange mesons and baryons. While pion interferometry in heavy-ion collisions is a well-established tool for studying the collision region (for recent theoretical progress, see Refs. [145, 146, 147]), the STAR collaboration has recently published the first observation of neutral kaon (K_s^0) interferometry [148]. In the analysis of K_s^0 - K_s^0 interferometry, the non-resonant contributions to the final state interactions between the kaons were estimated using three-flavor χ -PT, the low-energy effective field theory of QCD. Given the sometimes poor convergence of $SU(3)_L \otimes SU(3)_R$ χ -PT due to the relatively large kaon mass compared to the scale of chiral symmetry breaking ($\Lambda_\chi \sim 1$ GeV), particularly in the baryon sector, it is important to be able to verify that the non-resonant contributions to KK -scattering are indeed small, as estimated in χ -PT. To date, there have been no experimental determinations of the $I = 1$ KK scattering length, $a_{KK}^{I=1}$, but recently it has been calculated at NLO in χ -PT [31].

2. Mixed-Action χ -PT at One Loop

In Ref. [31], the expression for the $I = 1$ KK scattering length was determined to NLO in χ -PT, including corrections due to mixed-action lattice artifacts. As with the $I = 2$ $\pi\pi$ scattering length [30], it was demonstrated that when the mixed-action extrapolation formula is expressed in terms of the lattice-physical parameters there are no lattice-spacing-dependent counterterms at $\mathcal{O}(b^2)$, $\mathcal{O}(b^2 m_K^2)$ or $\mathcal{O}(b^4)$. There are finite lattice-spacing-dependent corrections, proportional to $b^2 \Delta_I$, and therefore entirely determined to this order in MA χ -PT. Again, as with the $I = 2$ $\pi\pi$ system, the NLO MA formula for $m_K a_{KK}^{I=1}$ does not depend upon the mixed valence-sea meson masses, and therefore does not require knowledge of the mixed-meson masses [140]. This allows for a precise determination of the predicted MA corrections to the scattering length. At NLO in MA χ -PT, the scattering length takes the

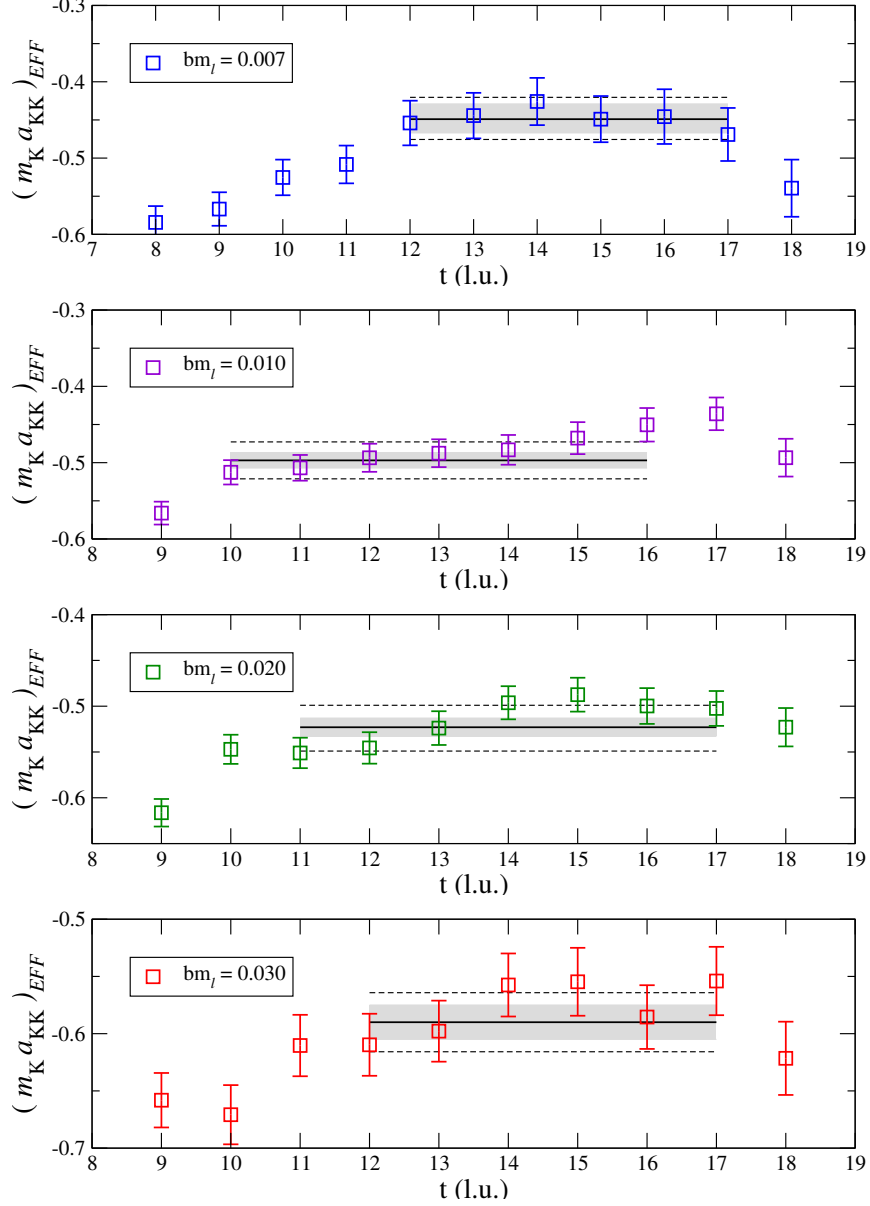


FIG. 12: The effective K^+K^+ scattering length times the effective m_{K^+} as a function of time slice. The solid black lines and shaded regions are fits with 1- σ statistical uncertainties. The dashed lines correspond to the statistical and systematic uncertainties added in quadrature. (See Ref. [149] for data tables.)

form

$$m_K a_{KK}^{I=1}(b \neq 0) = -\frac{m_K^2}{8\pi f_K^2} \left\{ 1 + \frac{m_K^2}{(4\pi f_K)^2} \left[C_\pi \ln \left(\frac{m_\pi^2}{\mu^2} \right) + C_K \ln \left(\frac{m_K^2}{\mu^2} \right) + C_X \ln \left(\frac{\tilde{m}_X^2}{\mu^2} \right) + C_{ss} \ln \left(\frac{m_{ss}^2}{\mu^2} \right) + C_0 - 32(4\pi)^2 L_{KK}^{I=1}(\mu) \right] \right\}, \quad (72)$$

where the various coefficients, C_i , along with \tilde{m}_X^2 and m_{ss}^2 , can be found in Appendix E of Ref. [31]. To account for the predicted MA corrections, one can use Eq. (72) to

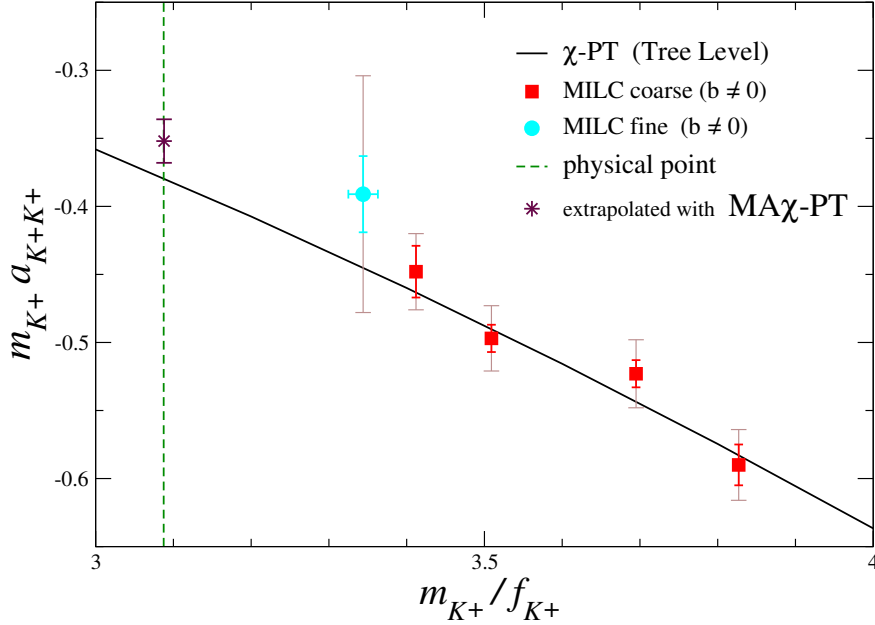


FIG. 13: $m_{K^+} a_{K^+K^+}$ versus m_{K^+}/f_{K^+} . The points with error-bars are the results of this lattice calculation (not extrapolated to the continuum) on both the coarse and fine MILC lattices. The solid curve corresponds to the tree-level prediction of χ -PT, and the point denoted by a star and its associated uncertainty is the value extrapolated to the physical meson masses and to the continuum.

directly fit the results of the lattice calculation. Further sources of systematic errors can be identified; higher-order effects in the chiral expansion, $\Delta_{NNLO}(m_K a_{KK}^{I=1})$; exponentially-suppressed finite-volume effects, $\Delta_{FV}(m_K a_{KK}^{I=1})$; residual chiral symmetry breaking effects from the domain-wall action, $\Delta_{m_{res}}(m_K a_{KK}^{I=1})$; and the error in truncating the effective-range expansion with the inverse scattering length, $\Delta_{range}(m_K a_{KK}^{I=1})$. For a detailed discussion of these various sources of uncertainty, we refer the reader to Ref. [149].

3. Extrapolation to the Physical Point

The results of the lattice calculations were pruned (defined in Section IV A 2) to explore the convergence of the chiral expansion, giving fits A, B, and C [78, 115, 133] for the low-energy constant $L_{KK}^{I=1}(\mu = f_K)$. The results of these fits are collected in Table VI. The extracted values of $L_{KK}^{I=1}$ from each of the fits are consistent with each other within the uncertainties. In analogy with the comparison convention employed for $\pi^+\pi^+$, the results of the lattice calculation are extrapolated to the physical values of $m_{\pi^+}/f_{K^+} = 0.8731 \pm 0.0096$, $m_{K^+}/f_{K^+} = 3.088 \pm 0.018$ and $m_{\eta}/f_{K^+} = 3.425 \pm 0.0019$ assuming isospin symmetry, and the absence of electromagnetism. Taking the range of values of $L_{KK}^{I=1}$ spanned by these fits, gives

$$m_{K^+} a_{K^+K^+} = -0.352 \pm 0.016 \quad , \quad 32(4\pi)^2 L_{KK}^{I=1}(\mu = f_K) = 7.1 \pm 0.7, \quad (73)$$

TABLE VI: The results of fitting three-flavor MA χ -PT at NLO to the computed scattering lengths, as described in the text. The values of $m_K + a_{K+K+}$ are those extrapolated to the physical (isospin-symmetric) meson masses and to the continuum.

FIT	$32(4\pi)^2 L_{\bar{K}K}^{I=1}(f_K)$	$m_{K+} + a_{K+K+}$ (extrapolated)	χ^2/dof
A	7.3(1)(4)	$-0.347 \pm 0.003 \pm 0.009$	0.22
B	7.3(2)(5)	$-0.347 \pm 0.004 \pm 0.011$	0.32
C	6.9(2)(6)	$-0.355 \pm 0.005 \pm 0.013$	0.14

where the statistical and systematic errors have been combined in quadrature. The results are shown in Fig. 13.

D. Thoughts on Meson-Meson Scattering

The lattice results for meson-meson scattering pose an interesting puzzle. In Fig. 6 one sees that the $I = 2$ $\pi\pi$ scattering length tracks the current algebra result up to pion masses that are expected to be at the edge of the chiral regime in the two-flavor sector. While in the two flavor theory one expects fairly good convergence of the chiral expansion and, moreover, one expects that the effective expansion parameter is small in the channel with maximal isospin, the lattice calculation clearly imply a cancellation between chiral logs and counterterms (evaluated at a given scale). As one sees in Fig. 13, the same phenomenon occurs in K^+K^+ where the chiral expansion is governed by the strange quark mass and is therefore expected to be more slowly converging. The π^+K^+ scattering length (see Fig. 9) indicates similar behavior but one should keep in mind that this data is expected to contain larger lattice spacing corrections. This mysterious cancellation between chiral logs and counterterms for the meson-meson scattering lengths begs for an explanation.

E. NN Scattering

One of the ultimate goals of nuclear physics is to compute the properties and interactions of nuclei directly from QCD. The first, pioneering study of NN scattering with Lattice QCD was performed more than a decade ago by Fukugita *et al* [99]. This calculation was quenched and at relatively large pion masses, $m_\pi \gtrsim 550$ MeV. A fully dynamical Lattice QCD calculation of the NN scattering lengths in both the 1S_0 -channel and $^3S_1 - ^3D_1$ -coupled-channels at pion masses of $m_\pi \sim 350$ MeV, 490 MeV and 590 MeV in the isospin-limit was performed within the last few years [150]. The dependence of the NN scattering lengths upon the light-quark masses has been determined to various non-trivial orders in the EFT expansion [151, 152, 153], and is estimated to be valid up to $m_\pi \sim 350$ MeV. The pion mass dependence of nuclear observables may also be explored using a lattice formulation of the low-energy EFT of nucleons [154]. The results of the Lattice QCD calculation at the lightest pion mass and the experimentally-determined scattering lengths at the physical value of the pion mass are used to constrain the chiral dependence of the scattering lengths from $m_\pi \sim 350$ MeV down to the chiral limit.

For an arbitrary nucleus (or bound and continuum nucleons), of atomic number A and charge Z , there are naively $(A + Z)!(2A - Z)!$ contractions that must be performed to

produce the nuclear correlation function ²⁴. Therefore, in the 1S_0 channel there are 48 contractions, while in the $^3S_1 - ^3D_1$ coupled channels system there are 36. The two-nucleon correlator that projects onto the s-wave state in the continuum limit is

$$C_{NN}^{IS}(t) = X_{\alpha\beta\sigma\rho}^{ijkl} \sum_{\mathbf{x}, \mathbf{y}} \langle N_i^\alpha(t, \mathbf{x}) N_j^\beta(t, \mathbf{y}) N_k^{\sigma\dagger}(0, \mathbf{0}) N_l^{\rho\dagger}(0, \mathbf{0}) \rangle, \quad (74)$$

where I denotes the isospin of the NN system and S denotes its spin, $\alpha, \beta, \sigma, \rho$ are isospin-indices and i, j, k, l are Dirac-indices. The tensor $X_{\alpha\beta\sigma\rho}^{ijkl}$ has elements that produce the correct spin-isospin quantum numbers of two-nucleons in an s-wave. The summation over \mathbf{x} (and \mathbf{y}) corresponds to summing over all the spatial lattice sites, thereby projecting onto the momentum $\mathbf{p} = \mathbf{0}$ state. The interpolating field for the proton is $p_i(t, \mathbf{x}) = \epsilon_{abc} u_i^a(t, \mathbf{x}) (u^{bT}(t, \mathbf{x}) C \gamma_5 d^c(t, \mathbf{x}))$, and similarly for the neutron.

At the pion masses used in these calculations the NN scattering lengths are found to be of natural size in both channels, and are much smaller than the $L \sim 2.5$ fm lattice spatial extent. It is noteworthy that the scattering lengths at the heaviest pion mass are not inconsistent with the lightest-mass quenched values of Ref. [99]. However, one should keep in mind the effects of quenching on the infrared properties of the theory [156].

A pion mass of $m_\pi \sim 350$ MeV is expected to be at the upper limit of where the EFT describing NN interactions will be valid [157, 158, 159, 160, 161, 162]. The chiral extrapolation is performed with BBSvK power-counting [162] (\equiv KSW power-counting [160, 161]) and W power-counting [157, 158, 159] in the 1S_0 -channel and BBSvK power-counting in the $^3S_1 - ^3D_1$ coupled channels. The Lattice QCD determinations of the light-quark axial-matrix element in the nucleon by LHPC [63] and its physical value are used to constrain the chiral expansion of g_A . The lattice calculations of the nucleon mass and pion decay constant [78] —as well as their physical values— are used to constrain their respective chiral expansions. In addition to the quark-mass dependence these three quantities contribute to the NN systems, there is dependence on the quark masses at next-to-leading order (NLO) from pion exchange, and from local four-nucleon operators that involve a single insertion of the light-quark mass matrix, described by the “ D_2 ” coefficients [151, 152, 153]. The results of this Lattice QCD calculation constrain the range of allowed values for the D_2 ’s, and consequently the scattering lengths in the region between $m_\pi \sim 350$ MeV and the chiral limit, as shown in Fig. 14 and Fig. 15. With only one lattice point at the edge of the regime of applicability of the EFT, a prediction for the scattering lengths at the physical pion mass is not possible: the experimental values of the scattering lengths are still required for an extrapolation to the chiral limit and naive dimensional analysis (NDA) is still required to select only those operator coefficients that are consistent with perturbation theory. The regions plotted in the figures correspond to values of C_0 – the coefficient of the leading-order quark-mass independent local operator – and D_2 that fit the lattice datum and the physical value, and are consistent with NDA. In both channels the lightest lattice datum constrains the chiral extrapolation to two distinct bands which are sensitive to both the quark mass dependence of g_A and the sign of the D_2 coefficient. As the lattice point used to constrain the EFT is at the upper limits of applicability of the EFT, we expect non-negligible corrections to these regions from higher orders in the EFT expansion. It is clear from Fig. 14 and Fig. 15 that

²⁴ The sum over all contractions can be shown [155] to scale as A^3 , rather than $\sim (A!)^2$.

even a qualitative understanding of the chiral limit will require lattice calculations at lighter quark masses.

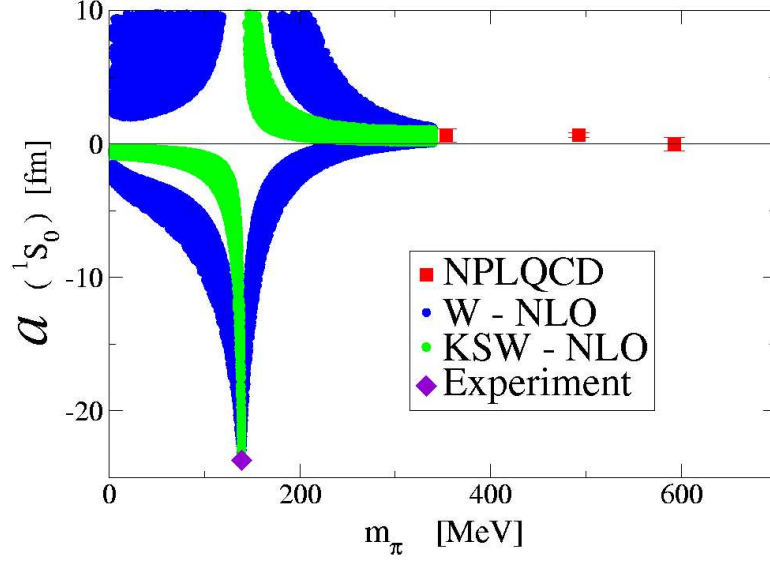


FIG. 14: Allowed regions for the scattering length in the 1S_0 channel as a function of the pion mass. The experimental value of the scattering length and NDA have been used to constrain the extrapolation in both BBSvK [160, 161, 162] and W [157, 158, 159] power-countings at NLO.

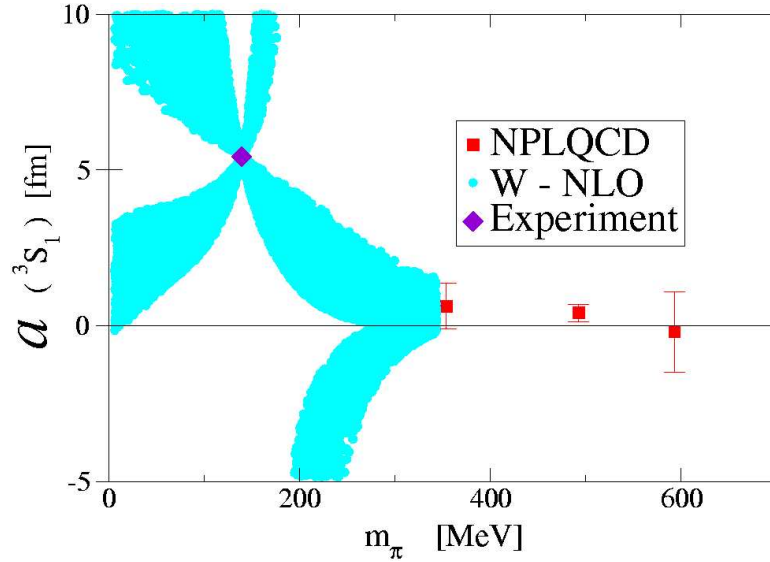


FIG. 15: Allowed regions for the scattering length in the $^3S_1 - ^3D_1$ coupled-channels as a function of the pion mass. The experimental value of the scattering length and NDA have been used to constrain the extrapolation in BBSvK [162] power-counting at NLO.

Without the resources to perform similar Lattice QCD calculations in different volumes, and observing that most energy-splitting are positive, it is assumed that scattering states

are found in each case. Calculations in larger volumes will be done in the future to verify the expected power-law dependence upon volume that scattering states exhibit. In addition to discriminating between bound and continuum states, calculations in a larger volume would reduce the energy of the lowest-lying continuum lattice states, and thus reduce the uncertainty in the scattering length due to truncation of the ERE. Further improvement would result from measuring the energy of the first excited state on the lattice, either with a single source or by using the Lüscher-Wolff [12] method. The lattice spacing effects in the present calculation appear at $\sim \mathcal{O}(b^2)$ (or exponentially suppressed $\mathcal{O}(b)$ effects), and are expected to be small. However, the finite lattice spacing effects should be determined by performing the same calculation on lattices with a finer lattice spacing. A theoretical investigation of mixed-action EFT for NN scattering which would allow a continuum extrapolation remains to be carried through ²⁵. In addition to more precise Lattice QCD calculations through an increase in computing resources, formal developments are also required. In order to have a more precise chiral extrapolation, calculations in the various relevant EFTs must be performed beyond NLO. Furthermore, it is clear that lattice calculations at lower pion masses are essential for the extrapolation to the chiral limit, and will ultimately allow for a “prediction” of the physical scattering lengths.

F. YN Scattering

1. Introduction

In high-density baryonic systems, the large value of the Fermi energy may make it energetically advantageous for some of the nucleons to become hyperons, with the increase in rest mass being more than compensated for by the decrease in Fermi energy. This is speculated to occur in the interior of neutron stars, but a quantitative understanding of this phenomenon depends on knowledge of the interactions among the hadrons in the medium. In contrast to NN interactions, where the wealth of experimental data has allowed for the construction of high-precision potentials, the hyperon-nucleon (YN) interactions are only very-approximately known. Experimental information about the YN interaction comes mainly from the study of hypernuclei [164, 165], the analysis of associated Λ -kaon and Σ -kaon production in NN collisions near threshold [166, 167, 168, 169, 170, 171], and hadronic atoms [172]. There are a total of 35 cross-sections measurements [173] of the processes $\Lambda p \rightarrow \Lambda p$, $\Sigma^- p \rightarrow \Lambda n$, $\Sigma^+ p \rightarrow \Sigma^+ p$, $\Sigma^- p \rightarrow \Sigma^- p$ and $\Sigma^- p \rightarrow \Sigma^0 n$, and unsurprisingly, the extracted scattering parameters are highly model dependent. The theoretical study of YN interactions is hindered by the lack of experimental guidance. The “realistic” potentials developed by the Nijmegen [174, 175] and Jülich [176, 177, 178] groups are just two examples of phenomenological models based on meson exchange. These are soft-core potentials with one-boson exchange models of the NN interaction. Since $SU(3)$ flavor symmetry is broken by the differences in the quark masses, the corresponding couplings are not completely determined by the NN interaction and are instead obtained by a fit to the available data. In Ref. [174, 175], for example, six different models are constructed, each describing the available YN cross-section data equally well, but predicting different values for the phase

²⁵ See Ref. [34] for preliminary work in this direction. The masses and magnetic moments of the octet baryons have been calculated at NLO in MA χ -PT in Ref. [163].

shifts. The effective field theory approach [179, 180, 181, 182, 183] is less developed and suffers from a large number of couplings that need to be fit to the data.

In view of the large uncertainties in the YN scattering amplitudes and their importance for modeling neutron stars and the study of hypernuclei, a first-principles QCD calculation of YN scattering is highly desirable. The only way to achieve this is through numerical calculations using Lattice QCD. Some of the present authors were part of a work [182] that outlined a program to address this issue with a combination of lattice calculations and the use of effective field theories.

We have computed the low-energy s-wave phase shifts for YN scattering [184] in the 1S_0 channel and $^3S_1 - ^3D_1$ coupled-channels at particular energies, using Lüscher's finite-volume method [16, 18, 19]. No attempt was made to extrapolate to the physical pion mass as it is likely that all but one of the data points lies outside the regime of applicability of the YN EFTs.

An interpolating field of the form $n \times \Sigma^-$ (a simple product of the single baryon interpolating fields) was used to determine the energy-eigenvalues of the s-wave strangeness = 1, isospin = $\frac{3}{2}$ eigenstates in both spin channels, and an interpolating field $n \times \Lambda$ to determine the energy-eigenvalues of the s-wave strangeness = 1, isospin = $\frac{1}{2}$ eigenstates in both spin channels.

2. Results

A typical example of the quality of the output of the lattice calculation can be seen in the effective mass plots for $n\Lambda$ in the 1S_0 -channel, as shown in Fig. 16. The plateaus in the

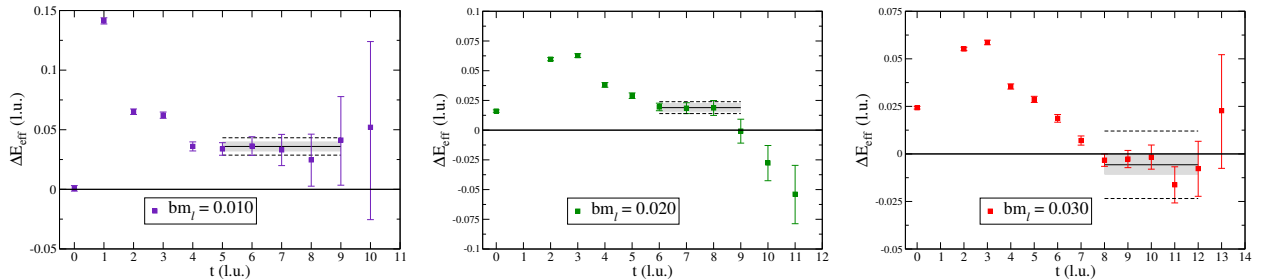


FIG. 16: The effective mass plots for $n\Lambda$ in the 1S_0 -channel at pion masses of $m_\pi \sim 350$ MeV (left panel), $m_\pi \sim 490$ MeV (center panel) and $m_\pi \sim 590$ MeV (right panel). The straight line and shaded region correspond to the extracted energy shift and associated uncertainty. The dashed lines correspond to the statistical and systematic errors added linearly.

effective energy plots persist for only a small number of time-slices. At small t there is the usual contamination from excited states whereas at larger t the signal-to-noise ratio degrades exponentially with t . The Dirichlet boundary at $t = 22$ introduces a systematic uncertainty due to backward propagating states. However, in practice, the statistical noise becomes a limiting factor at far earlier time slices and the boundary at $t = 22$ is not an issue for this calculation. We obtained a non-zero energy shift larger than the statistical error in ten of the correlation functions.

It is not clear that we have been able to identify the ground states in all of the correlation functions, e.g. $n\Sigma^-$ in the 1S_0 -channel at $m_\pi \sim 490$ MeV, and $n\Lambda$ in the 1S_0 -channel at

$m_\pi \sim 490$ MeV, as the statistics are not sufficient to determine whether the large-time behavior we observe is due to noise or due to the presence of any states with lower energy than those found. Indeed, it would be very exciting if there were states with lower energy, as they would likely be bound states (based on naturalness arguments and the exact Lüscher relation).

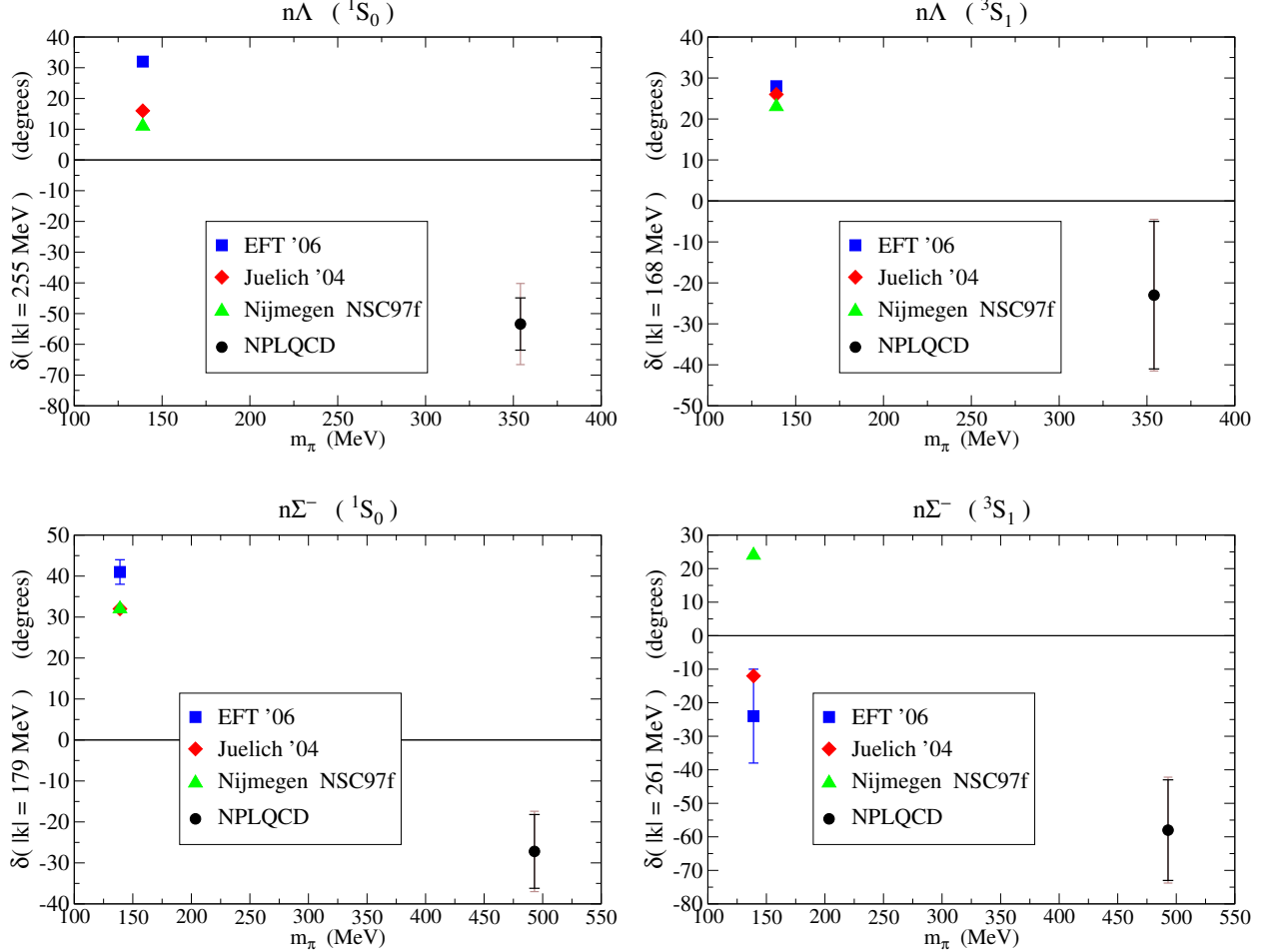


FIG. 17: Comparison of the lowest-pion-mass lattice results in each channel with a recently developed YN EFT [183] (squares), and several potential models: Nijmegen [174] (triangles) and Jülich [178] (diamonds). The dark error bars on the lattice data are statistical and the light error bars are statistical and systematic errors added in quadrature.

3. Discussion

The lightest pion mass at which a signal was extracted is at the upper limits of the regime of applicability of the effective field theories that have been constructed, thus precluding a chiral extrapolation. However, this work does provide new rigorous theoretical constraints on effective field theory, and potential model constructions of YN interactions. In Fig. 17 we compare the lattice values of the phase shifts to recent EFT results [183] (squares), and to several potential models: Nijmegen [174] (triangles) and Jülich [178]. At face value these

results appear quite discrepant, however one should keep in mind that extrapolation to the physical pion mass will seriously alter individual contributions to the YN interaction.

While the measurements of the momenta and phase shifts are unambiguous, their physical interpretation is not entirely resolved. Each of the phase shifts at the lowest pion masses are negative. Assuming that the observed state is the ground state in the lattice volume, this implies that the interactions are all repulsive. The $n\Sigma^-$ interaction in the $^3S_1 - ^3D_1$ coupled channels is strongly repulsive at $m_\pi \sim 490$ MeV, while the interaction in the 1S_0 -channel is only mildly repulsive. The opposite is found to be true for the $n\Lambda$ systems at $m_\pi \sim 350$ MeV, where the interaction in the 1S_0 -channel is found to be strongly repulsive, while that in the $^3S_1 - ^3D_1$ coupled channels is mildly repulsive. However, there may be channels for which there exist states of lower, negative energies, some of which may correspond to bound states in the continuum limit. If such states are present, then we would conclude that the interaction is attractive, and that the positive-shifted energy state we have identified corresponds to the first continuum level. Current statistics are sufficiently poor that nothing definitive can be said about the existence of such states.

G. Exploratory Quenched Calculations

1. BB Potentials

Energy-independent potentials can be rigorously defined and calculated for systems composed of two (or more) hadrons containing a heavy quark in the heavy-quark limit, $m_Q \rightarrow \infty$. This is interesting for more than academic reasons as the light degrees of freedom (dof) in the B-meson have the same quantum numbers as the nucleon, isospin- $\frac{1}{2}$ and spin- $\frac{1}{2}$. As such, the EFT describing the interactions between two B-mesons has the same form as that describing the interactions between two nucleons, but the counterterms that enter into each EFT are different. Therefore, a deeper understanding of the EFT description of nuclear physics can be gained by Lattice QCD calculations of the potentials between B-mesons. A number of quenched explorations of these potentials have been performed previously [185, 186, 187, 188, 189, 190, 191, 192, 193], but there was little evidence for any potential simply due to limited computational resources. We returned to this problem [194] and computed the potential between two B-mesons in the four possible spin-isospin channels (neglecting $B_d^0 - \bar{B}_d^0$ mixing) in relatively small volume DBW2 lattices with $L \sim 1.6$ fm, with a pion mass of $m_\pi \sim 403$ MeV, and lattice-spacing of $b \sim 0.1$ fm. The calculation was quenched and the naive Wilson action was used for the quarks. At this relatively fine lattice spacing, much finer than previous calculations, were able to extract a non-zero potential, but the small volume meant that the contributions to the potential from image B-mesons (periodic BC's) were visible.

Constructing the t-channel potentials, defined via the quantum numbers of the exchange particles, in keeping with nuclear physics tradition, isolated statistical fluctuations into the channel associated with the “ σ ”-meson, leaving the channels with the quantum numbers of the π , ρ and ω with relatively small statistical errors. The potentials are shown in Fig. 18.

Given the uncertainties in the potentials, and the number of counterterms that appear in the EFT describing the long- and medium- distance interactions between the B-mesons, it was possible to make only a parameterization of each potential beyond the leading light-meson contribution. Since only the longest range contribution to the potential in each

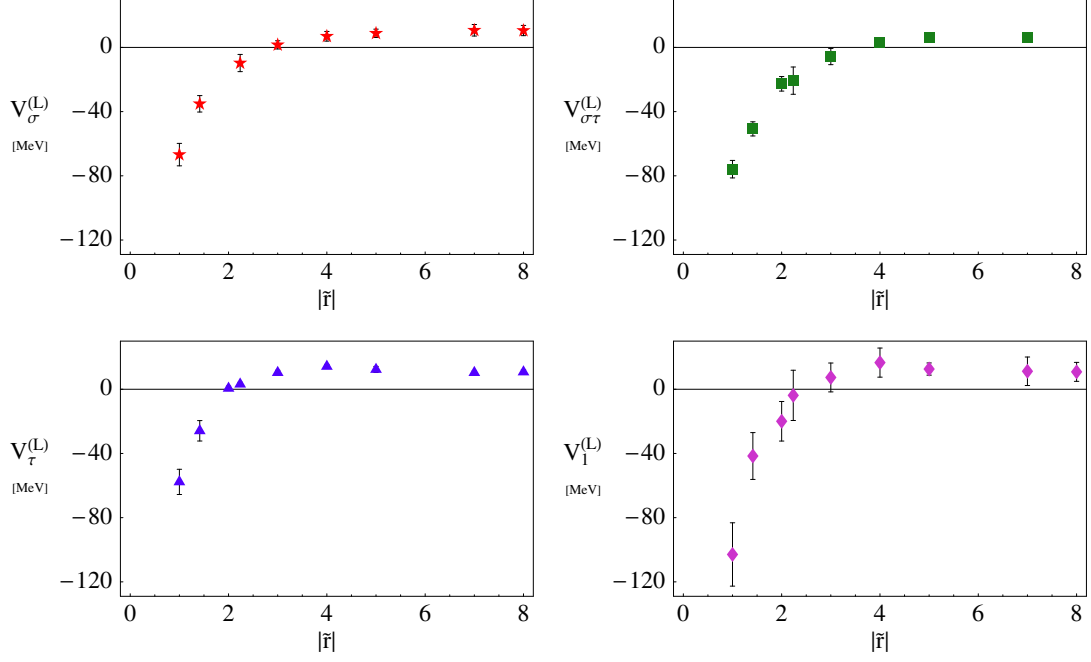


FIG. 18: The t-channel potentials between two B-mesons in the finite lattice volume. $V_{\sigma}^{(L)}$, $V_{\tau}^{(L)}$, $V_{\sigma\tau}^{(L)}$, and $V_1^{(L)}$ correspond to the potentials in the exchange-channels with spin-isospin of $(J, I) = (1, 0)$, $(0, 1)$, $(1, 1)$ and $(0, 0)$.

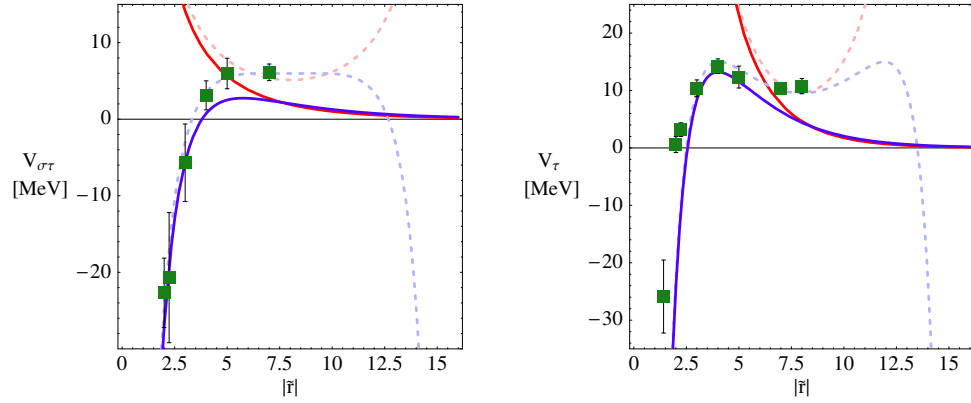


FIG. 19: Fits to the finite-volume isovector t-channel potentials between two B-mesons. The dashed lines correspond to the finite-volume fits to the lattice data, and the solid curves are the infinite-volume extrapolations.

channel can be identified, we fit our results at large separations, $|\mathbf{r}| > \Lambda_{\chi}^{-1}$, using the finite-

volume versions of the simplified infinite-volume potentials,

$$V_{\sigma\tau}^{(\infty)}(\mathbf{r}) \xrightarrow{|\mathbf{r}| \rightarrow \infty} \frac{g^2 m_\pi^2}{24\pi f_\pi^2} \frac{e^{-m_\pi|\mathbf{r}|}}{|\mathbf{r}|} + \alpha'_\chi \frac{e^{-\Lambda_\chi|\mathbf{r}|}}{|\mathbf{r}|} \quad , \quad (75)$$

$$V_\tau^{(\infty)}(\mathbf{r}) \xrightarrow{|\mathbf{r}| \rightarrow \infty} \frac{g_\rho^2}{4\pi} \frac{e^{-m_\rho|\mathbf{r}|}}{|\mathbf{r}|} + \alpha_\chi \frac{e^{-\Lambda_\chi|\mathbf{r}|}}{|\mathbf{r}|} \quad . \quad (76)$$

The short distance forms in the above equations are entirely model dependent and are the simplest forms that we could find that provide a reasonable description of the data. Using the measured values and uncertainties of m_π and m_ρ and the physical value of f_π we first determine the couplings g and g_ρ by setting $\alpha_\chi = \alpha'_\chi = 0$ and fitting the finite-volume potentials at the two largest separations.²⁶ These fits are shown by the dashed red curves in Fig. 19 and the resulting couplings are found to be

$$g_\rho = 2.17 \pm 0.08 \quad , \quad g = 0.57 \pm 0.06 \quad . \quad (77)$$

Having determined these parameters, we reconstruct the infinite-volume potentials that are shown in the figure as the solid red lines.

Clearly the lattice calculations that exist of the potentials between B-mesons must be viewed as nothing more than exploratory. Further, the analysis of the output of the calculations should be model-independent in order to impact our understanding of the NN interaction.

2. J/ψ -Hadron Scattering

The interactions between quarkonia and the light hadrons is interesting from both the theoretical and experimental standpoints. Theoretically, near the heavy-quark limit, the quarkonia are compact objects for which a multipole expansion of the chromo-electric and magnetic fields can be performed, with the leading interactions scaling as $r_{\bar{Q}Q}^3$, where $r_{\bar{Q}Q}$ is the radius of the $\bar{Q}Q$ state. This has lead to predictions for the binding of such states to nuclear matter [195] and interactions with light nuclei [196]. On the experimental side, the number and distribution of quarkonia observed in heavy ion collisions as a function of nuclear size provides important information on both the production and attenuation of such states in nuclear matter under extreme conditions. The first quenched lattice studies of the low-energy interactions of charmonium with a π , ρ or nucleon have been recently performed [197]. This work is quite encouraging, and we look forward to fully-dynamical calculations at smaller pion masses.

V. N-BODY INTERACTIONS

The simplest multi-hadron systems consist of n pseudoscalar mesons of maximal isospin. Although such systems are of limited phenomenological interest for $n > 3$ (three pion interferometry is currently a topic of interest in heavy-ion collisions [198, 199, 200]), they

²⁶ Simple fits using the infinite-volume long range behavior were considered in Ref. [185].

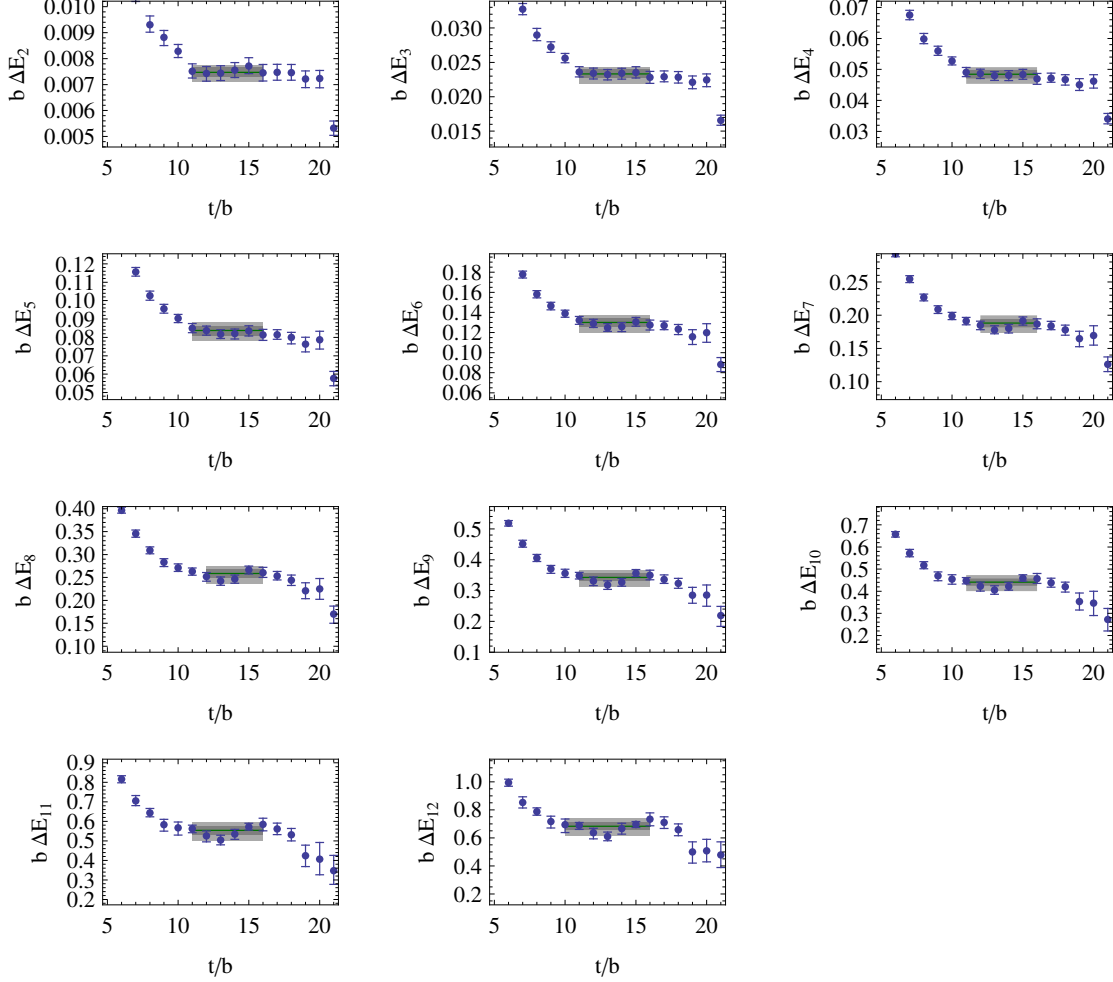


FIG. 20: The effective energy plots associated with the correlation functions of $n = 2, 3, \dots, 12$ π^+ 's with the pion rest mass removed for a pion mass of $m_\pi \sim 290$ MeV.

serve as a testing ground for more complicated many-body systems. We performed the first Lattice QCD calculation of multi-hadron ($n > 2$) interactions [22, 23] by calculating the ground-state energies of $\pi^+\pi^+$, $\pi^+\pi^+\pi^+$, $\pi^+\pi^+\pi^+\pi^+$ up to $(\pi^+)^{12}$ in a spatial volume of $V \sim (2.5 \text{ fm})^3$ with periodic boundary conditions. These systems serve as an ideal laboratory for investigating multi-particle interactions as chiral symmetry guarantees relatively weak interactions among pions, and multiple pion correlation functions computed with Lattice QCD do not suffer from signal to noise issues (as can be seen in Fig. 20) that are expected to plague analogous calculations in multi-baryon systems, as discussed in section II E. The $\pi^+\pi^+$ scattering length is extracted from the n -pion ($n > 2$) systems with precision that is comparable to (and in some cases better than) the $n = 2$ determination [115].

Using the expression for the energy shift of n - π^+ 's in a finite volume due to their two- and three-body interactions, as given in Eq. (14), the three- π^+ interaction

$$\overline{\eta}_3^L = \overline{\eta}_3^L \left[1 - 6 \left(\frac{a}{\pi L} \right) \mathcal{I} \right] , \quad (78)$$

is determined at four different quark masses. The extracted values of $\overline{\eta}_3^L$ in units of the NDA

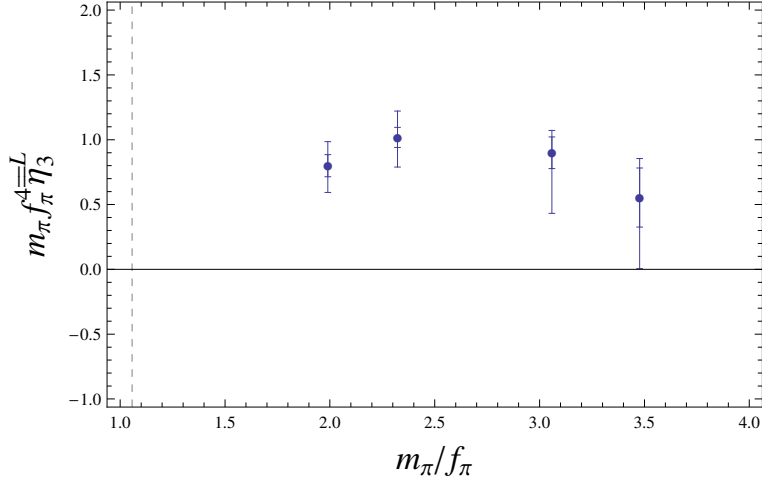


FIG. 21: The $\pi^+\pi^+\pi^+$ interaction, $\overline{\eta}_3^L$, in units of the NDA estimate of $1/(m_\pi f_\pi^4)$ as a function of m_π/f_π .

estimate of $1/(m_\pi f_\pi^4)$ are shown in Fig. 21 as a function of m_π/f_π . There is clear evidence for a three- π^+ interaction, and further, it is of a magnitude that is consistent with NDA.

The study of systems with arbitrary numbers of π^+ 's in a fixed volume enables the study of the isospin chemical potential as a function of isospin density. For the systems containing less than twelve π^+ 's with the coarse MILC lattices with $L \sim 2.5$ fm, the results are shown in Fig. 22 [23]. This is a first step toward a general study of multi-hadron systems.

VI. RESOURCE REQUIREMENTS FOR FURTHER PROGRESS

To understand more concretely the resources that will be required to compute the interactions between two or more nucleons, we determined the uncertainty in the nucleon-nucleon scattering length, at a scattering length of $a = 2$ fm (independent of the pion mass) as a function of the computational resources available to this program. Our estimates, shown in Fig. 23, are for computations on lattices with a lattice spacing of $b \sim 0.125$ fm and a spatial lattice extent of $L \sim 5$ fm. The following procedure was used to determine the uncertainties in the scattering length:

1. The results obtained by NPLQCD indicate that the uncertainty in the scattering lengths depend (approximately) exponentially upon the pion mass. The argument and coefficient of the exponential were fit to these results.
2. The computational requirements for propagator generation scale as $T_{\text{cpu}} = (A + B/m_q)V$. A and B were determined by the timings on the $b \sim 0.125$ fm, $20^3 \times 64$ MILC lattices for domain-wall propagator generation. The lattice volume is in lattice units.
3. The value of the energy splitting between the two nucleons in the volume and two isolated nucleons in the volume was tuned to produce a scattering length of 2 fm.

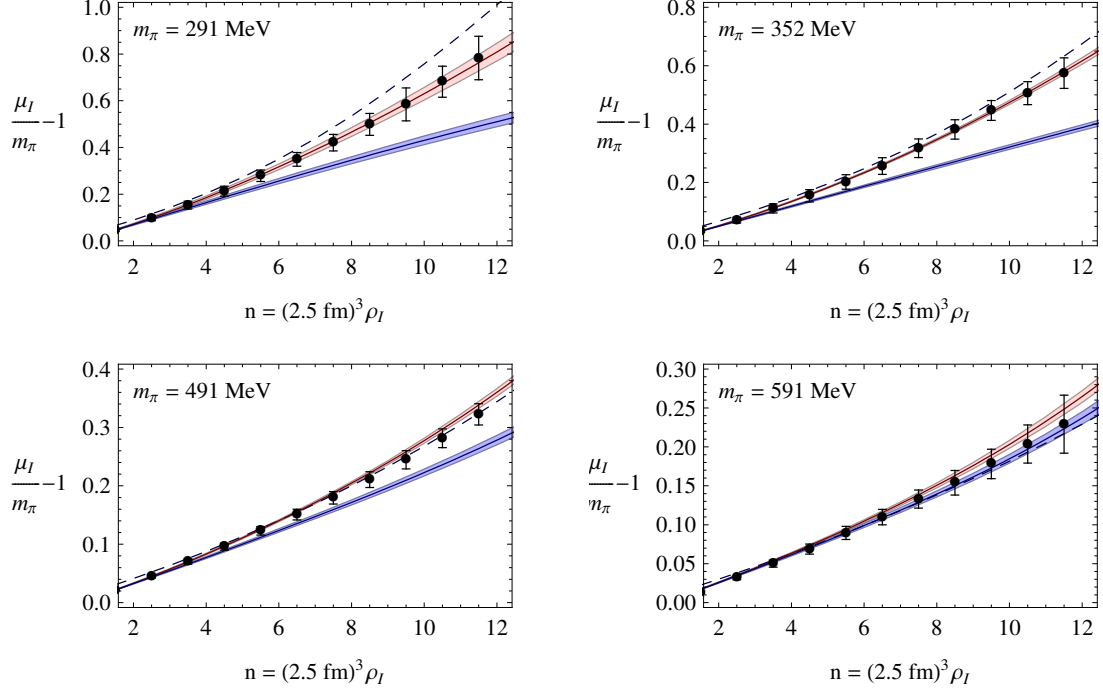


FIG. 22: The isospin chemical potential as a function of the number of pions (equivalent to the isospin density ρ_I) at a fixed volume with and without the contribution from the $\pi^+\pi^+\pi^+$ -interaction, $\overline{\eta}_3^L$. The solid red (lighter) curves and bands result from the analytic expression for the energy of the ground state in the large volume expansion, Eq. (14), using the fit values for $a_{\pi^+\pi^+}$ and $\overline{\eta}_3^L$ and their correlated uncertainties. The solid blue (darker) curves and bands are similarly the results for the fitted value of $a_{\pi^+\pi^+}$ and $\overline{\eta}_3^L=0$. The dashed curve corresponds to the leading order prediction of χ -PT.

4. The statistical uncertainty on the projected energy-splitting was determined by the number of propagators that could be generated with the given computational resources. Synthetic data was then processed using the jackknife procedure with the exact Luscher formula to produce the uncertainty in the scattering length.
5. We have not included the effect of the improved signal in going to larger volumes, possibly a $1/\sqrt{V}$ factor, as we have no data to extrapolate from.

The quoted resource requirements are for propagator generation ONLY, and do not include the resource requirements for lattice generation. Each data point requires the resource indicated in the legend of Fig. 23. Therefore, the computational resources required to generate the data indicated by the purple squares in Fig. 23 with the precision that is shown, is 0.12 Pflop-yrs. We assume that the lattices will be generated by others in the USQCD collaboration, and will be made available (in a timely fashion). Further, these resources are for the generation of Domain-Wall fermions. If, instead, Clover-Wilson fermions are used on dynamical Clover-Wilson lattices, the resource requirements for propagator generation are reduced by a factor of ~ 10 . Additional factors of $\sim 5 - 8$ (included in these estimates) are gained using the newly developed Incremental and EigCG deflation method [201]. Provided that gauge field configurations become available, the task of computing NN scattering lengths

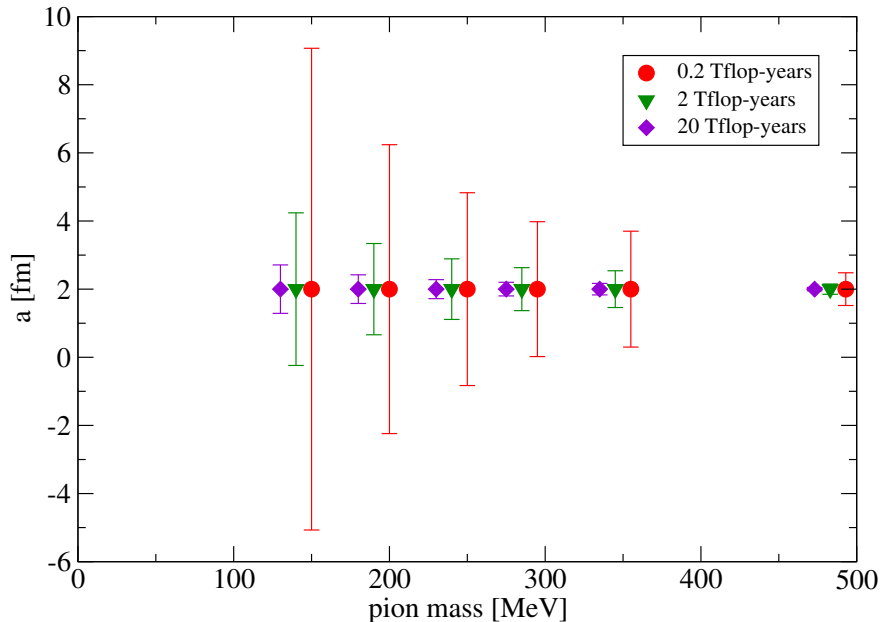


FIG. 23: The expected uncertainty in nucleon-nucleon scattering in the ${}^3S_1 - {}^3D_1$ coupled channels for a 2 fm scattering length as a function of the pion mass for domain wall valence quarks on the coarse MILC lattices ($b \sim 0.125$ fm) for given computational resources (there is a further reduction by an order of magnitude for clover quarks in the valence sector). Each data point requires the full computational resource, i.e. to generate the complete set of six triangular (green) data requires 12 Tflop-yrs.

and phase-shifts from lattice QCD could be accomplished with present-day computational resources.

VII. CONCLUDING REMARKS

Lattice QCD, when combined with effective field theory, is presently able to provide quantitative information about the interactions among hadrons directly from QCD. During the last five years a number of two-hadron processes have been investigated in fully-dynamical lattice QCD, including both meson-meson and baryon-baryon processes. While, it is fair to say that the study of hadronic interactions with Lattice QCD is still in its infancy, the computational resources that will likely become available during the next five years will allow for a complete study such systems. This will amount to nothing short of a revolution in nuclear physics.

The study of systems containing baryons is much more computationally intensive than that of systems containing only pions, due to the exponential degradation of the signal-to-noise in (multi-)baryon correlators. This is presently a serious roadblock for the direct study of nuclei and nuclear interactions with Lattice QCD. Further, the study of systems such as $\pi^+\pi^- \rightarrow \pi^+\pi^-$ are presently out of reach due to the need to calculate disconnected diagrams, which require approximately an order of magnitude increase in computational

time over the connected contributions.

For the calculations that are of interest to the nuclear physics community, it is important to step back and consider which lattice calculations are the most important to perform, and what the criterion “important” actually means! There may be some use in performing a high precision calculation, say $\sim 0.1\%$ -level, of a mesonic quantity, such as f_π , which is already known to high precision experimentally, but there may be equivalent use in performing a low precision calculation, say at the $\sim 20\%$ -level, of the weak pion-nucleon coupling constant, $h_{\pi NN}^{(1)}$, that is expected to provide a significant contribution to parity violating observables in many light nuclei and for which there is still a substantial amount of uncertainty as regards its value. This is clearly something for future discussions and we do not attempt to resolve this issue in this review.

The near future will see remarkable progress in this field. One can expect calculations in large volumes, small lattice spacings and at the physical quark masses, and also the inclusion of electromagnetism. With sufficient resources dedicated to this area of Lattice QCD, the interactions between two and three hadrons will be calculated at high precision, with complete control over all systematic uncertainties that arise. At that time, calculations of processes relevant to areas of nuclear physics, such as the interactions between hyperons and nucleons that impact the equation of state of nuclear matter in the interior of neutron stars, or the interactions between multiple nucleons, will be calculable directly from QCD. However, it is crucial to appreciate the fact that in order for this program in multi-baryon physics to be realized a significant amount of computational power will need to be directed exclusively at multi-baryon calculations.

Finally, in direct analogy with the experimental programs, it is not sufficient to have just one calculation of any given quantity. Lattice calculations with different discretizations, lattice volumes, lattice spacing, performed by different lattice collaborations are required in order to have confidence in the “Lattice QCD” value of the quantity. This concerted effort does not yet exist for any scattering process, and we look forward to such a coherent effort taking shape in the near future.

We would like to thank Paulo Bedaque, William Detmold, Tom Luu, Elisabetta Pallante, Assumpta Parreño, Aaron Torok and Andre Walker-Loud who have all contributed to the work described in this review. Our computations were performed at JLab, FNAL, LLNL, NCSA, and CNdS (Barcelona). We acknowledge DOE Grants No. DE-FG03-97ER4014 (MJS), DE-AC05-06OR23177 (KO) and NSF CAREER Grant No. PHY-0645570 (SB). KO acknowledges the Jeffress Memorial Trust, grant J-813 and a DOE OJI grant DE-FG02-07ER41527.

-
- [1] D. Page and S. Reddy, *Ann. Rev. Nucl. Part. Sci.* **56**, 327 (2006) [arXiv:astro-ph/0608360].
 - [2] S. C. Pieper, “Quantum Monte Carlo Calculations of Light Nuclei,” Lecture notes for International School of Physics ‘Enrico Fermi’: Course 169: Nuclear Structure far from Stability: New Physics and New Technology, Varenna, Italy, 17-27 Jul 2007. arXiv:0711.1500 [nucl-th].
 - [3] R. B. Wiringa, V. G. J. Stoks and R. Schiavilla, *Phys. Rev. C* **51**, 38 (1995) [arXiv:nucl-th/9408016].

- [4] *The Antropic Cosmological Principle*, by J.D. Barrow and F.J. Tipler, Oxford University Press, 1986. ISBN 0-19-282147-4.
- [5] K. Symanzik, Nucl. Phys. B **226**, 205 (1983).
- [6] R. G. Edwards and B. Joo [SciDAC Collaboration], “The Chroma software system for Lattice QCD,” [arXiv:hep-lat/0409003].
- [7] C. McClendon, “Optimized Lattice QCD Kernels for a Pentium 4 Cluster”, JLAB-THY-01-29, http://www.jlab.org/~edwards/qcdapi/reports/dslash_p4.pdf
- [8] *Quarks, gluons and lattices*, by M. Creutz, Cambridge Monographs on Mathematical Physics, Cambridge University Press 1983. ISBN 0 521 24405 6.
- [9] *Lattice Gauge Theories An Introduction*, by H.J. Rothe, World Scientific Notes in Physics - Vol59, World Scientific 1997. ISBN 981-02-3032-X.
- [10] *Lattice Methods for Quantum Chromodynamics*, by T DeGrand and C. DeTar, World Scientific 2006. ISBN 981-256-727-5.
- [11] M. Lüscher, Commun. Math. Phys. **104**, 177 (1986).
- [12] M. Lüscher and U. Wolff, Nucl. Phys. B **339**, 222 (1990).
- [13] L. Maiani and M. Testa, Phys. Lett. B **245**, 585 (1990).
- [14] K. Huang and C. N. Yang, Phys. Rev. **105**, 767 (1957).
- [15] M. Lüscher, Commun. Math. Phys. **105**, 153 (1986).
- [16] M. Lüscher, Nucl. Phys. B **354**, 531 (1991).
- [17] J.E. Mandula, G. Zweig and J. Govaerts, *Nucl. Phys.* **B228**, 91 (1983).
- [18] H. W. Hamber, E. Marinari, G. Parisi and C. Rebbi, Nucl. Phys. B **225**, 475 (1983).
- [19] S. R. Beane, P. F. Bedaque, A. Parreño and M. J. Savage, Phys. Lett. B **585**, 106 (2004) [arXiv:hep-lat/0312004].
- [20] E. Elizalde, *Commun. Math. Phys.* **198**, 83 (1998), hep-th/9707257.
- [21] S. Sasaki and T. Yamazaki, Phys. Rev. D **74**, 114507 (2006) [arXiv:hep-lat/0610081].
- [22] S. R. Beane, W. Detmold, T. C. Luu, K. Orginos, M. J. Savage and A. Torok, Phys. Rev. Lett. **100**, 082004 (2008) [arXiv:0710.1827 [hep-lat]].
- [23] W. Detmold, M. J. Savage, A. Torok, S. R. Beane, T. C. Luu, K. Orginos and A. Parreño, arXiv:0803.2728 [hep-lat].
- [24] S. R. Beane, W. Detmold and M. J. Savage, Phys. Rev. D **76**, 074507 (2007) [arXiv:0707.1670 [hep-lat]].
- [25] S. Tan, arXiv:0709.2530 [cond-mat.stat-mech].
- [26] W. Detmold and M. J. Savage, Phys. Rev. D **77**, 057502 (2008) [arXiv:0801.0763 [hep-lat]].
- [27] O. Bar, G. Rupak and N. Shoresh, Phys. Rev. D **67**, 114505 (2003) [arXiv:hep-lat/0210050].
- [28] O. Bar, G. Rupak and N. Shoresh, Phys. Rev. D **70**, 034508 (2004) [arXiv:hep-lat/0306021].
- [29] O. Bar, C. Bernard, G. Rupak and N. Shoresh, Phys. Rev. D **72**, 054502 (2005) [arXiv:hep-lat/0503009].
- [30] J. W. Chen, D. O’Connell, R. S. Van de Water and A. Walker-Loud, Phys. Rev. D **73**, 074510 (2006) [arXiv:hep-lat/0510024].
- [31] J. W. Chen, D. O’Connell and A. Walker-Loud, Phys. Rev. D **75**, 054501 (2007) [arXiv:hep-lat/0611003].
- [32] C. Aubin *et al.* [MILC Collaboration], Phys. Rev. D **70**, 114501 (2004) [arXiv:hep-lat/0407028].
- [33] J. Gasser and H. Leutwyler, Annals Phys. **158**, 142 (1984).
- [34] J. W. Chen, D. O’Connell and A. Walker-Loud, arXiv:0706.0035 [hep-lat].
- [35] N. Ishii, S. Aoki and T. Hatsuda, Phys. Rev. Lett. **99**, 022001 (2007) [arXiv:nucl-th/0611096].

- [36] G. P. Lepage, ‘The Analysis Of Algorithms For Lattice Field Theory,’ Invited lectures given at TASI’89 Summer School, Boulder, CO, Jun 4-30, 1989. Published in Boulder ASI 1989:97-120 (QCD161:T45:1989).
- [37] K. G. Wilson, Phys. Rev. D **10**, 2445 (1974).
- [38] J. B. Kogut and L. Susskind, Phys. Rev. D **11**, 395 (1975).
- [39] D. B. Kaplan, Phys. Lett. B **288**, 342 (1992) [arXiv:hep-lat/9206013].
- [40] Y. Shamir, Nucl. Phys. B **406**, 90 (1993) [arXiv:hep-lat/9303005].
- [41] V. Furman and Y. Shamir, Nucl. Phys. B **439**, 54 (1995) [arXiv:hep-lat/9405004].
- [42] R. Narayanan and H. Neuberger, Nucl. Phys. B **443**, 305 (1995) [arXiv:hep-th/9411108].
- [43] H. Neuberger, Phys. Lett. B **417**, 141 (1998) [arXiv:hep-lat/9707022].
- [44] K. Orginos, D. Toussaint and R. L. Sugar [MILC Collaboration], Phys. Rev. D **60**, 054503 (1999) [arXiv:hep-lat/9903032].
- [45] K. Orginos and D. Toussaint [MILC collaboration], Phys. Rev. D **59**, 014501 (1999) [arXiv:hep-lat/9805009].
- [46] Y. Shamir, Phys. Rev. D **75**, 054503 (2007) [arXiv:hep-lat/0607007].
- [47] C. Bernard, M. Golterman and Y. Shamir, Phys. Rev. D **73**, 114511 (2006) [arXiv:hep-lat/0604017].
- [48] C. Bernard, M. Golterman and Y. Shamir, Phys. Rev. D **77**, 074505 (2008) [arXiv:0712.2560 [hep-lat]].
- [49] C. Bernard, M. Golterman, Y. Shamir and S. R. Sharpe, arXiv:0711.0696 [hep-lat].
- [50] S. Dürr and C. Hoelbling, Phys. Rev. D **74**, 014513 (2006) [arXiv:hep-lat/0604005].
- [51] S. Dürr and C. Hoelbling, Phys. Rev. D **71**, 054501 (2005) [arXiv:hep-lat/0411022].
- [52] C. Aubin and C. Bernard, Phys. Rev. D **68** (2003) 034014 [arXiv:hep-lat/0304014].
- [53] C. Aubin and C. Bernard, Phys. Rev. D **68** (2003) 074011 [arXiv:hep-lat/0306026].
- [54] C. Bernard, Phys. Rev. D **73** (2006) 114503 [arXiv:hep-lat/0603011].
- [55] W. J. Lee and S. R. Sharpe, Phys. Rev. D **60**, 114503 (1999) [arXiv:hep-lat/9905023].
- [56] C. Bernard, M. Golterman, Y. Shamir and S. R. Sharpe, Phys. Lett. B **649**, 235 (2007) [arXiv:hep-lat/0603027].
- [57] M. Creutz, PoS **LATTICE2007**, 007 (2006) [arXiv:0708.1295 [hep-lat]].
- [58] C. W. Bernard *et al.*, Phys. Rev. D **64**, 054506 (2001) [arXiv:hep-lat/0104002], <http://qcd.nersc.gov/>.
- [59] R. G. Edwards *et al.* [LHPC Collaboration], PoS **LAT2006** (2006) 195.
- [60] D. B. Renner *et al.* [LHPC Collaboration], PoS **LATTICE2007**, 160 (2006) [arXiv:0710.1373 [hep-lat]].
- [61] Ph. Hagler *et al.* [LHPC Collaborations], arXiv:0705.4295 [hep-lat].
- [62] R. G. Edwards *et al.*, PoS **LAT2006** (2006) 121 [arXiv:hep-lat/0610007].
- [63] R. G. Edwards *et al.* [LHPC Collaboration], Phys. Rev. Lett. **96**, 052001 (2006) [arXiv:hep-lat/0510062].
- [64] M. G. Alford, W. Dimm, G. P. Lepage, G. Hockney and P. B. Mackenzie, Phys. Lett. B **361**, 87 (1995) [arXiv:hep-lat/9507010].
- [65] D. Toussaint and K. Orginos [MILC Collaboration], Nucl. Phys. Proc. Suppl. **73**, 909 (1999) [arXiv:hep-lat/9809148].
- [66] J. F. Lagae and D. K. Sinclair, Phys. Rev. D **59**, 014511 (1999) [arXiv:hep-lat/9806014].
- [67] G. P. Lepage, Phys. Rev. D **59**, 074502 (1999) [arXiv:hep-lat/9809157].
- [68] K. Orginos, R. Sugar and D. Toussaint, Nucl. Phys. Proc. Suppl. **83**, 878 (2000) [arXiv:hep-lat/9909087].

- [69] S. Naik, Nucl. Phys. B **316**, 238 (1989).
- [70] A. Hasenfratz and F. Knechtli, Phys. Rev. D **64**, 034504 (2001).
- [71] T. A. DeGrand, A. Hasenfratz and T. G. Kovacs, Phys. Rev. D **67**, 054501 (2003).
- [72] T. A. DeGrand, Phys. Rev. D **69**, 014504 (2004).
- [73] S. Dürr, C. Hoelbling and U. Wenger, Phys. Rev. D **70**, 094502 (2004).
- [74] D. B. Renner *et al.*, Nucl. Phys. Proc. Suppl. **140**, 255 (2005).
- [75] R. G. Edwards *et al.*, PoS **LAT2005**, 056 (2005).
- [76] J. Foley, K. Jimmy Juge, A. O’Cais, M. Peardon, S. M. Ryan and J. I. Skullerud, Comput. Phys. Commun. **172**, 145 (2005) [arXiv:hep-lat/0505023].
- [77] T. A. DeGrand and D. Toussaint, *Singapore, Singapore: World Scientific (1990) 750 p*
- [78] S. R. Beane, P. F. Bedaque, K. Orginos and M. J. Savage, Phys. Rev. D **73**, 054503 (2006).
- [79] S. Weinberg, Phys. Rev. Lett. **17**, 616 (1966).
- [80] J. Bijnens, G. Colangelo, G. Ecker, J. Gasser and M. E. Sainio, Phys. Lett. B **374**, 210 (1996) [arXiv:hep-ph/9511397];
- [81] J. Bijnens, G. Colangelo, G. Ecker, J. Gasser and M. E. Sainio, Nucl. Phys. B **508**, 263 (1997) [Erratum-ibid. B **517**, 639 (1998)] [arXiv:hep-ph/9707291].
- [82] S. Pislak *et al.* [BNL-E865 Collaboration], Phys. Rev. Lett. **87**, 221801 (2001) [arXiv:hep-ex/0106071].
- [83] S. Pislak *et al.*, Phys. Rev. D **67**, 072004 (2003) [arXiv:hep-ex/0301040].
- [84] B. Adeva *et al.* [DIRAC Collaboration], Phys. Lett. B **619**, 50 (2005) [arXiv:hep-ex/0504044].
- [85] J. R. Batley *et al.* [NA48/2 Collaboration], Phys. Lett. B **633**, 173 (2006) [arXiv:hep-ex/0511056].
- [86] G. Colangelo, J. Gasser and H. Leutwyler, Nucl. Phys. B **603**, 125 (2001) [arXiv:hep-ph/0103088].
- [87] H. Leutwyler, arXiv:hep-ph/0612112.
- [88] S. M. Roy, Phys. Lett. B **36**, 353 (1971).
- [89] J. L. Basdevant, C. D. Froggatt and J. L. Petersen, Nucl. Phys. B **72**, 413 (1974).
- [90] B. Ananthanarayan, G. Colangelo, J. Gasser and H. Leutwyler, Phys. Rept. **353**, 207 (2001) [arXiv:hep-ph/0005297].
- [91] I. Caprini, G. Colangelo and H. Leutwyler, Phys. Rev. Lett. **96**, 132001 (2006) [arXiv:hep-ph/0512364].
- [92] C. Bernard *et al.* [MILC Collaboration], PoS **LAT2006**, 163 (2006) [arXiv:hep-lat/0609053].
- [93] S. R. Sharpe, R. Gupta and G. W. Kilcup, Nucl. Phys. B **383**, 309 (1992).
- [94] R. Gupta, A. Patel and S. R. Sharpe, Phys. Rev. D **48**, 388 (1993) [arXiv:hep-lat/9301016].
- [95] Y. Kuramashi, M. Fukugita, H. Mino, M. Okawa and A. Ukawa, Phys. Rev. Lett. **71**, 2387 (1993).
- [96] Y. Kuramashi, M. Fukugita, H. Mino, M. Okawa and A. Ukawa, [arXiv:hep-lat/9312016].
- [97] M. Fukugita, Y. Kuramashi, H. Mino, M. Okawa and A. Ukawa, Phys. Rev. Lett. **73**, 2176 (1994) [arXiv:hep-lat/9407012].
- [98] C. Gattringer, D. Hierl and R. Pullirsch [Bern-Graz-Regensburg Collaboration], Nucl. Phys. Proc. Suppl. **140**, 308 (2005) [arXiv:hep-lat/0409064].
- [99] M. Fukugita, Y. Kuramashi, M. Okawa, H. Mino and A. Ukawa, Phys. Rev. D **52**, 3003 (1995) [arXiv:hep-lat/9501024].
- [100] H. R. Fiebig, K. Rabitsch, H. Markum and A. Mihaly, Few Body Syst. **29**, 95 (2000) [arXiv:hep-lat/9906002].
- [101] S. Aoki *et al.* [JLQCD Collaboration], Nucl. Phys. Proc. Suppl. **83**, 241 (2000) [arXiv:hep-

- lat/9911025].
- [102] C. Liu, J. h. Zhang, Y. Chen and J. P. Ma, [arXiv:hep-lat/0109010].
 - [103] C. Liu, J. h. Zhang, Y. Chen and J. P. Ma, Nucl. Phys. B **624**, 360 (2002) [arXiv:hep-lat/0109020].
 - [104] S. Aoki *et al.* [CP-PACS Collaboration], Nucl. Phys. Proc. Suppl. **106**, 230 (2002) [arXiv:hep-lat/0110151].
 - [105] S. Aoki *et al.* [JLQCD Collaboration], Phys. Rev. D **66**, 077501 (2002) [arXiv:hep-lat/0206011].
 - [106] S. Aoki *et al.* [CP-PACS Collaboration], Nucl. Phys. Proc. Suppl. **119**, 311 (2003) [arXiv:hep-lat/0209056].
 - [107] S. Aoki *et al.* [CP-PACS Collaboration], Phys. Rev. D **67**, 014502 (2003) [arXiv:hep-lat/0209124].
 - [108] K. J. Juge [BGR Collaboration], Nucl. Phys. Proc. Suppl. **129**, 194 (2004) [arXiv:hep-lat/0309075].
 - [109] N. Ishizuka and T. Yamazaki, Nucl. Phys. Proc. Suppl. **129**, 233 (2004) [arXiv:hep-lat/0309168].
 - [110] S. Aoki *et al.* [CP-PACS Collaboration], Phys. Rev. D **71**, 094504 (2005) [arXiv:hep-lat/0503025].
 - [111] S. Aoki *et al.* [CP-PACS Collaboration], Nucl. Phys. Proc. Suppl. **140**, 305 (2005) [arXiv:hep-lat/0409063].
 - [112] X. Li *et al.* [CLQCD Collaboration], JHEP **0706**, 053 (2007) [arXiv:hep-lat/0703015].
 - [113] K. Sasaki and N. Ishizuka, arXiv:0804.2941 [hep-lat].
 - [114] T. Yamazaki *et al.* [CP-PACS Collaboration], Phys. Rev. D **70**, 074513 (2004) [arXiv:hep-lat/0402025].
 - [115] S. R. Beane, T. C. Luu, K. Orginos, A. Parreño, M. J. Savage, A. Torok and A. Walker-Loud, Phys. Rev. D **77**, 014505 (2008) [arXiv:0706.3026 [hep-lat]].
 - [116] K. Maltman and C. E. Wolfe, Phys. Lett. B **393**, 19 (1997) [Erratum-ibid. B **424**, 413 (1998)] [arXiv:nucl-th/9610051].
 - [117] U. G. Meissner, G. Muller and S. Steininger, Phys. Lett. B **406**, 154 (1997) [Erratum-ibid. B **407**, 454 (1997)] [arXiv:hep-ph/9704377].
 - [118] M. Knecht and R. Urech, Nucl. Phys. B **519**, 329 (1998) [arXiv:hep-ph/9709348].
 - [119] M. Knecht and A. Nehme, Phys. Lett. B **532**, 55 (2002) [arXiv:hep-ph/0201033].
 - [120] B. Bloch-Devaux, *Recent results from NA48/2 on Ke_4 decays and interpretation in term of $\pi\pi$ scattering lengths*, Talk presented at Kaon 2007, May 21-25 (2007).
 - [121] J. Gasser, *Theoretical progress on cusp effect and Kl_4* , Talk presented at Kaon 2007, May 21-25 (2007).
 - [122] <http://dirac.web.cern.ch/DIRAC/future.html>
 - [123] P. Buettiker, S. Descotes-Genon and B. Moussallam, Eur. Phys. J. C **33**, 409 (2004) [arXiv:hep-ph/0310283].
 - [124] B. Ananthanarayan, P. Buettiker and B. Moussallam, Eur. Phys. J. C **22**, 133 (2001) [arXiv:hep-ph/0106230].
 - [125] B. Ananthanarayan and P. Buettiker, Eur. Phys. J. C **19**, 517 (2001) [arXiv:hep-ph/0012023].
 - [126] M. Jamin, J. A. Oller and A. Pich, Nucl. Phys. B **587**, 331 (2000) [arXiv:hep-ph/0006045].
 - [127] V. Bernard, N. Kaiser and U. G. Meissner, Nucl. Phys. B **357**, 129 (1991).
 - [128] V. Bernard, N. Kaiser and U. G. Meissner, Phys. Rev. D **43**, 2757 (1991).
 - [129] B. Kubis and U. G. Meissner, Phys. Lett. B **529**, 69 (2002) [arXiv:hep-ph/0112154].

- [130] J. Bijnens, P. Dhonte and P. Talavera, JHEP **0405**, 036 (2004) [arXiv:hep-ph/0404150].
- [131] C. Miao, X. i. Du, G. w. Meng and C. Liu, Phys. Lett. B **595**, 400 (2004) [arXiv:hep-lat/0403028].
- [132] S. Descotes-Genon and B. Moussallam, Eur. Phys. J. C **48**, 553 (2006) [arXiv:hep-ph/0607133].
- [133] S. R. Beane, P. F. Bedaque, T. C. Luu, K. Orginos, E. Pallante, A. Parreño and M. J. Savage, Phys. Rev. D **74**, 114503 (2006) [arXiv:hep-lat/0607036].
- [134] J. Gasser and H. Leutwyler, Nucl. Phys. B **250**, 465 (1985).
- [135] J. Gasser and H. Leutwyler, Phys. Lett. B **125**, 321 (1983).
- [136] S. R. Beane, P. F. Bedaque, K. Orginos and M. J. Savage, Phys. Rev. D **75**, 094501 (2007) [arXiv:hep-lat/0606023].
- [137] A. Roessl, Nucl. Phys. B **555**, 507 (1999) [arXiv:hep-ph/9904230].
- [138] J. Schweizer, Phys. Lett. B **625**, 217 (2005) [arXiv:hep-ph/0507323].
- [139] D. O'Connell, "Ginsparg-Wilson Meson Scattering on a Staggered Sea," *talk at LATTICE 2006*, Tucson, Arizona.
- [140] K. Orginos and A. Walker-Loud, arXiv:0705.0572 [hep-lat].
- [141] J. Nagata, A. Nakamura and S. Muroya, Nucl. Phys. A **790** (2007) 414.
- [142] J. M. Flynn and J. Nieves, Phys. Rev. D **75**, 074024 (2007) [arXiv:hep-ph/0703047].
- [143] J. M. Flynn and J. Nieves, PoS **LAT2007**, 352 (2007) [arXiv:0711.3339 [hep-lat]].
- [144] D. B. Kaplan and A. E. Nelson, Phys. Lett. B **175**, 57 (1986).
- [145] J. G. Cramer, G. A. Miller, J. M. S. Wu and J. H. S. Yoon, Phys. Rev. Lett. **94**, 102302 (2005) [arXiv:nucl-th/0411031].
- [146] G. A. Miller and J. G. Cramer, J. Phys. G **34**, 703 (2007) [arXiv:nucl-th/0507004].
- [147] G. A. Miller and J. G. Cramer, Nucl. Phys. A **782** (2007) 251.
- [148] B. I. Abelev *et al.* [STAR Collaboration], Phys. Rev. C **74**, 054902 (2006) [arXiv:nucl-ex/0608012].
- [149] S. R. Beane, T. C. Luu, K. Orginos, A. Parreño, M. J. Savage, A. Torok and A. Walker-Loud [NPLQCD Collaboration], arXiv:0709.1169 [hep-lat].
- [150] S. R. Beane, P. F. Bedaque, K. Orginos and M. J. Savage, Phys. Rev. Lett. **97**, 012001 (2006) [arXiv:hep-lat/0602010].
- [151] S. R. Beane and M. J. Savage, Nucl. Phys. A **713**, 148 (2003) [arXiv:hep-ph/0206113].
- [152] S. R. Beane and M. J. Savage, Nucl. Phys. A **717**, 91 (2003) [arXiv:nucl-th/0208021].
- [153] E. Epelbaum, U. G. Meissner and W. Gloeckle, Nucl. Phys. A **714**, 535 (2003) [arXiv:nucl-th/0207089].
- [154] D. Lee, arXiv:0804.3501 [nucl-th].
- [155] D.B. Kaplan, *The OFT*, talk presented at the workshop on **Domain Wall Fermions at 10 Years**, Brookhaven National Laboratory March 15-18, 2007. http://www.phys.washington.edu/users/dbkaplan/kaplan_talks.html.
- [156] S. R. Beane and M. J. Savage, Phys. Lett. B **535**, 177 (2002) [arXiv:hep-lat/0202013].
- [157] S. Weinberg, Phys. Lett. B **251**, 288 (1990).
- [158] S. Weinberg, Nucl. Phys. B **363**, 3 (1991).
- [159] C. Ordoñez, L. Ray and U. van Kolck, Phys. Rev. C **53**, 2086 (1996) [arXiv:hep-ph/9511380].
- [160] D. B. Kaplan, M. J. Savage and M. B. Wise, Nucl. Phys. B **534**, 329 (1998) [arXiv:nucl-th/9802075].
- [161] D. B. Kaplan, M. J. Savage and M. B. Wise, Phys. Lett. B **424**, 390 (1998) [arXiv:nucl-th/9801034].

- [162] S. R. Beane, P. F. Bedaque, M. J. Savage and U. van Kolck, Nucl. Phys. A **700**, 377 (2002) [arXiv:nucl-th/0104030].
- [163] B. C. Tiburzi, Phys. Rev. D **72**, 094501 (2005) [arXiv:hep-lat/0508019].
- [164] A. Gal, E. Hungerford, Nucl. Phys. A **754** 1-489 (2005).
- [165] O. Hashimoto and H. Tamura, Prog. Part. Nucl. Phys. **57**, 564 (2006).
- [166] J. Balewski et al., Phys. Lett. B **420**, 211 (1998).
- [167] R. Bilger et al., Phys. Lett. B **420**, 217 (1998).
- [168] S. Sewerin et al., Phys. Rev. Lett. **83**, 682 (1999).
- [169] P. Kowina et al., Eur. Phys. J. **A22**, 293 (2004).
- [170] M. Abdel-Bary et al., Phys. Lett. B **595**, 127 (2004).
- [171] A. Gasparyan, J. Haidenbauer, C. Hanhart, J. Speth, Phys. Rev. C **69**, 034006 (2004).
- [172] C. J. Batty, E. Friedman and A. Gal, Phys. Rept. **287** (1997) 385.
- [173] <http://nn-online.sci.kun.nl/index.html>.
- [174] V.G.J. Stoks and Th.A. Rijken, Phys. Rev. C **59**, 3009 (1999); Th.A. Rijken, V.G.J. Stoks and Y. Yamamoto, Phys. Rev. C **59**, 21-40 (1999).
- [175] Th.A. Rijken, Y. Yamamoto, Phys. Rev. C **73** 044008 (2006).
- [176] B. Holzenkamp, K. Holinde, and J. Speth, Nucl. Phys. A **500** (1989) 485.
- [177] A. Reuber, K. Holinde, H.-C. Kim, and J. Speth, Nucl. Phys. A **608** 243 (1996).
- [178] J. Haidenbauer and Ulf G. Meißner, Phys. Rev. C **72** 044005 (2005).
- [179] M. J. Savage and M. B. Wise, Phys. Rev. D **53**, 349 (1996).
- [180] C.L. Korpa, A.E.L. Dieperink, and R.G.E. Timmermans, Phys. Rev. C **65**, 015208 (2001).
- [181] H.W. Hammer, Nucl. Phys. A **705**, 173 (2002).
- [182] S. R. Beane, P. F. Bedaque, A. Parreño and M. J. Savage, Nucl. Phys. A **747**, 55 (2005) [arXiv:nucl-th/0311027].
- [183] H. Polinder, J. Haidenbauer and Ulf-G. Meißner, Nucl. Phys. A **779**, 244 (2006) [arXiv:nucl-th/0605050].
- [184] S. R. Beane, P. F. Bedaque, T. C. Luu, K. Orginos, E. Pallante, A. Parreño and M. J. Savage [NPLQCD Collaboration], Nucl. Phys. A **794**, 62 (2007) [arXiv:hep-lat/0612026].
- [185] C. Michael and P. Pennanen [UKQCD Collaboration], Phys. Rev. D **60**, 054012 (1999) [arXiv:hep-lat/9901007].
- [186] P. Pennanen, C. Michael and A. M. Green [UKQCD Collaboration], Nucl. Phys. Proc. Suppl. **83**, 200 (2000) [arXiv:hep-lat/9908032].
- [187] A. M. Green, J. Koponen and P. Pennanen, Phys. Rev. D **61**, 014014 (2000) [arXiv:hep-ph/9902249].
- [188] H. R. Fiebig [LHP collaboration], Nucl. Phys. Proc. Suppl. **106**, 344 (2002) [arXiv:hep-lat/0110163].
- [189] H. R. Fiebig [LHP Collaboration], Nucl. Phys. Proc. Suppl. **109A**, 207 (2002) [arXiv:hep-lat/0112010].
- [190] M. S. Cook and H. R. Fiebig, arXiv:hep-lat/0210054.
- [191] T. T. Takahashi, T. Doi and H. Suganuma, AIP Conf. Proc. **842**, 249 (2006) [arXiv:hep-lat/0601006].
- [192] T. Doi, T. T. Takahashi and H. Suganuma, AIP Conf. Proc. **842**, 246 (2006) [arXiv:hep-lat/0601008].
- [193] A. M. Green, arXiv:nucl-th/0409021.
- [194] W. Detmold, K. Orginos and M. J. Savage, Phys. Rev. D **76**, 114503 (2007) [arXiv:hep-lat/0703009].

- [195] M. E. Luke, A. V. Manohar and M. J. Savage, Phys. Lett. B **288**, 355 (1992) [arXiv:hep-ph/9204219].
- [196] S. J. Brodsky and G. A. Miller, Phys. Lett. B **412**, 125 (1997) [arXiv:hep-ph/9707382].
- [197] K. Yokokawa, S. Sasaki, T. Hatsuda and A. Hayashigaki, Phys. Rev. D **74**, 034504 (2006) [arXiv:hep-lat/0605009].
- [198] M. M. Aggarwal *et al.* [WA98 Collaboration], Phys. Rev. Lett. **85**, 2895 (2000) [arXiv:hep-ex/0008018].
- [199] I. G. Bearden *et al.* [NA44 Collaboration], Phys. Lett. B **517**, 25 (2001) [arXiv:nucl-ex/0102013].
- [200] J. Adams *et al.* [STAR Collaboration], Phys. Rev. Lett. **91**, 262301 (2003) [arXiv:nucl-ex/0306028].
- [201] A. Stathopoulos and K. Orginos, arXiv:0707.0131 [hep-lat].